Sample thickness influence on flexural strength under concentrated load of some Portuguese ornamental stones

João Carlos de Mendonça Senra

Dissertação para obtenção do Grau de Mestre em

Engenharia Geológica e de Minas

Orientadores:
Professora Doutora Maria Amélia Alves Rangel Dionísio
Professor Doutor Gustavo André Paneiro

Júri

Presidente: Professor José Manuel Vaz Velho Barbosa Marques
Orientadora: Professora Maria Amélia Alves Rangel Dionísio
Vogal: Doutora Vera Pires de Almeida Ribeiro

Outubro 2021

Declaration

I declare that this document is an original work of my own authorship and that it fulfills all the requirements of the Code of Conduct and Good Practices of the Universidade de Lisboa.

Acknowledgement

Firstly, I would like to thank both my supervisors, Professor Maria Amélia Dionísio and Professor Gustavo Paneiro, not only for all the support given but mostly for always being available for me at any given point in time during the realization my dissertation. Without a doubt, the work here presented would not have come to fruition without their willingness to always provide feedback and advice.

I would also like to thank SOCIMAR – Sociedade Industrial de Mármores, Lda., FILSTONE – Comércio de Rochas, S.A. and AFONSTONE - Rochas Ornamentais, Lda. for kindly providing the natural stone samples necessary for the realization of this work, as well as CERENA, whose laboratory and equipment made available were just as important.

Moreover, I would like to extend my gratitude to the people with whom I had the pleasure of sharing my time with during my laboratory work, particularly to my colleagues Leonor Gomes and Sérgio Tenjua who accompanied me through it and were always willing to given a hand when necessary.

Finally, I would also like to thank my family, who worked hard to support me through my educational journey and gave me all the help I could ever ask for.

Resumo

Recentemente, uma evolução no sentido de aplicações mais finas e leves de painéis de pedra natural em fachadas começou a desafiar as normas de ensaio existentes. A resistência à flexão, uma propriedade testada sob a norma EN 12372 (2006), é frequentemente utilizada para avaliar a resistência mecânica de tais painéis de pedra, mas as normas atuais estão desatualizadas em relação à aplicação moderna, uma vez que restrições de espessura mínima de 25 mm, mais espessa do que os painéis frequentemente utilizados, significam que os produtores não conseguem cumprir a norma existente. Para além disso, tem sido mostrado que a variação em resistência à flexão com a redução do tamanho da amostra não segue leis estatísticas conhecidas, tais como a lei Bažant, devido à sua heterogeneidade natural e uma estrutura complexa. De modo a analisar o comportamento da resistência à flexão na rocha ornamental portuguesa, dada uma variação da espessura das amostras, tanto dentro como abaixo do standard existente, foi testado um largo conjunto de amostras composto por 2 granitos, 2 mármores e 6 calcários: não só para resistência à flexão, mas também para outras propriedades físicas. As restrições de dimensionamento das amostras, que se baseiam na espessura, foram seguidas para quatro tamanhos de amostra: de 10/20/25/50 mm de espessura; e os resultados mostram que embora exista uma ténue correlação entre um leve aumento na resistência à flexão e a diminuição espessura da amostra, esta é insignificante dadas as incertezas estatísticas e o papel desta resistência no dimensionamento da rocha ornamental.

Palavra-chave: Rocha ornamental; Normalização; Resistência à flexão; Espessura da amostra.

Abstract

In recent times, an evolution towards thinner and lighter applications of natural stone panels in façades has begun to challenge existing test standards. Flexural strength, a property tested under the EN 12372 (2006) standard, is often used to assess the mechanical resistance of such stone panels, but the norms through which its measured are now at odds with modern applications methods, as restrictions to a minimum sample thickness of 25 mm, which is often thicker than the panels used, means that producers cannot comply with the existing standard. To add to this issue, flexural strength's relation with sample size reduction has been shown to not comply with known statistical laws, such as the Bažant law, due to their natural heterogenous disposition and complex structure. In this study, in order to analyze the behavior of bending resistance in Portuguese natural stones, given a sample's thickness variation from within, to below the existing standard, a large sample pool consisting of 2 granites, 2 marbles and 6 limestones were tested. This study also included the evaluation of other physical properties. The standards restrictions for sample dimension, which are based on thickness, were followed for four sample sizes: 10 mm, 20 mm, 25 mm and 50 mm thickness; and the results show that while there is a tenuous correlation between a small increase in flexural strength as sample thickness decreases, this effect is negligible given the statistical uncertainties and this resistance's role in the dimensioning of stone panels.

Keywords: Ornamental Stone; Standardization; Flexural strength; Sample thickness.

Contents

List of Figures

List of Tables

1. Introduction

Natural stone has had a long history when it comes to its use as a building material, dating to historic times where civilizations were built on a foundation of layered, quarried blocks of granite, marble or limestone, largely due to their availability and relative durability. In the 20th century, however, the architectural landscape has evolved, and the application of natural stone as a building material has shifted from its historic foundational purposes, to a piece of design, as technological advancements caused the emergence of new construction materials, namely concrete, which are cheaper and more adept for a structural role. Therefore, natural stones currently have a larger role in cladding, roofing or in a façade, and are sought after due its mixture of aesthetic and mechanical properties, besides its ecological character. It's in this scenario where the concept of flexural strength comes into play, as it is one of the most important properties that characterize a natural stone, particularly in its application as cladding material. Besides, stone dimensioning processes (and subsequently stone safety factors) did not change as the evolution of stone façades design progressed, and as such, the current applications of these materials are beginning to challenge norms established in past times. Such is the case of stone cladding, in which the application has trended toward the use of thinner and lighter stone (Schrenk, 2020), to the point where the standards used to measure flexural strength cannot take into consideration such uses, as its norms restrict test samples to a minimum set of dimensions which are thicker than the actual stone's dimensioning. As such, the question is raised of whether the resistance values obtained from standard tests, conducted on thicker samples, are still viable to describe resistance even on thinner stone applications, or are instead misleading the design of cladding anchorage with overrated flexural strength values.

1.1.1. Objectives

This dissertation's main goal is to study the effects of different test sample dimensions, particularly of variable sample thickness, in the values of flexural strength obtained under a concentrated load, following the standard EN 12372, for a set of 10 different Portuguese natural stones. More specifically, this standard currently employs restrictions to the dimensioning of test samples, and the objective is to observe whether utilizing test samples below the minimum allowed thickness of 25 mm results in any variation compared the expected flexural strength results from samples that follow the standard.

In order to accomplish this goal, several laboratory tests were made under controlled conditions to profile and analyze physical properties, such as open porosity, water absorption and P-wave propagation velocity propagation, as well as the mechanical property of flexural strength, in a total of 200 test samples, from 2 granites, 2 marbles and 6 limestones, all originated from Portugal, and with various dimensions.

1.1.2. Organization of the Dissertation

This present dissertation is divided in 5 main sections, with the first of these being the current introductory chapter, containing the motivational factors which originated this study, followed by a section which covers important previous works that have been made, over time, not only in the topic of flexural strength and its variation as a product of sample size, but also in fields of other physical properties, that will be analyzed in this work, and their relationship with flexural strength in natural stone.

The third section contains both an extensive description of the natural stones samples that were acquired, with their geological framework and general applications, as well as the methods that were used both in the experimental phase, and in the processing of the subsequently obtained results. Following this, these results are then presented in a fourth section, separated in three subsections for granite samples, marble samples, and limestone samples, with the goal of analyzing them in the context of the objectives described.

Finally, in a fifth section, concluding remarks are presented over the analysis made in the previous section and the overall work done, along with the closing thoughts on the topic in study and remarks regarding future works, should they address the notion of sample size thickness effect on flexural strength, taking into consideration the shortcomings of this work and the development towards a better understanding of this notion.

2. Literature Review

In this section, some information is provided regarding the physical properties being tested in this study, as well as their apparent correlations with flexural strength, in natural stone. The main goal is to understand if variation on these properties can translate into variation on the resulting flexural strength in a sample, and if so, as result of which particular characteristics of a stone sample. In the case of the mechanical property of flexural strength itself, after brief introduction to its definition, previous works by various authors on its relationship with changes in sample size are then analyzed.

2.1. Physical properties

2.1.1. Open porosity and apparent density

Porosity is a property with an important role as a descriptive parameter of natural stone, as it's often related to other properties, whether in a direct or indirect manner, and along with knowledge of these, it could lead into a better understanding of a stone's physical and mechanical responses, regarding both compressive and flexural tension (Çelik *et al.* 2014). In general, porosity refers to the relationship between the volume of void spaces, like pores, cracks and microcracks, that reside within a certain rock and that rock's total volume. More concretely, open porosity only measures a portion of this same volume of void spaces, the ones which are accessible by fluids or gases from the rock's surface, meaning that open porosity will always be smaller than total porosity. In this sense, open porosity can be measured through water absorption tests, and it's a good indicator for a natural stone's general quality from a weathering perspective, as in general a lower open porosity means a lower susceptibility of the rock matrix being altered through contact with external fluids (Camposinhos, 2014).

Although not necessarily based on the heterogeneity characteristic of natural stones, porosity has been associated with changes in flexural strength of low resistance hydraulic cements, in the work of Birchall *et al.* (1981), in which a set of cements based on calcium silicate, calcium aluminate and calcium sulphate, exhibiting flexural strengths of 3 to 10 MPa, have their resistance of bending stress increased to a maximum of 70 MPa, through a process that reduced the presence of voids which originated in the mixing process, with this reduction causing an exponential increase in flexural strength.

In the case of density, it's a property that's largely dependent on porous volume and on the mineral composition of the natural stone: a rock composed, in general, by less dense minerals such as quartz, feldspar or calcite, will inevitably be less dense that an igneous rock with denser minerals in its composition, such as olivine or pyroxene (Camposinhos, 2014). Density represents the ratio of mass per unit of volume of a material, and bulk density specifically is measured through the comparison between the volume of rock mass and the volume of voids present in the rock, hence an inversely proportional relationship between bulk density and measured porosity. Bulk density, like porosity, is also a property that allows to project both physical and mechanical resistances in natural stone, so it also serves as an important parameter to describe its durability.

2.1.2. Water absorption by capillarity

Water absorption through capillarity is a property that reflects the penetration of water into a material's surface, through the material's natural pore structure and other voids, connected into its inner mass, without the presence of external forces. Unlike open porosity, where the total volume of connecting voids in a given rock is characterized, water absorption describes the rate at which the penetration occurs as a flux of water, through the pore structure. Therefore, a rock with a high level of porosity might not always have an equally high level of water absorption, as the presence of a large volume of voids doesn't necessarily guarantee a high degree of connectivity between them. However, along with porosity, it's also desirable to have a low amount of water absorption in a natural stone, as the higher the absorption rate the higher the rate at which any fluid will propagate through the rock's surface, potentially accelerating the stone's weathering process (Camposinhos, 2014).

Usually, the process of water absorption can be divided in two separate stages (Figure 1): an initial stage, where a quicker intake of water can be observed, derived from the stones natural water absorption rate through its pore structure and connectivity; and a second stage, where a much slower absorption takes place, based on a process of diffusion of the remaining air trapped in the pore structure. The point between both phases indicates the ceiling for the absorption through capillarity, and the first stage is the one used to describe the water absorption. However, the absorption process can be divided in a larger number of phases when dealing with heterogeneous materials, as could be the case for an anisotropic sedimentary stone composed by several horizontal layers, each with its own gradient of grain size, where the point between each different receding phase indicated change of layer (Gonçalves, 2007).

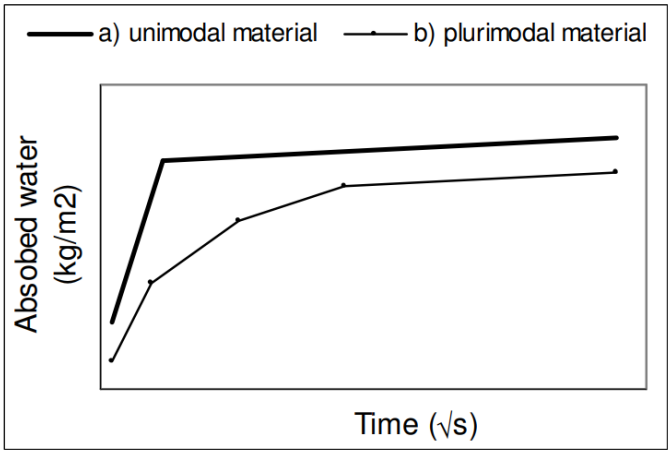

Figure 1 – Example of typical curves for water absorption in porous building materials for two phases (unimodal material) and multiple phases (plurimodal material), in kg/m2 of absorbed water per unit of time (adapted from Gonçalves, 2007).

2.1.3. P-wave propagation velocity

P-wave propagation velocity is often employed as a mean to determine geotechnical properties of a natural stone and rock mass quality in general, whether in an attempt to estimate and correlate with other properties, such as uniaxial compressive strength, porosity, dry or saturated density, amount and density of fractures and the degree of weathering; or even as a mean of evaluating the rock's elastic behavior (Yagiz, 2011; Aydin, 2013). The measuring of P-wave propagation velocity is based on the ultrasonic test, where a compression wave is induced, transmitted and received on the rock sample, and the elastic wave travel time, alongside the spatial distance are measured. The travel time of the wave is a product of the rock's structural characteristics and the specimen's geometry, and in this case rectangular blocks are utilized, as they provide a better means to evaluate the main axes of P-wave propagation velocity and measure anisotropy, given that sedimentary rock samples, like limestone, are likely to present an orientated disposition of its minerals that may impart directional dependencies to strength and deformation resistance (Aydin, 2013). Anisotropy, through this method, can be described as the difference in velocities observed between the aforementioned main axes, while the measurements of elastic constants can only be calculated in isotropic (or only slightly anisotropic) samples, according to the ASTM Standard D2845-00 (2008).

Kahraman *et al.* (2007), conducted a study on 22 large limestone blocks from a stone processing plant, looking to elaborate a quality classification method based on P-wave propagation velocities, on building stones. In this, the P-wave propagation velocity of core samples was measured, and the ratio between this and the velocity measured on the large limestone blocks was called the velocity ratio index (VRI), through which the quality classification was built upon. The quality classification was generally conducted through visual inspection and it evaluated the fracturing level of a processed limestone block, designated as slab efficiency. They concluded that by means of ultrasonic P-wave measurements, the estimated block quality matched the observed slab efficiency (Figure 2), in what proved to be a cheap, non-destructive and easily applicable method. However, Kahraman *et al.* (2007) pointed out that the study was carried out only in limestone, and that further studies would need to be made in order to evaluate this quality assessment method to other types of rock.

Recently, Nourani *et al.* (2017) applied P-wave propagation velocity analysis in classification and assessment of rock mass parameters in an iron mine, such as Q-system values and RMR (Rock Mass Rating), as well as other such as RQD (Rock Quality Designation), uniaxial compressive strength, joint roughness coefficient and Schmidt number. In this work, P-wave propagation velocity determination included both laboratory and in situ measurements, as well as an analysis on the ratio between both of these measurements, and in two different orthogonal directions. The results showed that the aforementioned rock mass parameters, which were already known, were all more or less well correlated with P-wave propagation velocity values obtained, particularly the Q-system values. Also, it was possible to estimate P-wave propagation velocity through these parameters with a high correlation coefficient of 91%, and the anisotropy observed through the studying of P-values measured meant these could be used to assess strong and weak excavation directions of the rock mass.

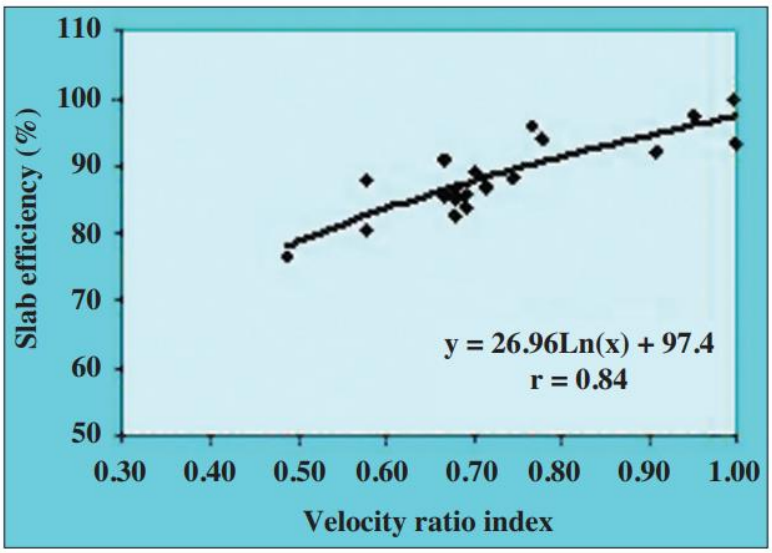

Figure 2 – Comparison of estimated block quality through the Velocity Ratio Index (VRI) against the visual observation for 22 limestone blocks (adapted from Kahraman et al., 2007).

In terms of correlation with other geotechnical parameters, Yagiz Saffet (2011) conducted a study on the estimation of properties in 9 different types of rock, including limestones, travertines and schists, from measured P-wave propagation velocities, relating them to properties such as uniaxial compressive strength, Schmidt hardness, Young's modulus, water absorption, open porosity, density and others, which were all predetermined. The conclusion of this study, formed by means of linear regression analysis, showed that P-wave propagation velocity had a high correlation coefficient with both uniaxial compression strength and the Young's modulus, with 92% and 95% respectively (Figure 3). Decent correlation coefficients with the other mentioned properties, with exception of dry and saturated densities, were also obtained. Yagiz also pointed out the importance of rock texture and mineralogical compositions to the geotechnical properties of rock, conducting petrographic and mineralogic studies on sections of the specimens tested.

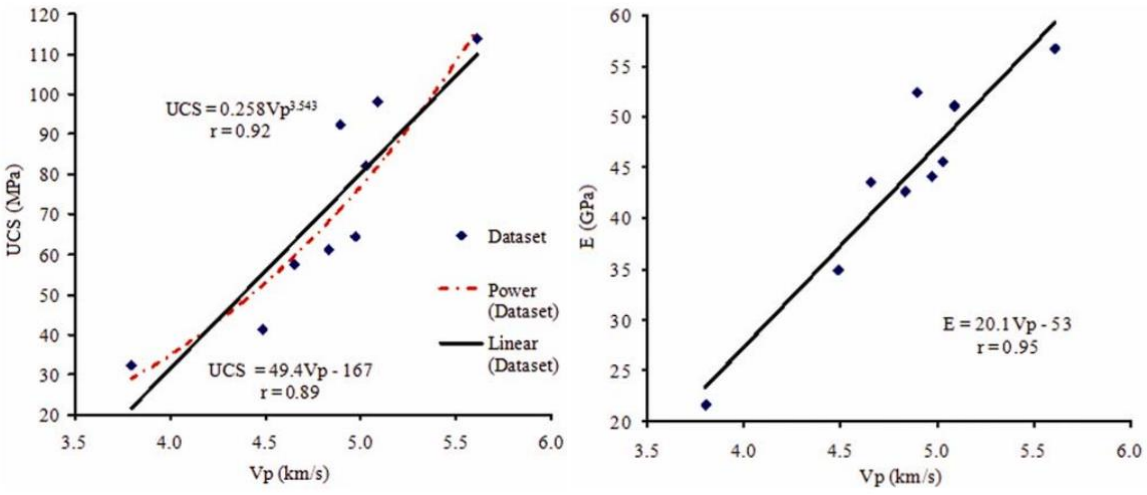

Figure 3 – Relationship of P-wave propagation velocities with uniaxial compression strength (on the left) and modulus of elasticity (on the right) (adapted from Yagiz, 2011). The P-wave propagation velocity shows a polynomial relation with UCS, with a correlation coefficient of 92%, and a linear relation with the modulus of elasticity, with a correlation coefficient of 95%.

In 2011, Fener studied the effects of rock sample dimension in measured P-wave propagation velocities on 9 different rock groups, each group with six different core sample diameters, through a comparison of P-wave propagation velocity for a singular distance and sample core diameter surrounding it (Figure 4). To do this, the test results were statistically analyzed to search for linear, polynomial or exponential regressions with a high correlation coefficient between the velocities obtained and the different diameters, much like in the previous works mentioned.

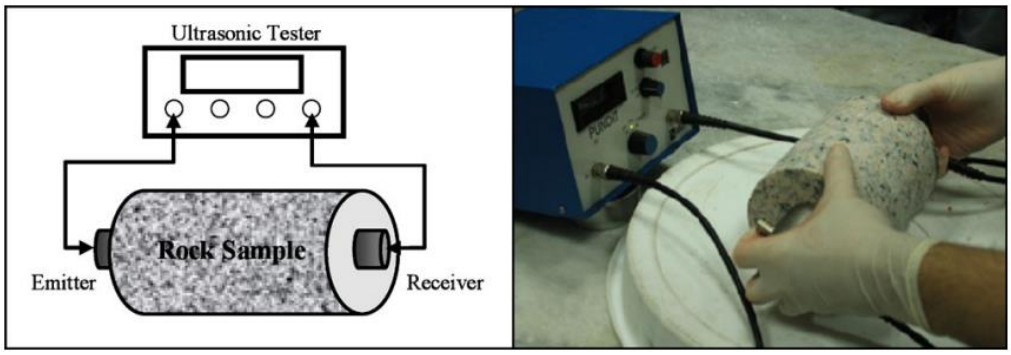

Figure 4 – P-wave propagation velocity measurement on the core samples, through ultrasonic testing (adapted from Fener, 2011).

The result showed that for most groups, there was a tendency for P-wave propagation velocity to decrease as the diameter of the core sample increased, although for some of the tested samples, the largest diameter samples recorded an increase in this velocity. It was concluded that the P-wave propagation velocity variation was stronger on rock types that presented higher porosity, and that this variation in velocity was well correlated with a variation in porosity and dry density.

2.2. Mechanical properties

2.2.1. Size Effect on stone flexural strength

Flexural strength, also known as bending strength or rupture modulus, is a mechanical property that defines the maximum amount of bending stress that a given material can withstand, in a flexural test, which occurs right as the material begins to either fracture or yield. The methods most commonly used in flexural testing involve a sample being placed between a pair of supporting rollers and either one, or two, central rollers, which will then apply a transversal bending load on the sample until it yields. The sample's flexural strength is then calculated based on the highest recorded load weight during the test (EN 12372:2006, EN 13161:2008). This type of testing is required for assessing the stone's mechanical resistance according to the CE marking, whose certification is necessary for economic trading of construction products, such as natural stone, within Europe (Bellopede, 2015).

Besides the highest recorded load weight, another property that goes into calculating flexural strength, through this method, is sample size, with the dimensions of the sample for flexural testing being based on the corresponding standards: EN 12372:2006 for 3-point bending tests and EN 13161:2008 for 4-points bending tests. The 3-point bending test, which was the one chosen for this

study, is commonly considered a simple method to evaluate a rock's strength to flexural loads, and it can be easily applied to different kinds of sample sizes and shapes (Fan *et al.*, 2019). For this case, following the EN 12372:2006 standard for determination of flexural strength under a concentrated load, the rectangular shape with 300mm x 50mm x 50mm is recommended, but other dimensions are possible. Sample thickness is particularly important as, according to the standard, it dictates the overall size of the sample, varying between 25mm and 100m. However, when it comes to the utilization of natural stone, applications such as wall cladding or roof slating often work with material whose thickness is smaller than the minimum standard value for flexural testing of 25mm (EN 12372:2006). Therefore, it's necessary to understand the impact of dimension scaling in stone's flexural strength, in this case related to the effect of thickness reduction, and if the standardized testing method for it is able to represent these smaller dimensions.

Studies on the impact of size scaling can date back to 1949, with Weibull's work on the statistical size effects on fracture occurrence (Weibull, 1949), predicting that the larger the dimensions of a material, the larger the chance of encountering internal microfracturing, which would imply a proportionate strength reduction in the material (Bažant, 1999). Z. P. Bažant reviewed the application of this theory on concrete structures, in 1999, concluding that Weibull's theory had certain limitations, appearing applicable to only "extremely thick plain (unreinforced) structures". Also, the Author claims that there was still a lot of progress to be made, in order to reach an understanding of these size scaling problems, particularly regarding heterogeneous materials as is the case with natural stone.

When it comes to the size effect on stone, there have only been a few studies over the years that regarded its impact on flexural strength in natural stone, with one of them being made by Labuz and Biolzi (2007). They analyzed tensile and flexural strength measurements through various methods (fixed platens, rotating platens, and 4-point bending tests) in sandstone specimens, on the subject of strength and stability issues in relation to inhomogeneity and size effect in rock. From this work, it was concluded that among other factors, a sample's heterogeneity had a role in the stress field that influenced crack localization, crack propagation, and nominal strength observed, and that size effect changes were only noticeable when in presence of a stress gradient (Figure 5)

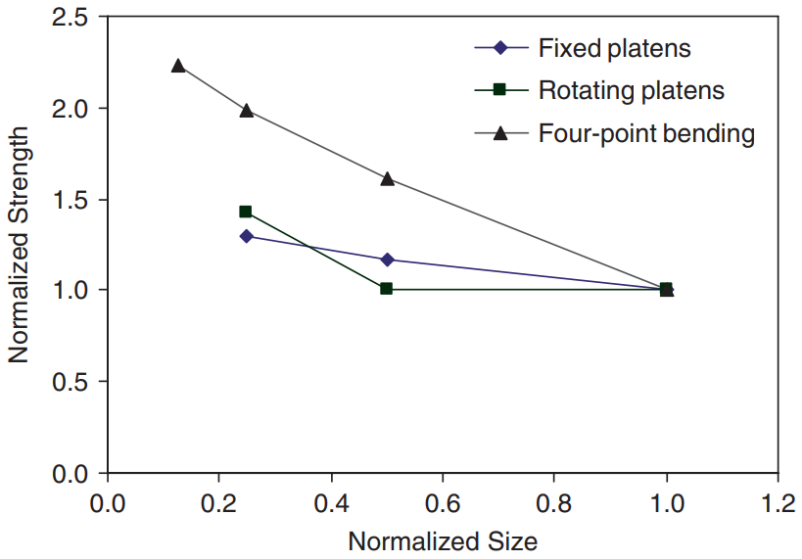

Figure 5 – Results from several uniaxial tensile and flexural tests (fixed/rotating platens and 4-point bending) of sandstone, with normalized measured values for sample size and flexural strength (adapted from Labuz & Biolzi, 2007).

Fernandes *et al.* (2010) compared 3-point and 4-point bending tests and their respective (and differing) sample dimensions, by applying Weibull's theory, in 5 different Portuguese limestones. This study confirmed that differences between flexural strength values measured between 3-point and 4-point bending tests, which employ different cross-section dimensions, could be explained through Weibull's strength scaling approach. However, this behavior didn't always occur with all limestones, something that was attributed to a structural difference between samples of the same rock. This, along with the work of Labuz and Biolzi (2007), makes it possible to assume that different stones, with different structural properties, do not always behave in a way that makes it possible to analyze size effects in stone as a whole, and that it's necessary to take into account their petrographic characteristics (Bellopede *et al.*, 2015).

In 2015, Bellopede *et al.* approached the subject of size effect in flexural strength's testing under a concentrated load, through analysis on data of 15 different types of stone in a wide variety of different sample sizes (including dimensions smaller than EN 12372 recommendations), to understand whether or not a variation in size, tied to the fact that marketed stone slabs could not be tested according to standardization due to a necessary minimum of 25mm of thickness, could be linked to a variation in flexural strength. From the obtained results, it was concluded that, in general, observed flexural strength variations in accordance to various specimens' thicknesses were negligible, such as the case of a sandstone (Sandstone S) which had the highest available number of samples with different thicknesses (Figure 2). In some particular cases, a low correlation between flexural strength and sample size was identified (Figure 6), as it seemingly followed Bažant's law, but it was considered too statistically inconsistent. This study also pointed towards intrinsic properties, such as porosity and mineral structure, and the uneven presence of fractures, voids and other defects, as the main causes behind the high level of dispersion in the flexural strength measurements, something that went along with the conclusions taken from previously mentioned works on this subject (Labuz and Biolzi, 2007; Fernandes *et al.*, 2010).

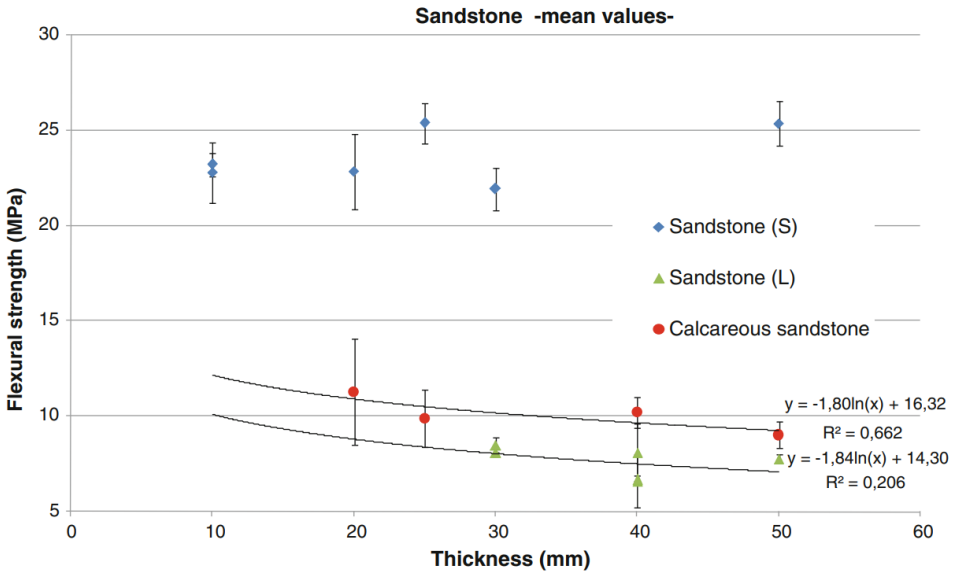

Figure 6 – Correlation between flexural strength values and specimen thickness for three different stones: Sandstone S, Sandstone L and Calcareous Sandstone (adapted from Bellopede et al., 2015).

The subject of size effect on flexural strength on natural stone would once again be approached by Marini *et al.* (2017), taking into consideration stone structure and heterogeneity, on four stones with anisotropic features (2 soapstones and 2 gneisses) and four with isotropic features (2 granites, 1 diorite and 1 marble). Once again, it was concluded that the effect of thickness on bending strength of the tested samples was relatively negligible (Figure 7). A statistical evaluation also indicated that characteristics such as anisotropy and a larger mean grain size contributed towards a larger spread in the measured flexural strength values. Finally, this work proposed that dimensions for the standardized testing of flexural strength should be reduced to 15 millimeters for fine-grained stones and 20 millimeters for coarse-grained stones.

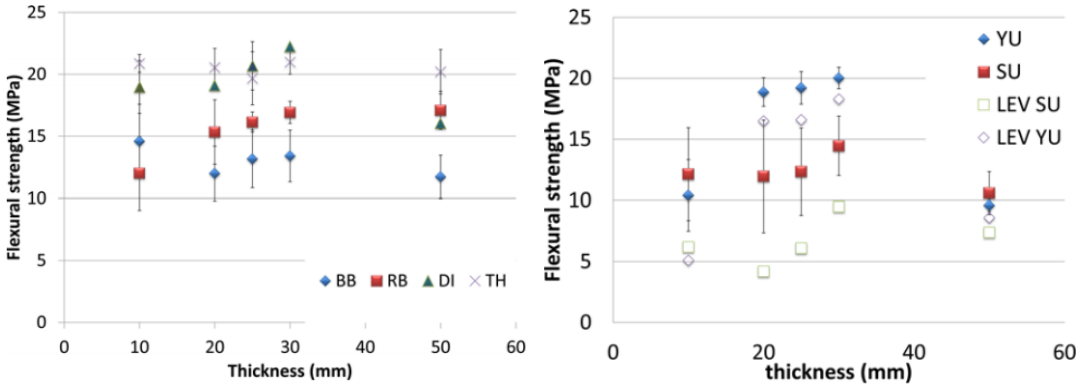

Figure 7 – Flexural strength as a function of thickness for stones with isotropic features (on the left) and some stones with anisotropic features (on the right) (adapted from Marini et al., 2017).

More recently, Fan *et al.* (2019) examined the bending properties of granites with a 3-point bending test, in samples that varied in either height or width, in a study of size effect on flexural strength of rock and the relationship between Brazilian splitting strength and bending strength. They concluded that the maximum load measured on the bending test was linearly proportional to the cross-section size

of the beam granite samples, including the height and width, and that, although the measured flexural strength varied slightly overall (Figure 8), it was not considered substantial enough, proportionately to the variations in both height and width.

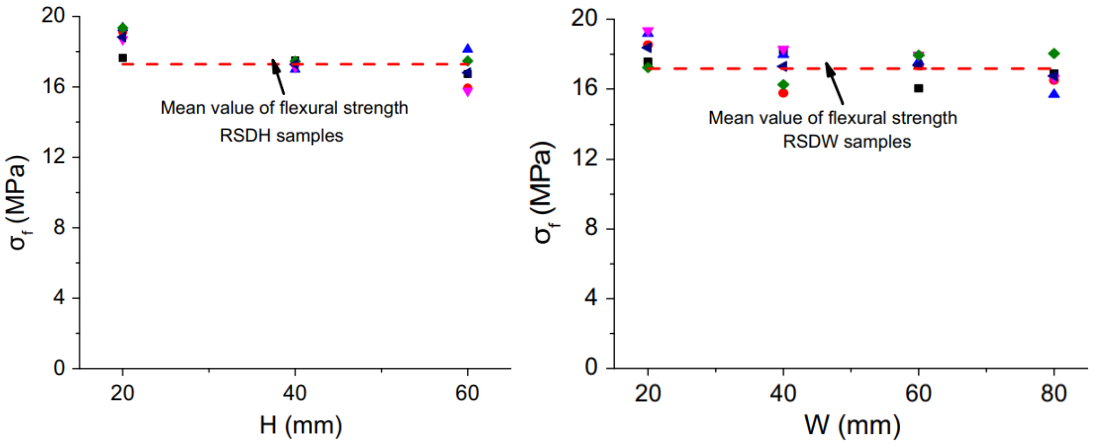

Figure 8 – Comparison between the measured flexural strength values against the variations in sample height (on the left) and sample width (on the right) (adapted form Fan et al., 2019).

3. Materials and Methods

To properly conduct a study on the size effects in flexural strength, a wide array of different natural stone test samples was acquired from a variety of Portuguese natural stone suppliers, which added to a total of 10 different rock types of Portuguese origin, with 2 types of granite samples, 2 types of marbles and 6 different types of limestone samples. All the granite and marble samples were provided by *SOCIMAR – Sociedade Industrial de Mármores, Lda.*, while in the case of the limestones, 3 types were provided by *FILSTONE – Comércio de Rochas, S.A.* while the other 3 types were provided by *AFONSTONE - Rochas Ornamentais, Lda.*

3.1. Natural Stone Samples

The set of tested granites was composed by the commercially named *Amarelo São Martinho*, designated as Granite AM in this work, a yellowish granite with a high degree of weathering and a medium to coarse grain size, and the *Cinzento Vimieiro*, designated as Granite CV, a granite of light grey color and a medium grain size, with a much lower degree of weathering relative to its counterpart.

In the case of marble samples, these were of *Ruivina Clara*, designated as Marble RC, a blueish-grey marble with some lighter veins, a medium to fine grain size, and of the *Estremoz Corrente*, designated as Marble EC, which differs from the *Ruivina Clara* due to its fine grain size and pearl white surface with pink and light brown colored veins.

In what concerns the limestones samples, these were of *FILSTONE Grey M*, designated in this study as Limestone GM, a light grey oolitic and bioclastic limestone with a fine to medium grain size, of *FILSTONE Beije MG*, designated as Limestone MG, a cream oolitic limestone, with a medium grain size and a slightly larger and more dense presence of bioclasts than the previous specimen, and of *FILSTONE Beije MMF*, designated as Limestone MMF, a fine grained and light cream-colored oolitic limestone, with a smaller and less dense composition of bioclasts than the GM and MG variants. The *Azul Valverde* is another of the limestones studied, designated as Limestone AV, a blueish-grey limestone with small patches of lighter color and a fine grain size, whereas the *Moca Creme*, designated as Limestone MC, is a cream-colored and heavily bioclastic limestone with fine to medium granularity, and the *Moleanos Macio*, designated as Limestone MM, is an oolitic limestone of a light cream color and slight bioclastic nature, with a fine grain size.

3.1.1. Geological Framework and General Application

In the case of the referred granites, Amarelo São Martinho originates from an outcrop of Monção's Granitic Massif, with the exploration in São Martinho, located in the district of Viana do Castelo, in the northwestern region of Portugal. This granite is considered to be from between the late period of the Hercynian orogeny, and the aftermath of it. The granite Cinzento Vimieiro, on the other

hand, is based around an extensive layer of granite, of around 40 km, elongated in the NNE-WSW direction, from the northern region of Alentejo, down to the district of Évora, where the exploration is located (Vimieiro). As in the previous case, this granite also originates from the same period, towards the end of the Hercynian orogeny. Both of these granites are recommended for interior and exterior cladding and flooring (IMGranit, ROP/LNEG).

For the marble stones tested, the marble Ruivina Clara originates from an exploration in Fonte da Moura, in the district of Évora, located in the southeastern end of the “marble triangle” of Estremoz, Borba and Vila-Viçosa, in the south-central region of Portugal. The geological age of this marble is considered to be between the Cambrian and the late Silurian periods. In terms of application, the Ruivina Clara is recommended for both indoors and outdoors, on walls and floors, and even in bathrooms, but it is not ideal for kitchen countertops (MARMOFOZ). The other marble in study, the Estremoz Corrente, is also explored in the same region, but in the SW flank of the previously mentioned “marble triangle”, located in the municipality of Estremoz, with a similar estimated age of in-between the Cambrian and superior Silurian periods. This marble can be utilized in most types of interior or exterior application (ROP/LNEG).

The limestone Azul Valverde originates from an outcrop of the Montejunto Formation, more precisely in the Estremenho Massif, located in the district of Santarém in the center region of Portugal. The outcrop extends in the EW direction for around 1 km and has a width of around 150 meters, between a fault in the northside (Mendiga fault) and a doleritic lode in the south, and the explored limestone is dated back to the Late Jurassic period, between the Oxfordian and the Kimmeridgian eras. The applications for the Azul Valverde range from several interior options, including flooring and wall cladding (ROP/LNEG). Similarly, the Moca Creme limestone also originates from the same Estremenho Massif, although its exploration is situated in Pé da Pedreira, whereas Azul Valverde is explored in Valverde, around 5 km northwest of the Moca Creme limestone exploration. This limestone is believed to belong to the Bathonian era of the Middle Jurassic period, and its application is usually reserved for interior cladding, facades or pavement with low circulation (Primeira Pedra). As for the limestone Moleanos Macio, it originates from the Moleanos Formation, with the exploration being located in Alcobaça, in the district of Leiria, on the central coastline area of Portugal. It’s presented as a long continuity along the western flank of the Candeeiros mountain range, with the dating of the limestone goes back to the Callovian era, of the Middle Jurassic period, and its applications involving wall cladding and flooring, for interiors, as well as stonemasonry (ROP/LNEG).

The limestones FILSTONE Grey M, Beije MG and Beije MMF all originate from an exploration in Casal Farto, also located in the district of Santarém, which is based on the Estremenho Massif as well, and more specifically from the Serra de Aire Formation. These limestones date back to the Bathonian Era of the Middle Jurassic Period, and their applications include mostly wall cladding, both interior and exterior, and interior flooring (ROP/LNEG).

3.1.2. Samples preparation

For each one of the 10 different types of stones, which were kindly offered, there were a total of 20 samples with varying sizes, for a grand total of 200 Portuguese natural stone samples to be studied. These natural stone samples were already cut to the necessary dimensions for this project, with the proportions between length, width and height defined by the standard EN 12372 (2006). Through this standard, the received specimen's dimensions, for the laboratory testing of flexural strength, were defined based on the following requirements:

1. Sample thickness h should be between 25 mm and 100 mm and should be greater than twice the size of the largest grain in the stone;
2. Sample total length L should be equal to six times the thickness;
3. Sample width b should be between 50 mm and three times the thickness (50 mm ≤ b ≤ 3h), and in no case should it be less than the thickness.

However, given the scope of this study, the very first requirement was superseded, as it was necessary to proceed with the behavior evaluation of the natural stone with thickness inferior to the minimum allowed through the EN 12372 (2006) standard for flexural strength testing. Given these restrictions, the sample's dimensions were divided by different values for thickness h, as it's the parameter utilized to define the total size of a sample, according to this standard. The chosen dimensions for the thickness were of 10 mm, 20 mm, 25 mm and 50 mm: the first two below the allowed values for sample thickness, and the latter two within regulation, including the thickness of 50 mm which is the one recommended by the EN 12372 (2006) standard. With the values for thickness defined, the values for sample length were automatically defined as well, as they're dependent on sample thickness h, and the sample width was defined at a constant 50 mm, a value within the standard's recommended, that was chosen due to constraints in the equipment utilized to determine flexural strength, which will be explained later on. Grouped by thickness, these were the final dimensions for the natural stone samples (Figure 9):

- Set 1: Length – 60 mm; Width – 50 mm; Height – 10 mm;
- Set 2: Length – 120 mm; Width – 50 mm; Height – 20 mm;
- Set 3: Length – 150 mm; Width – 50 mm; Height – 25 mm;
- Set 4: Length – 300 mm; Width – 50 mm; Height – 50 mm;

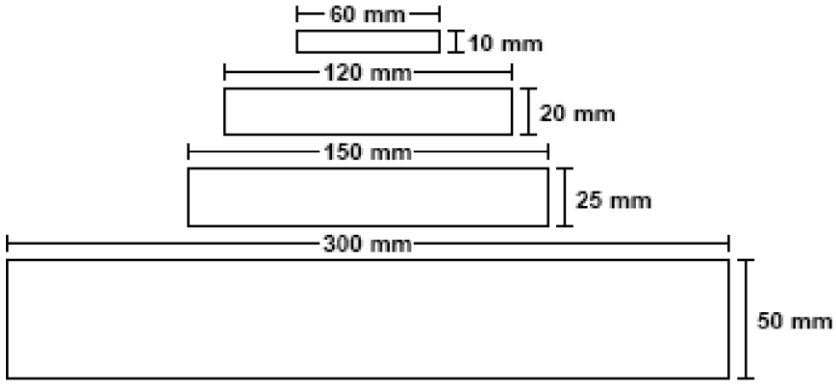

Figure 9 – Comparison of the profiles from the 4 chosen sample sizes, for natural stone testing of flexural strength, with thickness h (vertical) and length L (horizontal). For each of these, the equivalent width was of 50mm.

Given that there was a total of 20 samples per type of natural stone, the result were four sets of 5 rock samples of each of the aforementioned sizes per natural stone, for a grand total of 50 samples per size. However, an exception to these defined dimensions occurred with both granites, with the largest sample size of 300x50x50 mm, due to the provider being constricted to provide specimens with a maximum thickness of 30 mm, meaning that the largest sized set for the granite stones was 300x50x30 mm instead.

The received samples had smooth sawn surface finishes, and were then marked according to their rock type and an attributed number, from 1 to 20, from the smallest thickness set to the largest. This means that samples from each natural stone labeled 1 to 5 always refer to a thickness value of 10 mm and samples 15 to 20 always refer to the largest thickness value of either 50mm, or 30 mm in the case of granites specimens. Besides the number, the samples were also marked with the initials of the natural stone they represented, such as AM for *Amarelo São Martinho*, or EC for *Estremoz Corrente*. Limestone samples that were received from FILSTONE were already marked upon arrival, according to their designated grain size codename (MG, GM and MFF).

3.2. Testing workflow

In the following flowchart (Figure 10), it's possible to observe the general order in which the laboratory experiments were conducted, divided between the nature of properties being tested: basic petrographic macroscopic characterization, some physical and mechanical properties. Due to the nature of a flexural strength test, in which the sample is destroyed, it meant that every other type of test had to be done before it could happen, which meant that the realization of the mechanical testing was dependent on the completion and evaluation of every other type of sample testing. However, given that the tests for physical and petrographic properties were all non-destructive, it was possible to realize them in a different order whenever necessary. This was helpful due to the fact that some of the properties measured, such as porosity or water absorption, required passive testing, meaning their total duration was very large, but with a large amount of time between the necessary measuring, which in turn allowed

for other works to be done simultaneously. Still, in general, the testing order followed what's described on Figure 10.

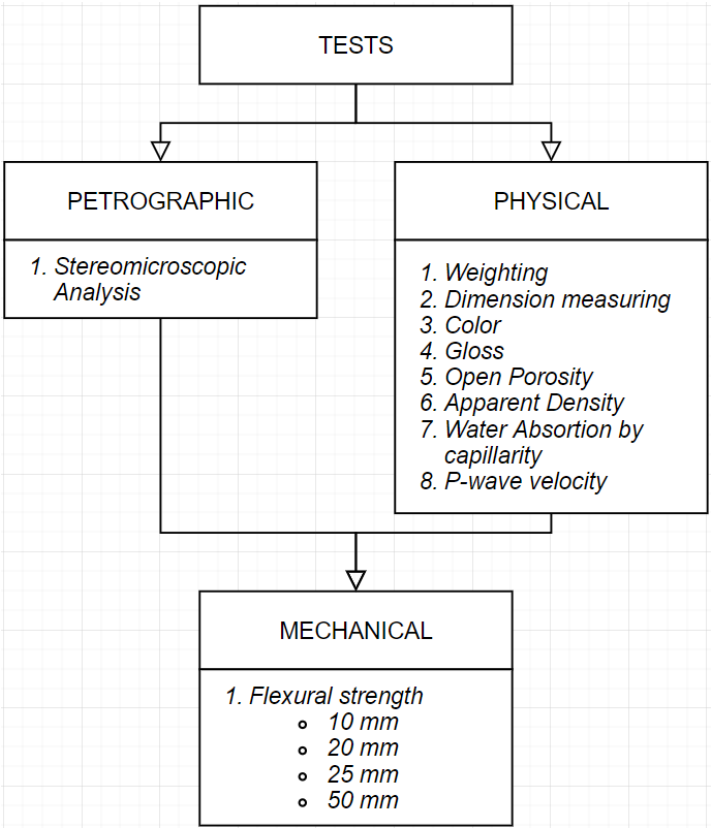

Figure 10 – Flowchart for all the designated tasks to be conducted throughout this project, separated between petrographic analysis, physical testing and finally, mechanical testing. Mechanical testing, due to its destructive nature, would only occur once the petrographic and physical tasks were completed.

3.3. Petrographic Analysis

3.3.1. Stereomicroscopic Analysis

The observation of the main petrographic characteristics of the received natural stone samples was done utilizing a stereomicroscope, an ISM-PM200S from *Insize* (Figure 11), and millimetric paper as a means of scale, as it allowed to give a general macro-analysis of the different sample's surfaces while having a capacity to observe properties like mineral composition, texture, grain size, fractures, color and overall weathering with higher precision, compared to the human eye. Due to its digital support, it also allowed to easily capture the observed details for posterior evaluation, as the analysis of properties such as size of largest grain and overall heterogeneity, which can be measured this way, plays an important role in studying size effect on flexural strength (Labuz and Biolzi, 2007; Bellopede *et al.*, 2015; Marini *et al.*, 2017).

Figure 11 – ISM-PM200S stereomicroscope, utilized in the petrographic analysis of the received natural stone samples.

3.4. Physical Properties

3.4.1. Weight and Size Measurements

The first step in the physical characterization of the natural stone samples involved the measurement of sample weight and dimensions, as these are the base properties necessary in order to have context in the evaluation of other parameters measured in the rest of the testing process (e. g. the determination of open porosity values is dependent on sample volume, P-wave propagation velocity is based on the relation between travel time and distance traveled on sample, etc.). Although the specific sample sizes were already described, there's still a degree of variation in these values, as the process of sawing the natural stone is susceptible to margins of error.

The measurements for dimension were taken with a digital caliper, (Figure 12), for dimensions that were bellow or around 150 mm, as that was the maximum length allowed by the digital caliper. This meant that all sample measurement of length, width and thickness could be measured through this method, with the exception of length in the larger 300x50x50 mm samples. For these samples, a ruler with a precision of 0.5 mm was used instead. The digital caliper measurements allowed to obtain values up to the thousandth of a millimeter, and for each instance of measuring a distance, the average of 4 different values was taken, usually from two opposing surfaces of the sample, in order to obtain a general value that was indicative of that sample's length/width/thickness.

Figure 12 – Application of the digital caliper in the measuring of width on Marble RC13 sample.

In the case of measuring sample dry mass (wd), a digital scale was used, a KERN EMB-V (Figure 13). Only natural stone samples with a thickness of up to 25 mm were weighed, as the largest category of size, of 300x50x50 or 300x50x30, were not subjected to physical testing that required the measurement of the original dry mass. This same digital scale would later be utilized on the determination of open porosity and apparent density, as well as in determining the water absorption through capillarity, in order to keep all weighing values throughout the project consistent, relative to each other.

Figure 13 – Digital scale KERN EMB-V, used in the dry weighing and other weighing measurements made throughout the physical testing phase.

3.4.2. Assessing Color and Gloss

Color is a visible physical property of an object, resulting from the observation of a part of the electromagnetic spectrum through the human eye (Tkalcic & Tasic, 2003). It is an important descriptive parameter, as it's usually one of the first characteristics detected, alongside shape, size or texture. In natural stones, color is a result of not only the color of its predominant mineral, but also the distribution, shape and size of its adjacent components (Wrinkler, 1997). Due to natural stone's role in modern architecture, where the aesthetic factor is a major component, color is often a criterion picked not only for choosing between a number of different rocks, but also for designating the natural stones themselves. However, despite being an important characteristic in the appearance of natural stones, its measurement is not a straightforward process, as the classification of color through human observation is subjective and often varies from individual to individual. Therefore, in order to attain an objective analysis of color, it's best to apply a mathematical model, or a color model, to describe it, such as the RGB, CMYK or CIE color models. In this study, the CIELAB color space was chosen, due to its widespread acceptance in scientific and industrial applications, as well as the ability to best describe color as observed through human vision (Tkalcic & Tasic, 2003; Hunt & Pointer, 2011; Sanmartín *et al.*, 2015), and the availability and inexpensiveness of the equipment required for its application.

The CIELAB color space is based on the CIE model for colorimetry, as an adaptation of the CIEXYZ color space. It's composed by three approximately uniform dimensions, which are defined by the L*, a* and b* coordinates. The L* coordinate represents the amount of lightness measured in an object, where white corresponds to a value of 100 and black to a value of 0. On the other hand, the a* and b* coordinates represent the chromatic colors, with a* measuring the amount of green (negative a* value) or red (positive a* value) colors and b* measuring the amount of blue (negative b* value) or yellow (positive b* value) colors. Every measured color is classified by a color point with coordinates L*, a* and b*, where null values on the a* and b* coordinates indicate a color on the grayscale.

For color measurements, a *PCE-CSM 1* handheld portable colorimeter (Figure 14) was used, from *PCE*, which allows to easily measure values in the CIELAB color space, with a D_{65} light source and an 8º incidence angle, while for calibration, a white *PCE-WTB-CSM 1-7* calibration disk was utilized. In order to measure a sample's color values, a total of 10 different values were taken from all of the surfaces of the sample, except when a surface was deemed not representative of the stone's natural color, as was the case for certain polished surfaces or surfaces that were written on. The *PCE-CSM 1* allow to automatically calculate the average values for CIELAB parameters, from all 10 measures taken for a single sample.

From the measurements made, the L*, a*, b* and C^*_{ab} values were taken and plotted against each other, with the results produced being 2 separate graphics that describe the stones color with L* as a product of C^*_{ab} (luminance versus chroma) and a* as a product of b* (green/red gradient versus blue/yellow gradient), per type of natural stone and independent of sample size.

Figure 14 – Measuring of color in the surface of a marble sample, using the handheld colorimeter PCE-CSM 1.

Another visible physical property that is often studied in the analysis of natural stone's appearance, related and evaluated alongside color, is gloss. Although historically it's not as studied as other visual properties of objects' surfaces, it has, since the 2000's, seen a renewal of interest in its perception, which re-emerged from research into other surface properties such as color and texture, with technological advances paving the way for new experimental techniques and measurements, according to Chadwick & Kentridge (2015). Gloss is a property whose characteristics are based on the geometrical distribution of the incident light on the stones surface and the subsequent transformations that take place upon reflection of such light (Hammond III & Nimeroff, 1950). These transformations are, like in the case of color, a product of properties like distribution, shape and size of the natural stone's minerals, hence the relationship between these two parameters. When it comes to the perception of gloss, Hunter (1937) describes that there are six different types: specular gloss, sheen, contrast gloss, absence-of-bloom gloss, distinctness-of-image gloss, and absence-of-surface-texture gloss. Of these six types, specular gloss is often the one evaluated in the study of ornamental rock, as it is related to surface roughness (Wang *et al.*, 2000).

In the case of the measurements of a sample surface's specular gloss, a gloss meter *PCE-IGM 100* from *PCE* was used. The value for gloss attributed to each sample was based on an average of 8 measurements taken from all 6 surfaces, except for the 60x50x10 mm samples in which all measures were taken on the 60x50 mm faces, due to the 10 mm faces being too small. No measures were taken on polished surfaces that were present in some sets of samples. As for the values obtained, only the

gloss values for a 60-degree incidence angle were taken into account, as it's the angle at which the gloss values better correlate with the actual surface appearance (Hunter, 1937; Hammond III & Nimeroff, 1950). As for the presentation of results, these were plotted with sample gloss value per set of samples, from the sets with 10 mm of thickness to the ones with 30/50 mm.

Figure 15 – Gloss Meter PCE-IGM 100 from PCE, utilized in the measuring of gloss on natural stone sample's surfaces.

3.4.3. Determination of apparent density and open porosity

The testing process for determining open porosity, and subsequently for apparent density, followed the EN 1936 (2006) standard, which, in the case of open porosity, described the method of complete water absorption in vacuum followed by a weighing of both saturated and submerged samples.

Before this testing process could begin, the stone samples had to first be dried in a stove with a temperature of 40ºC, to ensure they were properly dried, for a period of 24 hours. After this period, they were once again weighed in order to determine that the samples were at a point of constant mass, where the weight was equal to the previously measured dry mass (wd). This first step was particularly necessary for samples which had previously been through the water absorption test, as non-destructible physical testing order varied for different sets of samples. Afterwards, the samples had to cool down to ambient temperature for another 24 hours, before being placed inside a glass desiccator (Figure 17), the vacuum recipient in which the samples would be submerged in water. Inside, the samples sat for another 24 hours as a compressor (Figure 16) reduced the air pressure inside to 2 KPa, in order to remove all air trapped within the samples connected pore structure. The next step involved filling the desiccator with distilled water, until all samples were completely submerged, where they again saturated for another 24 hours, with the compressor still keeping the air pressure at 2 KPa. Following this period, the compressor was turned off and the lid from the vacuum recipient was opened, in order to let air pressure return to atmospheric levels. After another period of 24 hours, the samples were finally ready to be weighed.

Figure 16 – Desiccator used in the porosity testing (on the right) and the attached compressor (on the left) utilized to control air pressure inside the vacuum recipient.

The objective of this method was to completely saturate the open pore network of the samples, from which 2 values could be determined in the mass determination process: a saturated sample mass (w_s) and a submerged sample mass (w_h). With these, along with the already measured dry sample mass values (w_d), it's possible to determine the open porosity (p_o) from the following Equation 1:

$$p_o = \frac{w_s - w_d}{w_s - w_h} \qquad 1$$

The mass determination process for the saturated samples was relatively straightforward, using the *KERN EMB-V* digital scale to measure after the excess water was removed from the sample's surfaces. In the case of the submerged weight, however, it was necessary to set up a container with water with a supporting net which would support the sample inside. This supporting net would then be hung from a hook in the bottom of the digital scale and suspended inside the water container, in a way where the sample placed in it was completely submerged. After taring the digital scale, to account for the weight of the net, the submerged weight of a sample could then be taken. Due to size restrictions surrounding both the desiccator, water container and supporting net, and weight limits on the digital scale, this test was only on the sample sets with 10mm, 20mm and 25mm of thickness, leaving the larger 300x50x50 mm samples out.

For the apparent density (p_b), the resulting values were obtained from the same measurements performed on the determination of open porosity, although these were put though a different equation (Equation 2), with real water density (p_{rh}) considered to be 998 kg/m^3:

$$p_o = \frac{w_d}{w_s - w_h} \times p_{rh} \qquad 2$$

3.4.4. Determination of water absorption coefficient by capillarity

The procedure for the determination of water absorption in samples followed the standard EN 1925 (1999), which describes the method of surface water absorption in an ascending manner, whose measurements were made via the determination of sample mass after certain periods of time (Figure 17). Just as was described in the test process to determine open porosity, the natural stone samples were first dried in a stove with at 40ºC and then cooled down to ambient temperature, to the point where its measured mass was consistent with the known dry mass, due to some cases including samples for water absorption testing which were previously a part of tests for open porosity. Similarly, the same size constraints which were present on the open porosity testing applied to the water absorption test, with the set of 300x50x50 samples being left out to due to their large dimensions, but also the smallest set of 60x50x10, due to its volume, contact surface and height, which were deemed too small for the appropriate measurement of water absorption.

The assembly for the test of water absorption included a container with a tray, on which the samples would be placed, and enough water in it that allowed the samples, placed on the tray, to have a surface submerged around 3 mm deep (Figure 17). The same digital scale utilized previously, was also used the weighing the samples (Figure 18), while a wet piece of cloth was necessary to remove the excess water from the sample's surface and a chronometer or a similar device was used to time the mass measurements.

Figure 17 – Water absorption test, with the sample's surfaces on the supporting tray, 3 mm deep in water.

The period between mass determinations followed the scale presented in the standard with some changes, with each sample being weighed after 1, 3, 5, 10, 15, 30, 60, 120, 240, 360 and 1660 mins after being placed on the tray. If within this period of 24 hours the sample hadn't reached its maximum capacity for water absorption, through capillarity, then consequent measures were taken every 24 hours afterwards, until a constant mass value was achieved between 2 sequential measures.

Figure 18 – Weighing process in the water absorption test, where samples were first cleared of excess water in the contacting surface, before being weighed and place back into the container.

For this process, the water absorption was only measured in one direction: along its width; as the other possible placements would either have too large of a surface area compared to its height (being placed along its height) or too small of a surface area relative to its height (being place along its length). The results from this test are based on the values of the samples masses, relative to how long they had been exposed to the water, with a differential of mass between the measured and the original dry sample mass, relative to the surface area of contact with the water ($\Delta w/A$), per unit of time passed ($\sqrt{t}$), which translates to the following Equation 3 for a water absorption coefficient C ($g/m^2.\sqrt{s}$):

$$C = \frac{\Delta w}{A\sqrt{t}} \qquad 3$$

The final result is a graphic with the water mass relative to surface area plotted against the square root of time passed, in order to maintain a linear relationship between both variables, through which it's possible to define capillary water absorption coefficient, from the resulting curve for each sample.

3.4.5. Determination of P-wave propagation velocities

The testing process for determining P-wave propagation velocity was based on ISRM's (Aydin, 2013) suggested method for determining sound velocity by ultrasonic pulse transmission, utilizing a *Steinkamp Ultrasonic Tester BP-7* to measure the travel time of an ultrasonic longitudinal pulse, with a pair of exponential transducers (transmitter and a receiver) with 45 Hz frequencies, which were applied using the direct method (Figure 19).

Figure 19 – Ultrasonic testing equipment (Steinkamp Ultrasonic Tester BP-7) with the correspondent pair of exponential transducers, with 45 Hz frequencies.

Originally, the proposed methods by ISRM used to include three distinct approaches for determining sound velocity in a laboratory testing environment. The method described here, the pitch-catch approach, could be utilized in various transducer-pair configurations, depending on the accessibility of the sample's surfaces. However, the chosen direct-transmission arrangement (Figure 20) had the advantage over the others, since direction and length of the path, along which the waves traveled, were known with greater confidence, and any degree of damage or weathering of the sample's surfaces and edge (Aydin, 2013).

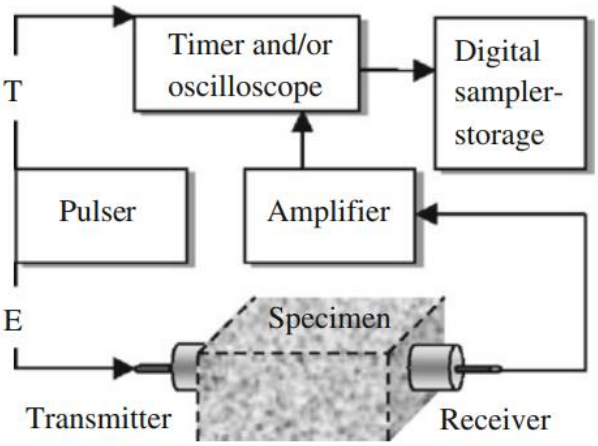

Figure 20 – The pitch-catch approach for measuring P-wave propagation velocities in natural stone samples, with the corresponding transmitter and receiver pair laid out in a direct-transmission arrangement.

To minimize discrepancies that could be obtained through this measurement method, the samples went first through a drying process, with the same characteristics as the one previously mentioned on the open porosity and water absorption tests, in a 40ºC stove for 24 hours, before cooling down for another day. In addition, a total of 6 points of contact for the transducers were marked on each sample tested, with 2 points per each of the 3 pairs of surfaces (Figure 21), for a measurement o P-wave propagation velocity across 3 different axes: along the length of a sample, along the width and along the height/thickness, in order to be able to characterize anisotropy in each sample. This way, of the two variables necessary to determine P-wave propagation velocity from this test, wave travel time

(t) and wave travel length (L), the latter was already known, as it corresponded with the previously measured sample dimensions. Wave travel time was obtained through the ultrasonic tester, and with these two values, of distance (L) and time difference (Δt), the P-wave propagation velocity (V_p) was calculated according to the following Equation 4:

$$V_p = \frac{L}{\Delta t} \qquad 4$$

Additionally, in order to describe the level of anisotropy in each sample, the Birch formula was applied, from the values of P-wave propagation velocity regarding the 3 different axes in which they were measured, with the lowest (V_{pmin}), highest (V_{pmax}), and median (V_{pmed}) velocity values measured for each natural stone sample, in order to obtain the Birch coefficient (k) (Birch, 1961) (Equation 5):

$$k = \left(\frac{V_{pmax} - V_{pmin}}{V_{pmed}}\right) \times 100 \qquad 5$$

Figure 21 – Example of the marking in the middle of the surfaces of RC Marble samples, on which the exponential transducers were placed in opposing faces, in order to carry out the measuring of P-wave travel time through each sample.

3.5. Determination of flexural strength

The testing process surrounding the determination of natural stone flexural strength followed the method described in the standard EN 12372 (2006), which describes the placement of the samples between two bottom supporting rollers and another top roller in the middle of the specimen's length, which then presses down, causing a concentrated bending load. As previously explained, the application of this standard was conditional, given that the tested specimen conditions went outside the minimum size restrictions. Nevertheless, the rest of the described testing process was followed accordingly. To determine the flexural strength (R_f), the main component needed is the load at which a sample fails

under bending stress (F), along with other measures such as distance between supporting rollers (l), and sample height (h) and width (b), described in Equation 6:

$$R_f = \frac{3Fl}{2bh^2} \quad (6)$$

However, not all natural stone samples were tested via the same equipment, due to regards with the magnitude of the bending load applied in the samples with sizes of 60x50x10 mm and of 300x50x50 mm being different. In order for them to rupture according to the testing standard, flexural strength tests were divided in 2 similar testing processes, varying mostly on the equipment utilized and subsequent *modus operandi* that was associated with them, as both processes achieved effectively the same in terms of results.

3.5.1. Flexural strength in samples with 10mm to 20mm thickness

The first of these testing methods was geared towards natural stone samples with dimensions of 60x50x10 mm and 120x50x20 mm (10 mm and 20 mm thickness), to which the used equipment, to apply the bending load, was a *DIGITAL TRITEST* from *ELE* (Figure 22). The reason for choosing this load equipment was based on the fact that these samples of smaller thickness required a lower loading rate, compared to what's standardly required for flexural strength tests, considering standardized dimensions. Along with the load frame equipment, a 100 (±0.02) kN load cell and its corresponding attachments, including software, were used to measure the applied loads over time, with a frequency of 100 Hz.

The testing process of flexural strength in the smaller samples, much like in the physical property testing phase, begun with the drying of samples on a stove at 40ºC, for a period of at least 24 hours, before letting the same samples return to ambient temperature. This was done to ensure that the samples were completely dry, as some had been previously subjected to open porosity and water absorption tests. To perform the 3-point bending test in this load frame, it was necessary to first mount metal supports which allowed for the precise placement of the rollers, on whom the sample would be placed onto, as well as the top roller that would press on the sample (Figure 23). For this, the metal pieces were cut beforehand to support the rollers, whose distances were based on the necessary roller distance, described by the standard EN 12372 as five times the thickness of the sample being tested.

Figure 22 – DIGITAL TRITEST, from ELE, and the respective loading cell on top, utilized in the determination of sample failure load in natural stone samples with 10 mm and 20 mm thickness.

Markings for roller placements on each sample were made, considering that the upper roller corresponded to the point at the middle of the sample's length, for the upper roller, and the two other points, which were distanced by five times the height/thickness of the sample, corresponded to the two bottom rollers. For any 60x50x10 mm sample, this distance was 50 mm or 25mm to the left/right of the middle point (Figure 23), while for the 120x50x20 mm samples it was a 100 mm distance, or 50mm to the left/right of the middle point.

To guarantee a stress rate of 0.25 MPa/s and considering the used load frame only considered strain rate control, the understanding the relation between stress rate and strain rate was mandatory. To do this, several dummy tests on spare samples from the received natural stones, were then performed to assess the stress rate for each for each considered rock type (granites, marbles and limestones).

For this assessment, a formula from the EN 12372 standard (Equation 7) was used to relate the stress rate in MPa/s (a) with a loading rate (V) in N/s, from distances such as width (b), height/ thickness (h) and distance between rollers (l):

$$V = \frac{3abh^2}{3l} \qquad 7$$

Figure 23 –Setup for the flexural strength testing on the DIGITAL TRITEST soil press, for a 60x50x10 mm RC Marble sample, with two supporting rollers separated at a distance equivalent of 5 times the samples thickness, and a pressing roller in the middle.

The value for loading rate (V) was obtained directly from the dummy testing of spare samples, simply measuring the growth rate of the weight being applied on each sample, which was easily observable from the loading cell's software. Through the results obtained from these dummy tests, it was then possible to approximate the relationship between deformability rate (mm/min) and loading rate (N/s), and subsequently with load rate (MPa/s), to a linear function, and subsequently figure out the necessary mm/min that would equate to a load rate of 0,25 MPa, for each of the three rock types studied.

3.5.2. Flexural strength in samples with 25mm to 50mm thickness

For the second stage in determining flexural strength in the natural stone samples, the process was relatively more straightforward, as a *FORM-TEST LEHRSYSTEME 506/1000/200 D* compression and bending hydraulic press (Figure 24) was utilized to conduct the tests on the larger samples (150x50x25 mm, 300x50x30 mm and 300x50x50 mm). Unlike the low-capacity load frame, the hydraulic press was designed for this type of test, and allowed the direct input of the loading rate, in N/s. For each set of sample size, this value was calculated using the same formula, from the EN 12372 standard, meaning that for each sample's size, there would be a different value for loading rate. In general, given the standard dimensions for the samples being tested, the following values were utilized for the loading rate setting:

- 150x50x25 mm samples: 41.67 N/s
- 300x50x30 mm samples: 50.00 N/s
- 300x50x50 mm samples: 83.33 N/s

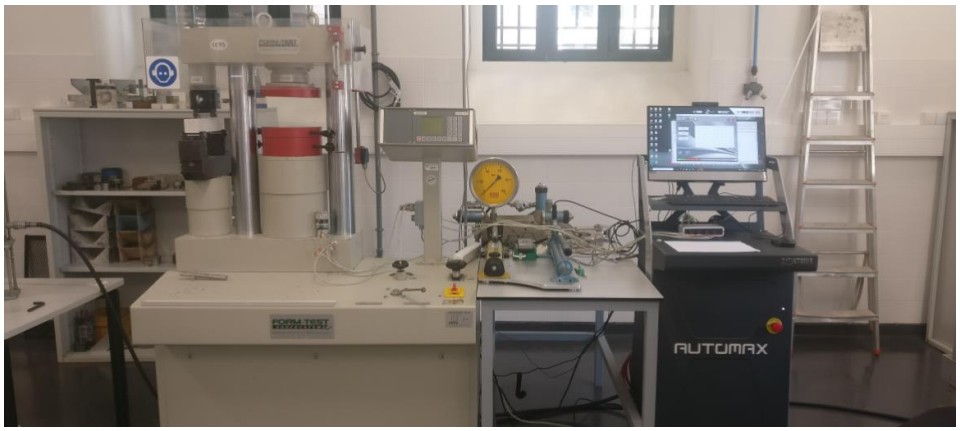

Figure 24 – Hydraulic press FORM-TEST LEHRSYSTEME 506/1000/200 D, a compression and bending testing machine which was used to measure the sample failure load.

The supporting rollers, where the natural stone samples were placed, were set in the desired distance in relation to the central roller, as the hydraulic press was naturally setup for this testing process (Figure 25). For the 150x50x25 mm samples, the distance between supporting roller was of 125mm, or 62.5 mm from the middle of the sample, while for the 300x50x30 samples, referring to granites only, the distance between supporting roller was 150 mm, or 75 mm from the center. Finally for the larger 300x50x50 samples, these distances were of 250 mm and 125 mm respectively. These distances were also marked on the samples, in order to correctly align them during the testing process. It terms of the placing of samples on the bending test setup, it's worth noting that the *FORM-TEST LEHRSYSTEME 506/1000/200 D* hydraulic press had a limit of 50 mm for the width of a sample being tested in the bending test part, which as mentioned when addressing sample specifications, meant that samples were to all have 50 mm of width, as this value is also the minimum required in the EN 12372 standard.

Figure 25 – Placement of a 300x50x50 sample on the FORM-TEST LEHRSYSTEME 506/1000/200 D hydraulic press, in which it was possible to set the desired distance, for the bottom rollers, thanks to its integrated ruler.

Once all results for flexural strength (R_f) were obtained, from the 2 described processes, the shortest distance between one of the two bottom supporting rollers and the resulting fracture (l_{fs}), from the test, was measured, in order to proceed with a correction for failure points which are offset from the

middle of the sample, according to the draft for flexural strength standard prEN 12372 (2021). From this draft, the corrected flexural strength values were then recalculated using the following formula:

$$R_f = \frac{3Fl_{fs}}{bh^2} \qquad 8$$

With both the original and the corrected flexural strength results obtained, a could graph could then be presented with both, with these values relative to sample thickness (which dictates the samples' overall dimensions) and per natural stone type, as a means to observe the quality of tests sample fracturing and to, through only the corrected values of flexural strength, analyze the relationship, in each of the natural stones tested, between sample size and the flexural strength.

3.5.3. Principal Component Analysis

Finally, in order to better help the understanding of the relationship between several of the parameters tested, through the previous mentioned methods, a principal component analysis (PCA) was then conducted, through the *RStudio* software, for each of the natural stones under study, in order to describe the variation behaviors of the different parameters in a smaller number of principal components. This process resulted in the construction of biplots for each of the natural stones, through which it was possible to observe how variation between some of the different parameters tested or measured, such as flexural strength, open porosity or sample dimensions, was positively, inversely, or not at all correlated, as well as which of these had more weight in overall variations, particularly from the point of view of the flexural strength results.

4. Results and Discussion

Given the methodology presented earlier, this section is be based around the results obtained through it, with a focus on interpreting each property individually, and then later attempting to understand their relationship with the results of flexural strength variation by sample size obtained, starting with the petrographic analysis and visually descriptive properties, and then moving into the physical properties of open porosity, apparent density, water absorption, P-wave propagation velocity and the corresponding Birch coefficient, before finally addressing the resulting values flexural strength test and the principal component analysis. This section is also be separated in three subsections, for the results obtained for granite, marble and limestone samples, in order to facilitate the process of understanding the correlations between different properties.

4.1. Results for Granite samples

4.1.1. Stereomicroscopic Analysis

As described in section 3.1, the Granite AM samples present a yellowish color, with a phaneritic texture, with a medium to coarse grain size and an intermediate degree of weathering, which is related to the presence of microfracturing in the samples studied. Upon closer inspection of the granite's surface (Figure 26), it's possible to observe that Granite AM samples were composed of mostly feldspar and quartz, with a high presence of both biotite and muscovite micas, while showing trace amounts of what appeared to be hornblende as well. The minerals of quartz, and in some cases biotite and muscovite, were observed to reach dimensions up to 7 mm of length, however most biotite and muscovite minerals measured around 2.5 mm in length.

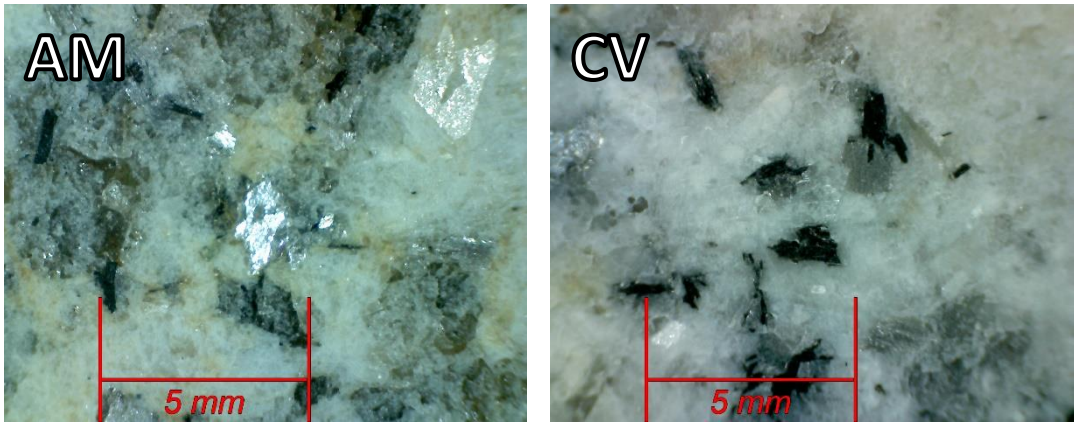

Figure 26 – Examples from the stereomicroscopic observation of the surfaces of Granites AM (left) and Granite CV (right), taken from samples AM2 and CV2 respectively.

In the case of the Granite CV, a light gray granite with a medium grain size, its texture appeared to have a slightly more porphyritic tendency when compared to the Granite AM, however its crystals appeared smaller in comparison to its counterpart. Stereomicroscopic observation, presented in Figure 27 as well, showed a composition of mostly feldspar with quartz, with a lesser presence of biotite and

to a lesser extent muscovite, in relation to the previously mentioned granite. The quartz grains, present as scattered gray quartz nodules, presented dimensions of around 3 mm in diameter, while the mica minerals measured around 1.5 mm. Overall, this granite presented a less altered state than what was observed in the Granite AM samples, with almost no noticeable amounts of fracturing or weathering in any of its sample's core mass.

4.1.2. Gloss and Color

Following the procedures described in section 3.4.2, for the granite samples, results from the measurements of the 4 color parameters (L*, a*, b* and C^*_{ab}) seem to indicate that a difference is present between Granite AM and Granite CV samples, something that's most likely associated with the disparity among the weathering degree of these two granite types. In Figure 27, which describes the relationship between the green/red coordinate (a*) and the blue/yellow coordinate (b*) values, it's possible to observe that the Granite AM displays, relatively, a much higher value for the b* parameter, with an average value of 10.13, and a slightly higher value for the a* parameter, with an average of 1.82, which indicates a strong tendency for the surface of these samples to be colored towards the yellow and slightly towards the red. On the other hand, the Granite CV samples present values with more proximity to 0 on both axes, indicative of its grey/white coloring, with average values of a* and b* of -0.08 and 1.68 respectively.

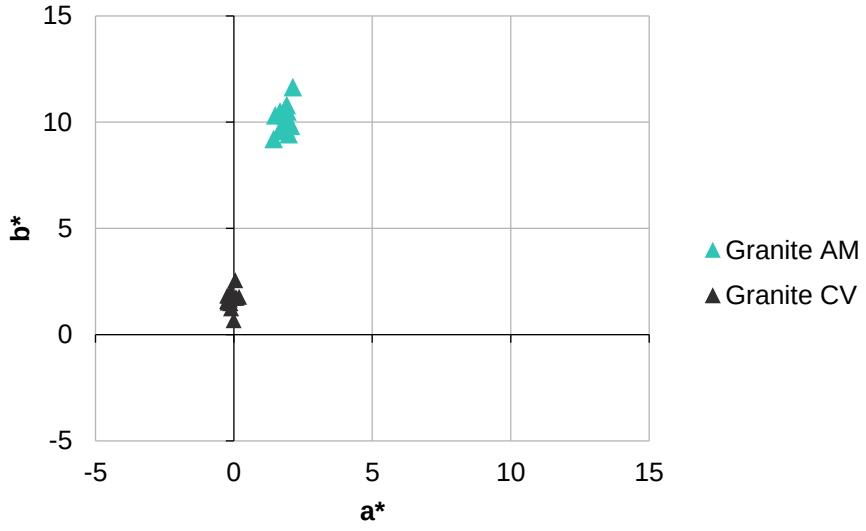

Figure 27 – Comparison between Granites' AM and CV sample results obtained for a (green/red color gradient) and b* (blue/yellow color gradient) parameters.*

As a consequence of the presented a* and b* parameters obtained for Granite AM and Granite CV, the resulting values for the chroma value (C^*_{ab}) also presented a much higher value for the Granite AM, as this parameter is directly correlated with the a* and b* coordinates, presenting an average of 10.30, while in the case of the Granite CV this value remained relatively low, at an average of 1.72 (Figure 28).

The luminosity values of L*, however, were similar for both granite types, as their each's samples averaged values for this coordinate of around 75. It's also possible to observe that the Granite AM samples tended to display higher variability in both L* and C^*_{ab} values, with respective standard deviations of 2.08 and 0.63, compared to what was obtained for Granite CV samples, which had a standard deviation of 1.38 for the L* coordinate and 0.38 for C^*_{ab}. Taking into consideration the other types of natural stone studied, these values tend to be on the high end, particularly the dispersion in lightness, which is a direct result of the heterogeneity seen in the granites' surfaces.

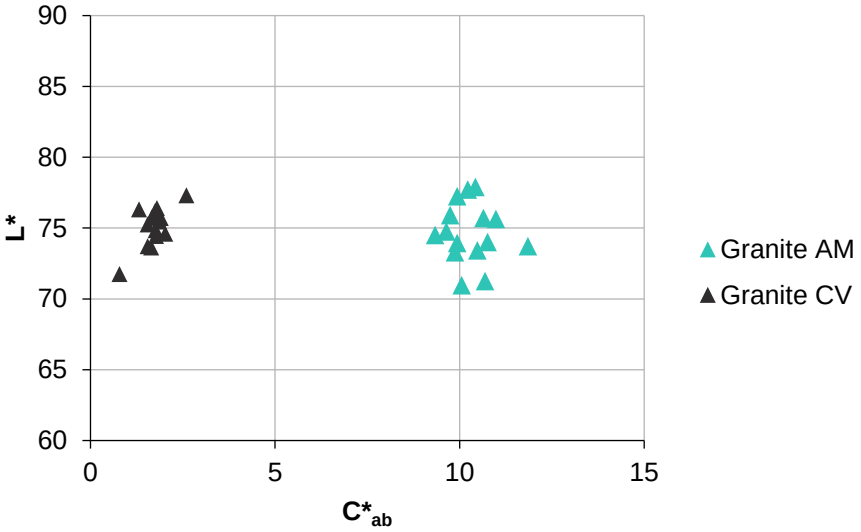

Figure 28 – Comparison between Granites' AM and CV sample results obtained for L (luminosity parameter) and C^*_{ab} (chroma gradient) values.*

For the result obtained in the determination of specular gloss (Figure 29), there is an easily observable difference between the Granite AM and Granite CV sample values. The former presents an average gloss value of 1.36, while the latter an average of 1.93, a difference that's directly related to the difference in the degree of natural weathering, as previously observed between these granites.

Besides the variation between natural stone type, no particular variation was observed in between the 3 sets of sample sizes tested, supporting the idea that all of them presented a similar surface finish, as standard deviation values for gloss were just 0.07 and 0.14 for granites AM and CV respectively.

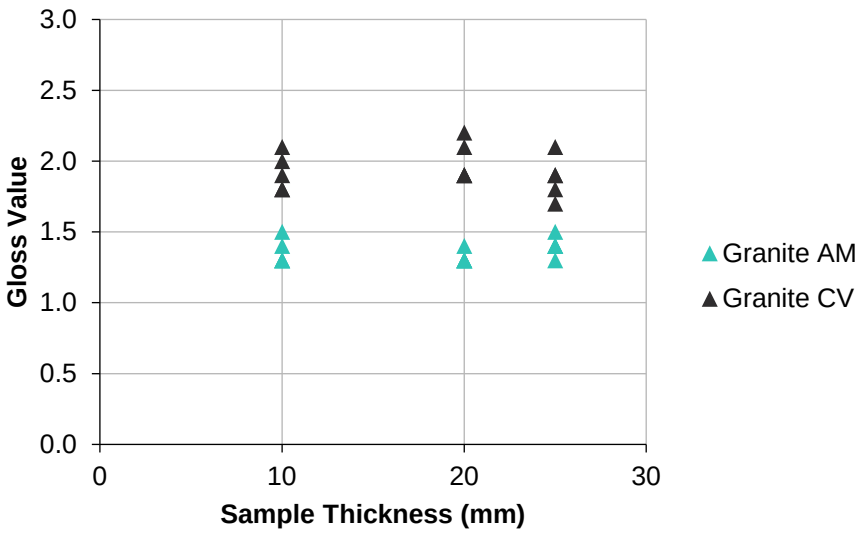

Figure 29 – Comparison between Granites' AM and CV sample results obtained for gloss values in relation to the different sets of sample sizes.

4.1.3. Apparent density and Open porosity

In the results obtained from the determination of open porosity described in section 3.4.3 (Figure 30, Table 1) the Granite AM displayed an average percentage twice as high as the healthier Granite CV, averaging 2.39% across all 3 sample sizes tested, with the highest percentage, of 2.48%, recorded on a 10 mm thick sample and the lowest, of 2.32%, on a 20 mm thick sample. The results for open porosity on this granite's samples are relatively consistent, regarding any size variation. On the Granite CV, however, a very slight decrease in open porosity percentage can be observed, as sample size increases.

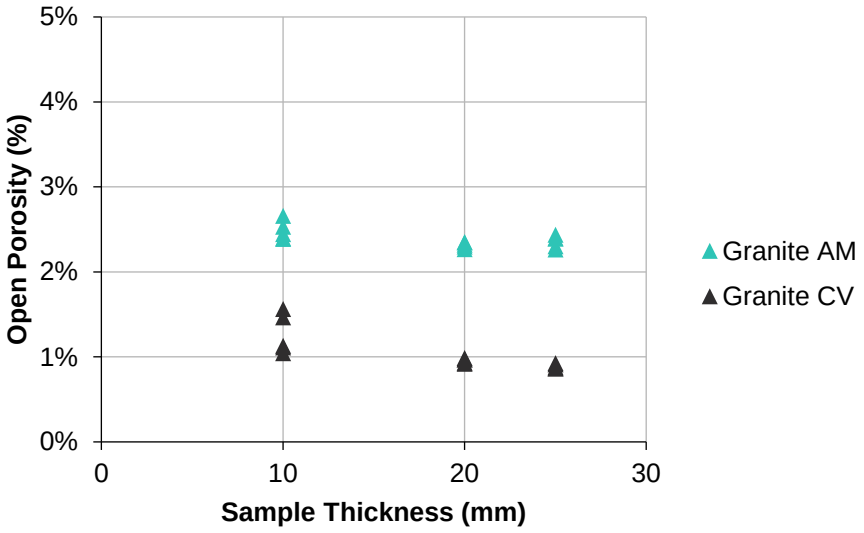

Figure 30 – Comparison between Granites' AM and CV sample results obtained for open porosity percentages and sample dimension (mm).

Table 1 – Average open porosity results for Granite AM and Granite CV samples of sizes with 10 mm, 20 mm and 25 mm thickness.

	Average open porosity (%)		
	10mm	20mm	25mm
Granite AM	2.48 ± 0.11	2.32 ± 0.03	2.36 ± 0.07
Granite CV	1.26 ± 0.23	0.95 ± 0.03	0.89 ± 0.03

The average percentage for the 10 mm, 20 mm and 25 mm thick samples were of 1.26%, 0.95% and 0.89% respectively, indicative of this decrease, but it's worth noting that for the 10 mm samples, samples CV1 and CV3 stood out from the other three, with values of 1.56% and 1.47% respectively, while the rest of the 10 mm Granite CV samples averaged 1.09% with a low standard deviation, of just 0.05%.

In terms of the calculated apparent density, from Equation 2, the behavior of the results obtained (Figure 31) mirrors those of the open porosity determination, with the Granite CV samples averaging a higher value compared to their counterpart, of 2617.05 kg/m^3, with a peak value of 2636.56v kg/m^3 and a minimum of 2604.83 kg/m^3, forming a standard deviation of 7.48 kg/m^3 from the average. It's worth noting that the CV1 and CV3 samples mentioned earlier also presented a lower value compared to the other 10 mm samples of Granite CV. As density and porosity are inversely related, the previous slight decrease observed, due to size effect, manifests itself as a slight increase in apparent density, whereas in the case of Granite AM samples, there continues to be no variation discernable from the different sample dimensions tested, which averaged 2580.14 kg/m^3 overall of apparent density.

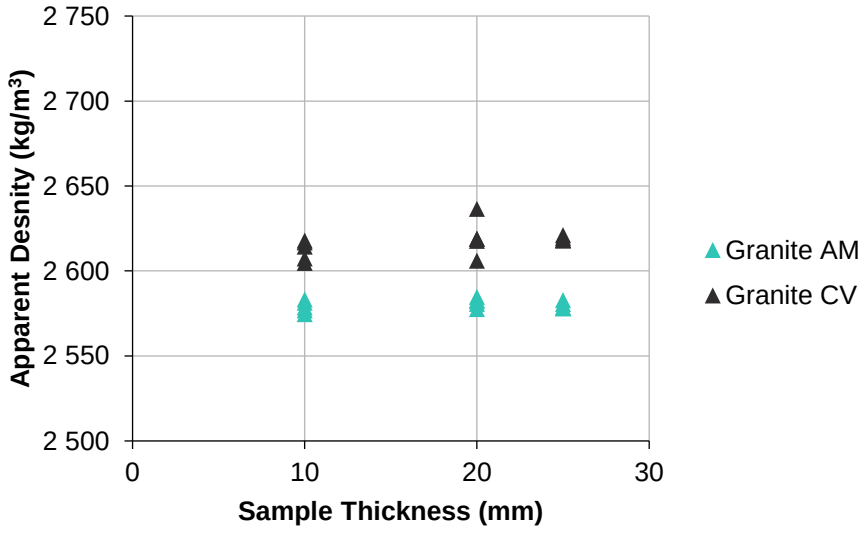

Figure 31 – Comparison between Granites' AM and CV sample results obtained for apparent density (kg/m^3) and sample dimension (mm).

4.1.4. Water absorption coefficient by capillarity

From the methods described in section 3.4.4, for water absorption coefficient determination, two separate graphs for granite stones were obtained for the Granite AM samples and the Granite CV samples (Figure 32, Table 2). In the former, the two different sized sets of samples present an identical water absorption curve, with a fast absorption rate which quickly reached its peak after just 2 hours, or 120 $\sqrt{s}$. The first phase of the curve, whose slope is equivalent to the water absorption rate, has a linear approximation to an average of 12.27 g/m^2.s^{½}, for the 20 mm thick samples, and 12.83 g/m^2.s^{½}, for the 25 mm thick samples. The estimated linear growth of each individual sample has an approximation accuracy of between 99.45% and 99.97%, the minimum and maximum respectively, to the values measured in the test.

Table 2 – Average water absorption coefficients for Granite AM and Granite CV samples of sizes with 20 mm and 25 mm thickness.

Water Absorption Results in 20 mm thick samples			
	Average Coefficient	Standard Deviation	Average R² (%)
Granite AM	12.27	0.50	99.76%
Granite CV	1.02	0.03	96.54%
Water Absorption Results in 25 mm thick samples			
	Average Coefficient	Standard Deviation	Average R² (%)
Granite AM	12.83	0.70	99.90%
Granite CV	1.15	0.05	99.31%

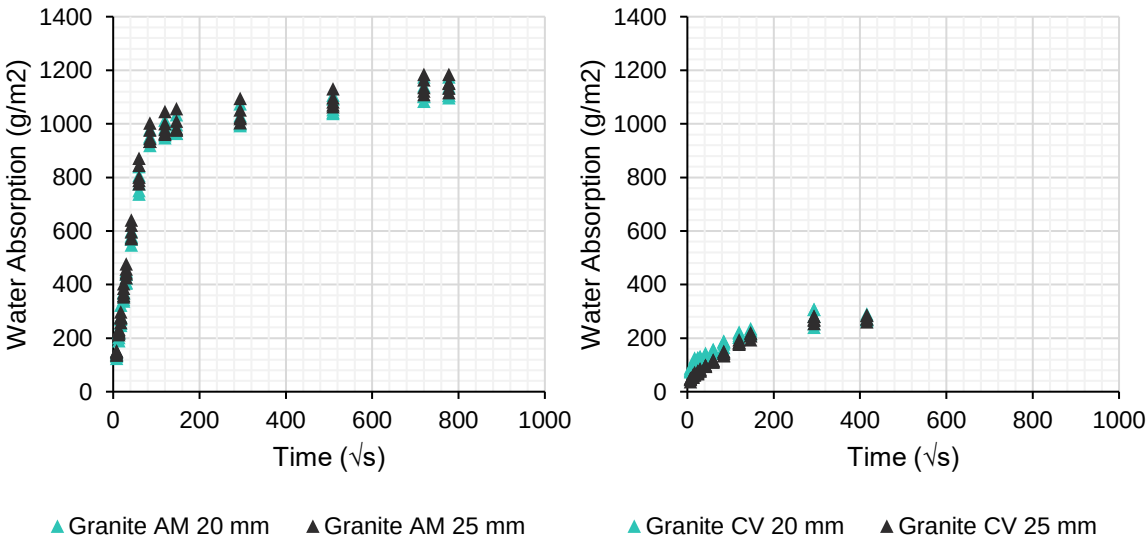

Figure 32 – Comparison between sample sizes' (of 20 mm and 25 mm thickness) and results obtained for water absorption (g/m^2), from Granite AM (left) and Granite CV (right) samples.

In the case of water absorption in the Granite CV samples, there is a much lower volume of water absorbed, which is a product the fact that this granite's samples have a lower open porosity on average, relative to samples of Granite AM. It also has a lower rate of absorption, maxing out at the 24

hour mark (293.94 $\sqrt{s}$), whose determination resulted in average values of 1.02 g/m^2.s^{½} in 20 mm thick samples and 1.15 g/m^2.s^{½} in 25 mm thick samples, for the predicted water absorption coefficient.

However, the general approximation of this estimation wasn't as high as in the previous granite, with the 20 mm and 25 mm samples averaging an accuracy of 96.54% and 99.31% respectively, which could be due to the fact that the smaller growth values of absorbed water, which are more notable in the first few measures, were too small to be accurately measured with a digital scale which only went down to the centigram.

4.1.5. P-wave propagation velocities

Following the determination of P-wave propagation velocity, described in section 3.4.5, the obtained values were divided in two different scatter plots, for each of the granites tested (Figure 33). For the samples of Granite AM, the overall P-wave propagation velocities measured were by far the lowest among all the natural stones tested, between 2600.52 m/s and exactly 3000.00 m/s. Among all three measurement directions, it's possible to observe a decrease of 12.31% in average P-wave propagation velocity as sample size increases from 10 mm, to 20 mm and 25 mm samples, with decreasing average velocities in all axes of respectively 2889.26 m/s, 2690.06 m/s and 2533.43 m/s. The exception to this behavior is in the larger samples, of 30 mm thickness, which have an average P-wave propagation velocity of 2715.14 m/s.

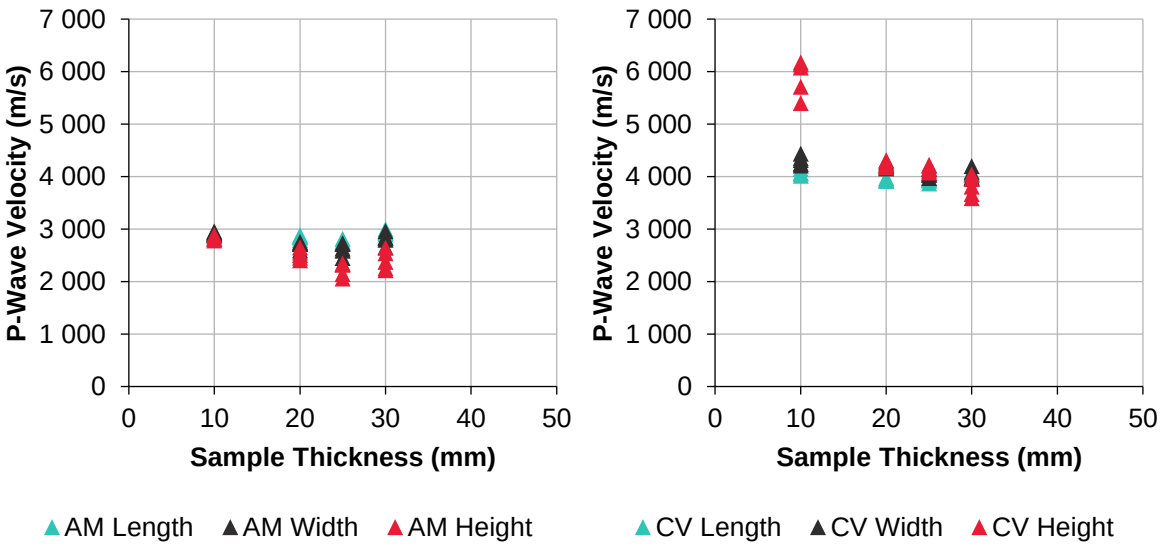

Figure 33 – Comparison between sample sizes' (from 10 mm to 30 mm thickness) and results obtained for P-wave propagation velocity (m/s), from Granite AM (left) and Granite CV (right) samples.

In terms of the relationship between the different measured directions, the average Birch coefficient, and subsequently the assumed anisotropy, also increased as sample size increased, with average values for the coefficient of 3.13%, for the 10 mm thick samples, increasing to an average of

19.35% on the 25 mm and 30 mm thick samples, where, generally, the values alongside sample length have the higher P-wave propagation velocity.

The results for the samples of Granite CV showed a similar decrease in P-wave propagation velocity as sample size increased, however, this pattern was exacerbated in the values of P-wave propagation velocity measured along the height of the samples, with an average value of 5901.10 m/s. This is likely a result of a clash between the 10 mm distance and the previously observed large grain size of the granite, as measurements for other directions with a higher distance are placed around the 4000 m/s mark instead.

Otherwise, the average velocities obtained of 4132.75 m/s, 4048.03 m/s and 3972.39 m/s (for 20 mm, 25 mm and 30 mm sample sets) describe a consistent decrease of 5.64% in P-wave propagation velocity, which Is not as accentuated as the observed decrease in the Granites AM samples. The anisotropy observed in the Birch Coefficient was much higher the 10 mm thick samples, with an average of 37.49%, while in the rest of the sample sizes it was not as emphasized, with values barely going above the 5% mark, a product of the variations observed in the P-wave measurements parallel to sample height.

4.1.6. Flexural strength

Following the determination of flexural strength on the granite samples, described in section 3.5, the obtained results were displayed on a graph relating bending strength and sample size, by thickness, for each tested rock type (Figure 34). In the results displayed for the Granite AM samples, it's possible to observe a slight decrease in a sample's flexural strength as sample size increases. From 10 mm to 30 mm thick samples, the average flexural strength decreases from 6.58 MPa to 4.93 MPa, with an average standard deviation per sample size of just 0.50 MPa. This decrease can be defined through a linear regression with a slope of -0.09 and coefficient of determination of 61.73%.

The sample dimensions within the EN 12372 standard, of 25 mm and 30 mm thickness, had the lowest measured value, of just 4.57 MPa, while the smallest samples of just 10 mm thickness had the highest, of 7.55 MPa. The overall flexural strength values obtained from this test were on the low end for a natural stone, which is likely a result of this rock's weathered condition.

In Granite CV samples' results, there is a higher overall dispersion in the values obtained, with standard deviations ranging from 0.80 MPa, in the 25 mm thick samples, to 1.76 MPa, in the samples of 10 mm thickness. This granite also presents higher values of flexural strength, with an overall average of 16.33 MPa, almost 3 times the strength observed on the Granite AM samples.

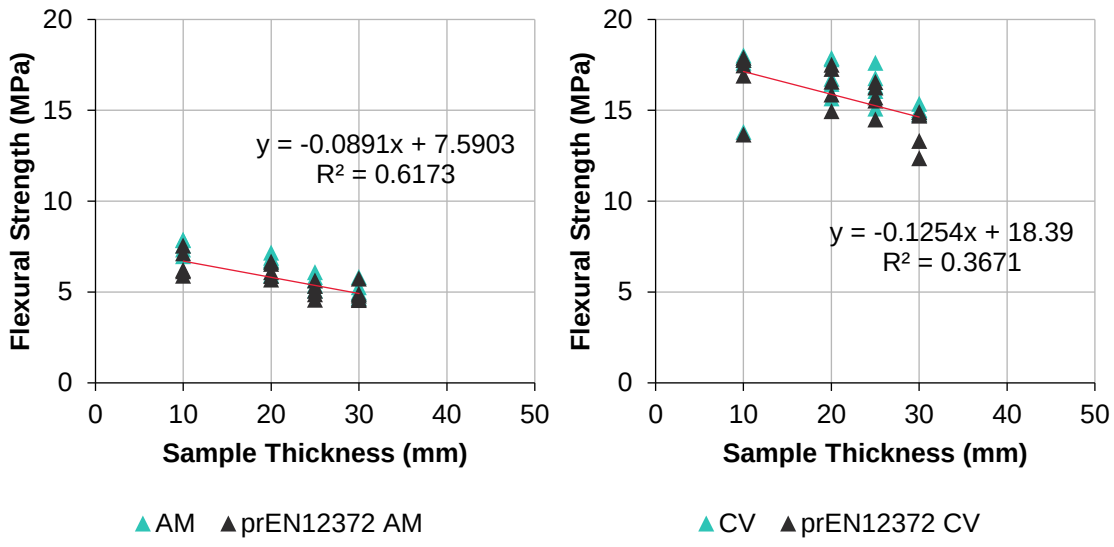

Figure 34 – Comparison between sample sizes' (from 10 mm to 30 mm thickness) and flexural strength results (MPa), obtained for Granite AM (left) and Granite CV (right) samples.

The size effect on flexural strength for the Granite CV is not as concise as seen in its counterpart, mostly due to a larger dispersion of results, but the decreasing behavior is still present, as the average flexural strength per sample size falls a total of 16.36% from 16.75 MPa, on the smaller 10 mm samples, to 14.01 MPa, on the 30 mm set. This is also while taking into account the measured value from sample CV2, of only 13.81 MPa, which could feasibly be considered as an outlier compared to the rest of the values obtained in the 10 mm range. An approximation of the decrease observed to a linear regression shows a higher slope of -0.13, marking a larger decrease in flexural strength from samples size increase, but with a much lower coefficient of determination, of just 36.71%, which is natural given the higher dispersion presented in the results.

In general, for all granites tested there's a tenuous indication of sample size affecting the measured flexural strength, and although this decrease can be confirmed for the Granite AM samples, for the Granite CV, a concrete observation of this behavior is marred by a high dispersion level in the values measured, with any approximation resulting in a relatively low coefficient of determination. Still, in relation to the minimum requirements regarding test sample dimensions (Table 3), of 25 mm thickness according to the EN 12372 standard, the average flexural strength results obtained from 10 mm and 20 mm thick samples are above the required sample size, particularly for the Granite AM.

Table 3 – Comparison between average flexural strength results for Granite AM and Granite CV samples of sizes with 10 mm, 20 mm and 30 mm thickness, with samples of 25 mm thickness, the minimum required.

	Average flexural strength (MPa)				*Ratio of average flexural strengths*		
	10mm	20mm	25mm	50mm	10/25mm	20/25mm	30/25mm
Granite AM	6.58 ± 0.71	6.17 ± 0.42	5.1 ± 0.41	4.93 ± 0.47	**1.29**	**1.21**	0.97
Granite CV	16.75 ± 1.76	16.44 ± 1.05	15.71 ± 0.80	14.01 ± 1.12	**1.07**	**1.05**	**0.89**

4.1.7. Principal Component Analysis in granite samples

To better understand how other parameters might be related to the variation of flexural strength in samples of different dimensions, for the granites tested, a principal component analysis (PCA), was conducted, using the following data obtained from the tests and measurements previously analyzed: flexural strength (MPa), sample thickness (mm), P-wave propagation velocity in the direction of length, width and height (m/s), the Birch coefficient (%) and open porosity (%). These were chosen to include the largest array of parameters possible while being able to keep the most possible sets of sample sizes, which in this case included the 10 mm, 20 mm and 25 mm thick samples.

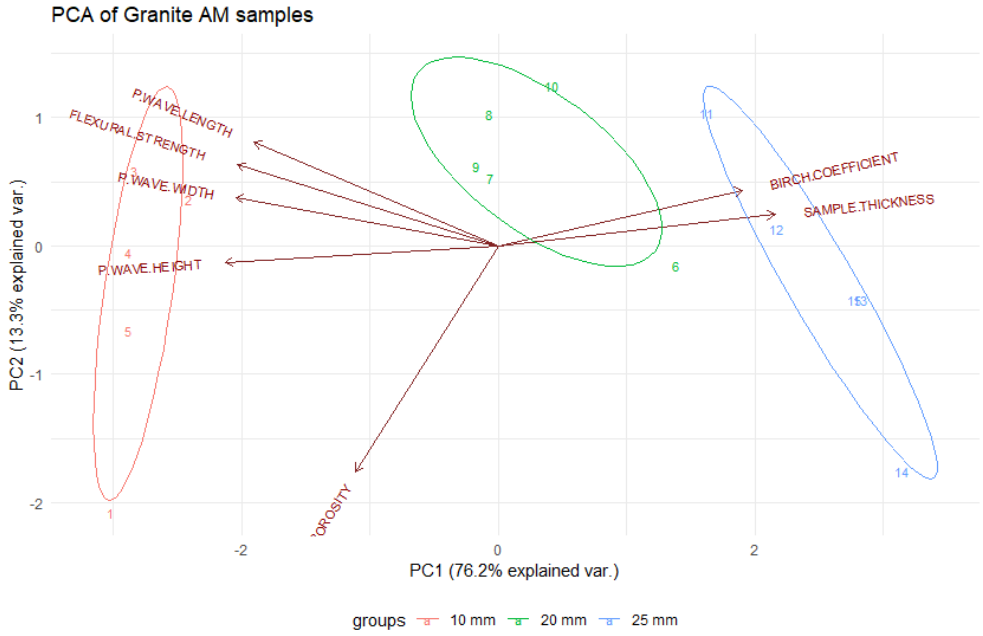

Figure 35 – PCA plot of the two main components PC1 and PC2, for the parameters of flexural strength (MPa), sample thickness (mm), p-wave propagation velocity in the direction of length, width and height (m/s), the Birch coefficient (%) and open porosity (%), obtained in Granite AM samples.

For the samples of Granite AM, a plot of the two main principal components of PC1 and PC2 describes 89.5% of variation in the 7 parameters analyzed, with PC1 being strongly defined by variations of flexural strength, P-wave propagation velocity, sample thickness and Birch coefficient, while open porosity has more weight on PC2 (Figure 35). Through this, it's possible to observe that for Granite AM samples, flexural strength and P-wave propagation velocity are positively correlated, and these two are slightly and inversely correlated with sample thickness.

Given the fact that Granite AM has a considerable degree of weathering and microfracturing, these relationships could imply that the reduction in flexural strength (and P-wave propagation velocity) that occurs as sample size increases would be a product, at least in the case of this granite, of the fact that in smaller dimensions, a lower chance of encountering internal microfracturing could result in a proportionate augment in material strength (Bažant, 1999).

As for the Granite CV samples, the principal component analysis captures 91.3% of all variation in the parameters described earlier, with just its two main components (Figure 36). In this granite, PC1 is weighed mostly by P-wave propagation velocities, sample thickness and Birch coefficient, while PC2 is largely defined by variation of flexural strength data, and as such, unlike what was observed in the Granite AM, there's a very low likelihood of correlation between it and sample thickness or P-wave propagation velocity. This goes along with the conclusion derived from the previous section 4.1.6, as the dispersion from flexural strength results is too high, particularly in the 10 mm, 20 mm and 25 mm thick samples.

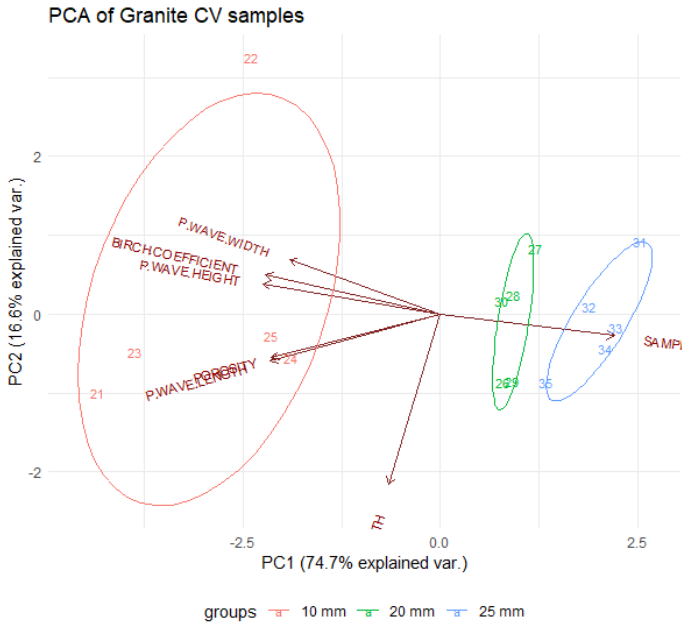

Figure 36 – PCA plot of the two main components PC1 and PC2, for the parameters of flexural strength (MPa), sample thickness (mm), p-wave propagation velocity in the direction of length, width and height (m/s), the Birch coefficient (%) and open porosity (%), obtained in Granite CV samples.

4.2. Results for Marble samples

4.2.1. Stereomicroscopic Analysis

Through the stereomicroscopic analysis of marble samples, performed as described in section 3.1 and whose results are exemplified in Figure 37, it's possible to observe that the Marble RC, of a blueish-grey color, white colored streaks and a granoblastic texture, is composed almost entirely of calcite minerals with a fine grain size, ranging from between 0.2 mm and 0.6 mm in diameter, with no particular orientation, while the crystals observed in this marble's matrix can have sizes of up to 1 mm in length.

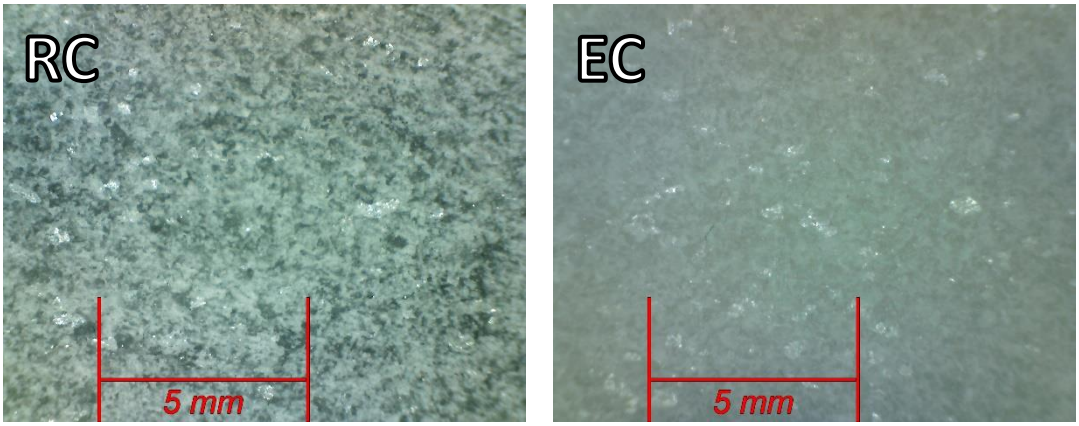

Figure 37 – Examples from the stereomicroscopic observation of the surfaces of Marble RC (left) and Marble EC (right), taken from samples RC3 and EC12 respectively.

In the case of the Marble EC samples (Figure 37), which present a white color with pink and light brown streaks with a granoblastic texture, they were also composed in large part by only calcite minerals, as was the case for the Marble RC, forming a homogenous matrix of a fine grain size of just approximately 0.1 mm. However, in the Marble RC samples the presence of crystals is more common and of slightly larger dimensions, with an average length of around 1.2 mm.

4.2.2. Gloss and Color

The measurements of the 4 color parameters of L*, a*, b* and C^*_{ab}, for the marble samples, whose description and assessment method are presented in section 3.4.2, show that between the Marble RC and Marble EC samples, there are some similar and some differing aspects, which are in agreement with what was previously observed in the micro-stereoscopic analysis. In terms of chroma (C^*_{ab}) characterization (Figure 38), through the coordinates a* (green/red gradient) and b* (blue yellow), it's possible to conclude that both marbles have little pigment, as both these parameters are close to 0 in average. For Marble RC samples, these averaged a value of -1.17 for a* and -1.85 for b*, which indicate a tendency towards green and blue respectively, while for Marble EC samples a* averaged -0.33 and b* averaged 1.73, which is a result of this marble's white color with reddish veins, resulting in

more prominent positive b* values. Due to this effect, it's also worth noting that Marble EC measurements have a higher dispersion, in relation to their counterparts.

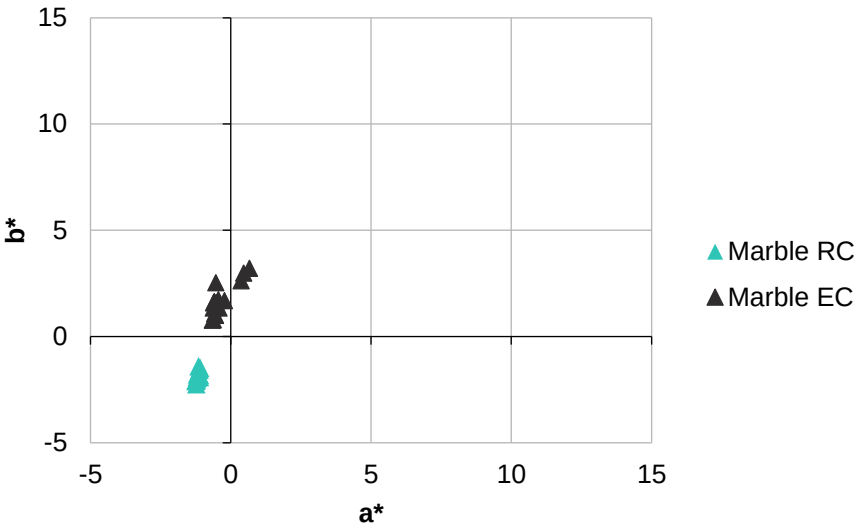

Figure 38 – Comparison between Marbles' RC and EC sample results obtained for a (green/red color gradient) and b* (blue/yellow color gradient) parameters.*

As a result of the parameters a* and b*, which were typically close to null in value, for both marbles in question, the resulting chroma coordinate (C^*_{ab}) is also low in value, representing the tendency towards a lack of strong colors previously mentioned, averaging around 2.20 for the Marble EC samples and 1.87 for the Marble EC samples (Figure 39). The higher general dispersion in a* and b*, mentioned for the Marble EC, is also reflected in a higher standard deviation for its C^*_{ab} parameter, with a value of 0.73, compared to the Marble RC, whose value is 0.21.

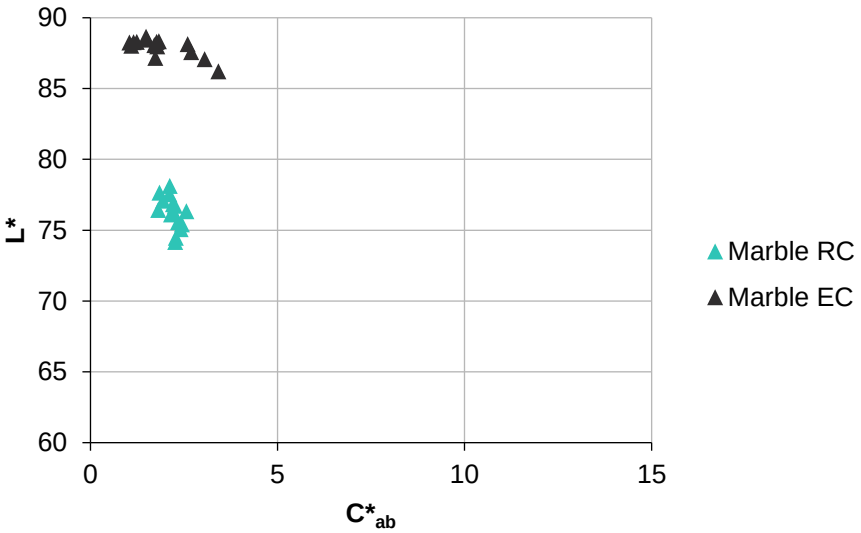

Figure 39 – Comparison between Marbles' RC and EC sample results obtained for L (lightness parameter) and C^*_{ab} (chroma gradient) values.*

In the lightness coordinate of L*, the difference in brightness between both marbles comes to light, as the darker Marble RC samples average around 76.25 with a standard deviation of 1.15, while the lighter colored samples of Marble EC average an L* of 87.93 with a lesser standard deviation of 0.65.

In relation to gloss results, presented in Figure 40 and in Table 4 as a variable dependent on sample size, it's possible to observe that between Marble RC And Marble EC samples, the latter have a higher value for gloss across all samples, with an overall average of 2.21, while the samples of Marble RC average only 1.67. Both of these natural stones have a generally higher variance in gloss value than the granites studied in section 4.1.2, likely due to the marbles composition of mostly calcite forming heterogenic clusters of crystals throughout its surfaces.

Unlike what was observed in granites, marble samples present a variation of gloss depending on the sample size, with the smaller samples of 10 mm thickness having an average of 1.76 for Marble RC and 2.28 for Marble EC, while in the larger 25 mm thickness samples, the average values are respectively 1.60 and 2.10, with the averages for the 25 mm samples in between the other two sets. However, this tendency is marginal at best, as there is still a large overlap between values from the different size sets, regarding gloss, so it can be assumed that no particular disparity in rugosity/surface finish exists between these two marbles.

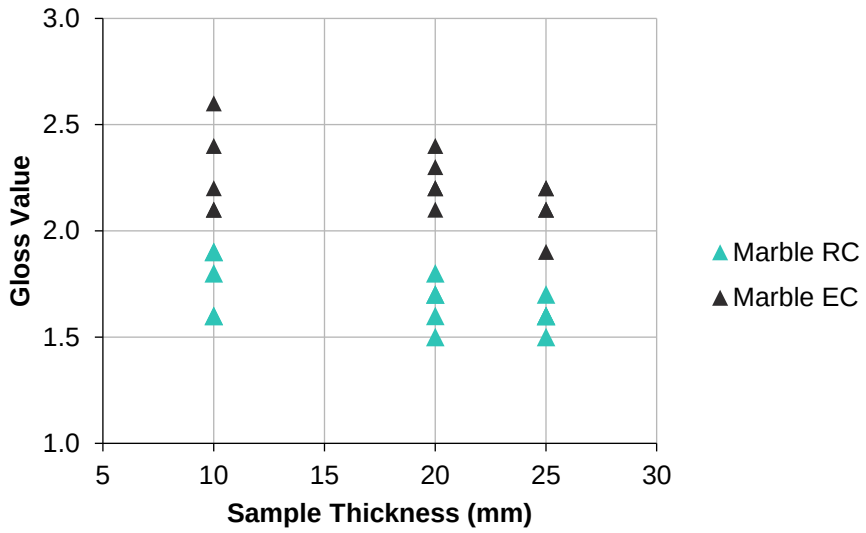

Figure 40 – Comparison between Marbles' RC and EC sample results obtained for gloss values in relation to the different sets of sample sizes, represented by their correspondent sample thickness (mm).

4.2.3. Apparent density and Open porosity

From the open porosity determination method, described in section 3.4.3, the obtained results (Figure 41, Table 4) show that for both marbles the average open porosity behavior is similar, with the Marble RC samples averaging around 0.48%, for open porosity percentage, while the samples of Marble EC averaged 0.59%.

However, what's more noticeable is the decrease in percentage that occurs on the samples with 25 mm thickness, for both marbles, where in the case of Marble RC samples, the average of these samples is 34.33% below what's seen in the smaller sample sizes while for the Marble EC samples this decrease is 31.48%. Besides this phenomenon, there are also two samples from two different dimensions, EC4 and EC6, which have a value for open porosity that's twice as high as the rest of the samples from the same groups, at around 1% open porosity. Putting these aside would make it possible to conclude that the general standard deviation in both marbles is low, at 0.09% for Marble RC samples and 0.08% for Marble EC samples, the latter of these growing to 0.18% when accounting for the two outlying samples.

Table 4 – Average open porosity results for Marble RC and Marble EC samples of sizes with 10 mm, 20 mm and 25 mm thickness.

	Average open porosity (%)		
	10mm	20mm	25mm
Marble RC	0.53 ± 0.03	0.54 ± 0.04	0.37 ± 0.03
Marble EC	0.68 ± 0.18	0.65 ± 0.21	0.44 ± 0.03

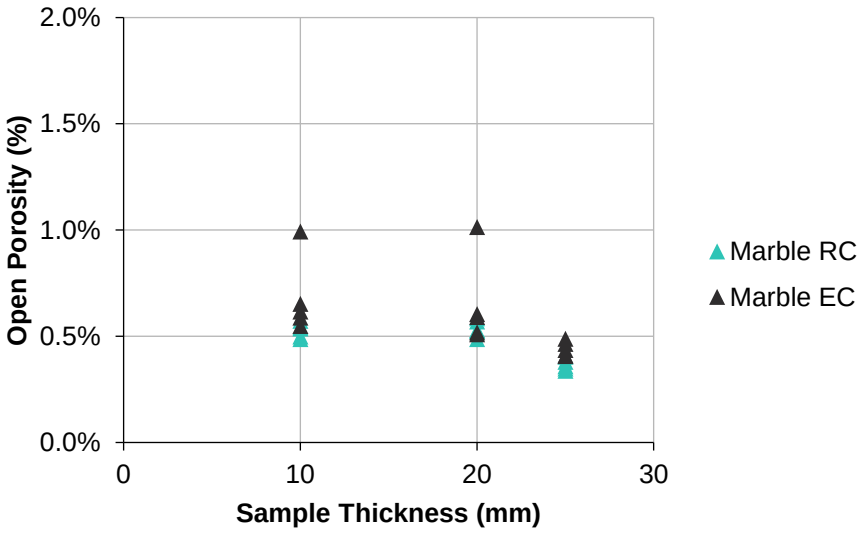

Figure 41 – Comparison between Marbles' RC and EC sample results obtained for open porosity percentages and sample dimension (mm).

As for the apparent density, the results represented in Figure 42 show that, much like in the case of the granites, the values obtained mirror the behavior observed in open porosity, with the Marble

RC samples averaging 2699.40 kg/m^3, edging out the average for samples of Marble EC at 2692.75 kg/m^3, still with both marbles having relatively similar values.

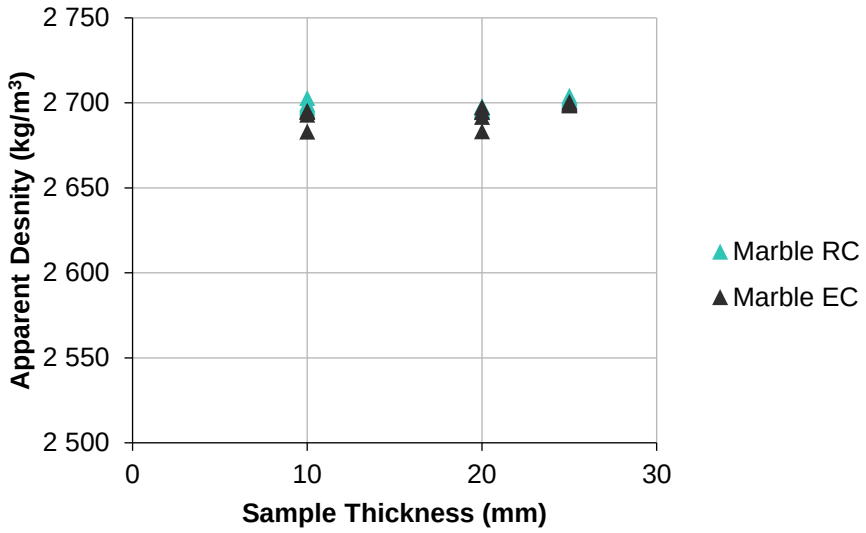

Figure 42 – Comparison between Marbles' RC and EC sample results obtained for apparent density (kg/m^3) and sample dimension (mm).

On the other hand, the characteristic of the samples with 25 mm thickness previously mentioned, of having a decrease in open porosity, has a much more subdued effect in apparent density, as relative to the other samples sizes, there is only an increase of 0.17% in Marble RC and of 0.26% for the Marble EC, which are negligible. The same occurs when looking at the values obtained for the Marble EC samples EC4 and EC6, whose value for open porosity was twice as high as the average, but in the case of apparent density it only represents a mirrored decrease of 0.34% when compared to the other samples from the 10 mm as 20 mm groups.

4.2.4. Water absorption coefficient by capillarity

The determination of water absorption in marbles, as described in section 3.4.4, resulted in two separate curves for each of the natural stones in study (Figure 43, Table 5), for the Marble RC and Marble EC samples. For both of these, the respective curves are formed of relatively low values for water absorption, between both the Marble RC and the Marble EC samples, an observation that's natural given the low open porosity values obtained.

The two sample sets of Marble RC, with different sizes based on a 20 mm and a 25 mm thickness, both present a relatively similar curve with a high level of dispersion, which reached the end of the first phase after about 6 hours or 146.97 $\sqrt{s}$ for the 20 mm thick samples, and for the 25 mm thick ones, after 24 hours or 293.94 $\sqrt{s}$. The smaller samples, of 20 mm thickness, have an approximate water absorption coefficient of 0.75 g/m^2.s^{½}, while the larger set have an average rate of 0.62 g/m^2.s^{½}. The accuracy of the estimated water absorption rates was lower the lowest from all tested natural stones

in this study, of only an average 85.92% for the 20 mm samples and an average 88.43% for the 25 mm samples, with the lowest percentage being registered on the RC9 sample, with a correlation coefficient of just 73.78%. These low estimate accuracies are due to the high dispersion in the values obtained, which occurred likely from the fact that the sensitivity of digital scale used, down to the centigram, was not enough to define such small growth values in weight in the early stages of measuring water absorption in the marbles.

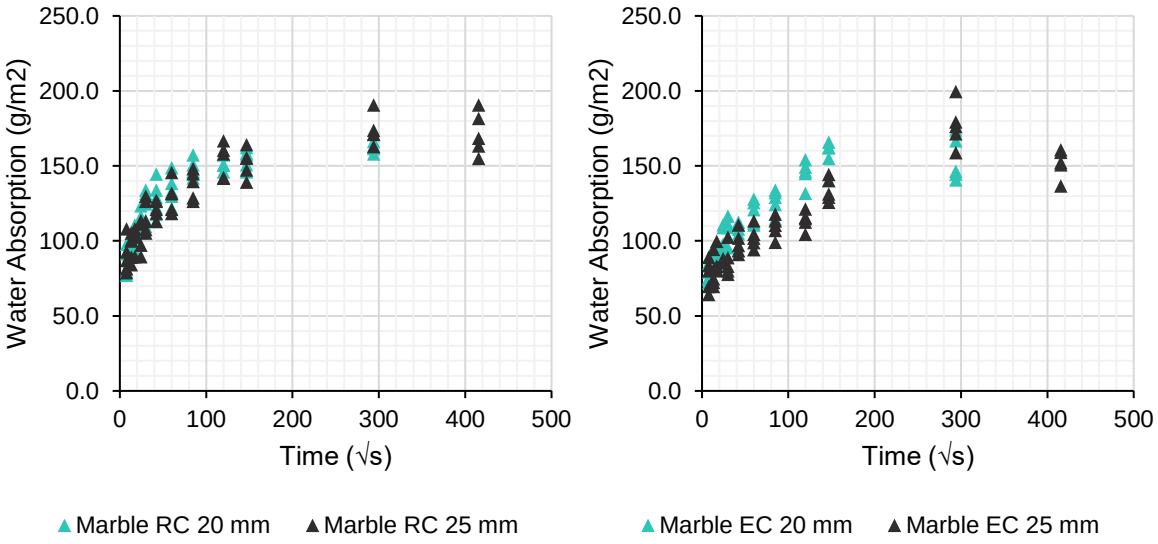

Figure 43 – Comparison between sample sizes' (of 20 mm and 25 mm thickness) and results obtained for water absorption (g/m²), from Marble RC (left) and Marble EC (right) samples.

As for the two set of sample sizes tested, of Marble EC, they have an absorption coefficient of 0.52 g/m².s½ and 0.37 g/m².s½, for 20 mm and 25 mm thick samples respectively, which are slightly lower relative to the curves from Marble RC samples. The time it took for the first phase of the water absorption curve to end was similar to the observed in the Marble RC samples, with 6 hours or 146.97 $\sqrt{s}$ for the 20 mm thick samples, and 24 hours or 293.94 $\sqrt{s}$ for the 25 mm thick ones. The correlation coefficient of the estimated water absorption rates is slightly higher in the Marble EC samples, compared to its counterpart, at 92.43% and 90.60% average for the 20 mm and 25 mm samples respectively.

Table 5 – Average water absorption coefficients for Marble RC and Marble EC samples of sizes with 20 mm and 25 mm thickness.

Water Absorption Results in 20 mm thick samples			
	Average Coefficient	Standard Deviation	Average R² (%)
Marble RC	0.75	0.05	85.92%
Marble EC	0.52	0.06	92.43%
Water Absorption Results in 25 mm thick samples			
	Average Coefficient	Standard Deviation	Average R² (%)
Marble RC	0.62	0.11	88.43%
Marble EC	0.37	0.05	90.60%

4.2.5. P-wave propagation velocities

The results obtained from the determination of P-wave propagation velocity in Marble RC and Marble EC samples are presented in Figure 44. In the case of Marble RC samples, it can be observed that P-wave propagation velocities obtained tend to be higher, based on the average value, in the samples with 50 mm thickness, for all measured directions, while these tend to be lower on the 20 mm samples. However, this variation is not as strong in all directions, which is a characteristic that's reflected in the overall standard deviation for each direction: along height, the overall standard deviation was the highest, at 636.69 m/s, while along the length it was the lowest, at an averaging 384.82 m/s. For the samples with 10 mm thickness, of Marble RC, the lowest average velocity was measured along the 50 mm width, with a value of 3850.45 m/s, while for the 25 mm and 50 mm samples it was along the length, at averaging velocities of 3933.87 m/s and 4061.60 m/s. Finally, for the 20 mm it was across the height of the samples, at an average of 3446.28 m/s.

These different directions in which lower P-wave propagation velocities were measured might indicate separate anisotropy directions for the different sets of samples, however, the high standard deviations in height and width derived values, which constitute on average about 15% and 10% of their respective average values, blur the ability to conclude it as a certainty. In terms of the Birch coefficient, it has an average value of around 21.80% for the 10 mm, 20 mm and 50 mm thick samples. In the case of the 25 mm samples, this coefficient is lower, at 13.06%, which indicates a level of anisotropy bellow the rest of the marble RC samples.

For the samples of Marble EC, there's also a relatively high dispersion in the P-wave propagation velocities obtained, with no particular pattern in relation to changes in sample size, from an overall perspective. However, the velocities measured along the length of the samples specifically, do present a consistent increase in average value, as the sample size increases, since for 10 mm, 20 mm, 25 mm, and 50 mm samples, there are increasing averages of P-wave propagation velocity of 5175.40 m/s, 5355.33 m/s, 5537.39 m/s and 5615.58 m/s, respectively, which consists in a total increase of 8.51% in velocity. Also, for this direction in measuring P-wave propagation velocity, the standard deviation was also generally the lowest, not surpassing 200 m/s or around 3.5% of the average, for each of the sample sizes tested.

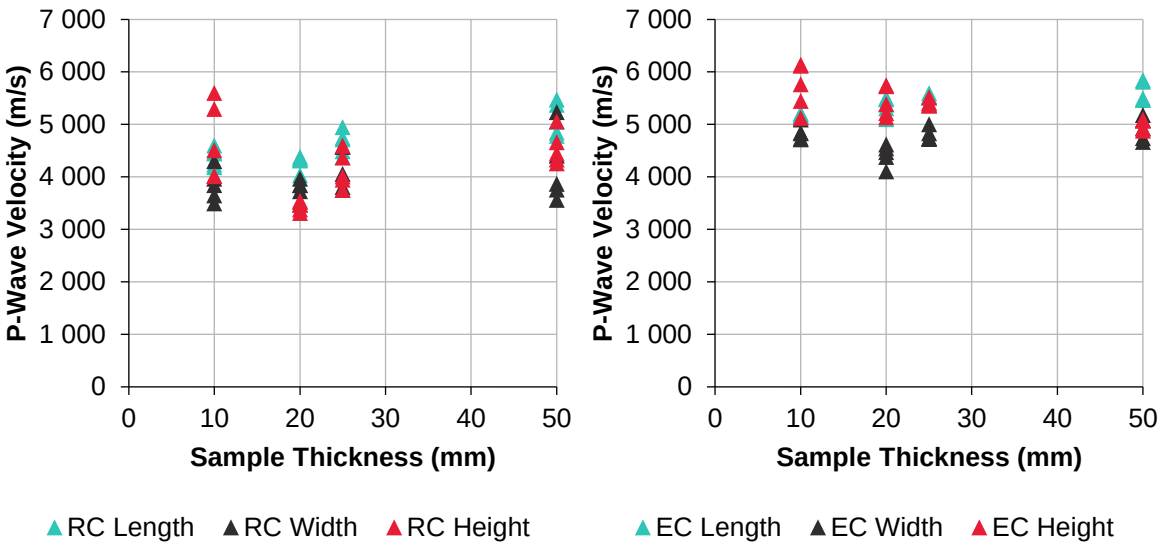

Figure 44 – Comparison between sample sizes' (from 10 mm to 50 mm thickness) and results obtained for P-wave propagation velocity (m/s), from Marble RC (left) and Marble EC (right) samples.

Unlike what was observed in the P-wave propagation velocities for the Marble RC samples, the values obtained for the samples of Marble EC show that the measures made along the width of the samples are on average the lowest, more pronounced in the 20 mm and 25 mm thickness samples. For the Birch coefficient, the values obtained are generally lower compared to the previously analyzed marble, with values of 16.65%, 21.21%, 13.95% and 13.83%, respective to samples of 10 mm, 20 mm, 25 mm, and 50 mm thickness, which indicated a slightly lower level of anisotropy is present in the Marble EC in relation to Marble RC natural stone.

4.2.6. Flexural strength

From the methods for measuring flexural strength described in section 3.5, the results obtained for the marble stone samples, in Figure 45 for both the Marble RC and Marble EC samples, present a slightly different reality regarding size effect on flexural strength, when compared to the previously analyzed granite natural stones, in section 4.1.6. In the case of the Marble RC samples, although there are variations between each set of sample dimensions, there is no discernable pattern which could be directly related with a change in these. For the samples with a thickness of 10 mm, 25 mm and 50 mm, the average values for flexural strength measured were of around 16.36 MPa, while the 20 mm thick samples averaged a lower 15.30 MPa, with standard deviations ranging between 1.01 MPa to 2.53 MPa. This difference in the 20 mm set, from others, might be due to specific characteristics in this particular sample size set, as in the P-wave propagation velocity tests the 20 mm thick samples of Marble RC also ranked below the rest, a factor that was not observed in other natural stones tested.

The relatively high dispersion in values obtained together with a lack of variation between each set of samples result in a negligible overall effect from size on the flexural strength values of Marble RC samples. A linear regression describes the variation of flexural strength as size increases with a positive

slope of 0.01, however, considering the result from sample RC19 as an outlier, as its value is vastly superior to the rest of the 50 mm thick samples, results in a linear regression with a slope of -0.02 and a coefficient of determination of 4.23%.

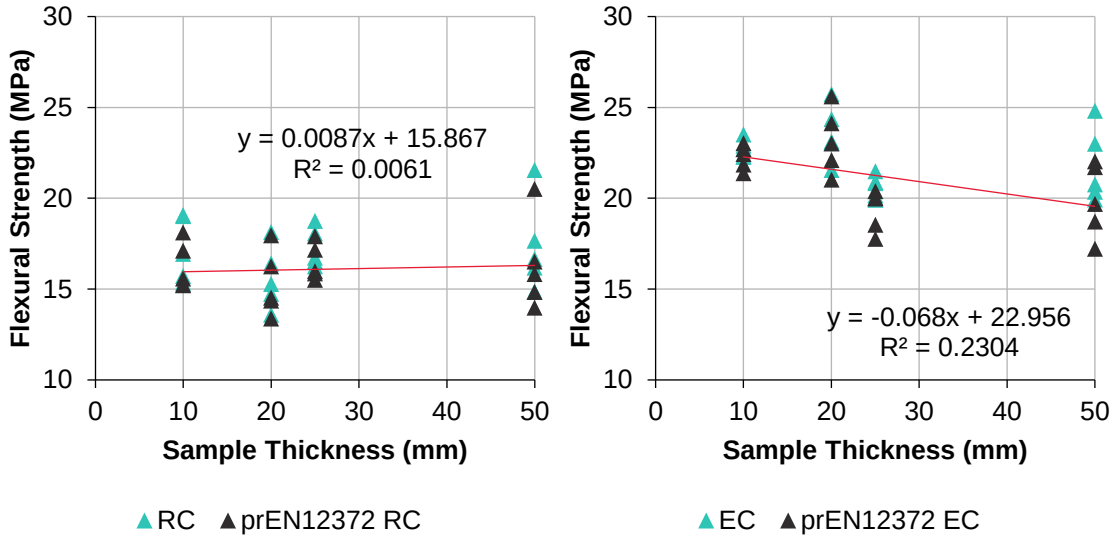

Figure 45 – Comparison between sample sizes' (from 10 mm to 30 mm thickness) and flexural strength results (MPa), obtained for Marble RC (left) and marble EC (right) samples.

The results from the Marble EC samples presented the highest values across all natural stone types in study, with an overall average of 22.18 MPa, the only one to average above 20 MPa in this parameter. Although slightly similar to what's presented for the Marble RC samples, the Marble EC samples also show a higher indication of a relationship between sample size and flexural strength values, more akin to what was previously observed in granite samples, with a relatively lesser degree of dispersion compared to its counterpart as well. The values obtained for the 10 mm and 20 mm thick samples averaged the highest flexural strength results, of 22.73 MPa, while the 25 mm and 50 mm thick samples averaged 19.61 MPa, with the 20 mm and 50 mm sets having relatively high standard deviations of a respective 1.78 MPa and 2.03 MPa. In the case of the Marble EC samples, a linear regression describes a slope of -0.07 with a coefficient of determination of 23.04%.

Given the results presented for the both the Marble RC and Marble EC natural stones, in terms of flexural strength in relation to samples size, no direct effect can be concluded in the case of the Marble RC, as the average values remain either constant, or with too low of a variation, while for Marble EC samples there are slight indications of a tendency of reduction in flexural strength, albeit marred by the high dispersion in the results obtained. As such, when compared to the minimum required sample thickness of 25 mm (Table 6), from the EN 12372 standard, the average result of flexural strength in Marble RC samples of 10 mm and 20 mm thickness is equal or slightly below the average obtained from the standard minimum sample size, while in the case of Marble EC samples the 25 mm thick samples showed values that are always bellow those obtained from smaller sample sizes.

Table 6 – Comparison between average flexural strength results for Marble RC and Marble EC samples of sizes with 10 mm, 20 mm and 50 mm thickness, with samples of 25 mm thickness, the minimum required.

	Average flexural strength (MPa)				*Ratio of average flexural strengths*		
	10mm	20mm	25mm	50mm	10/25mm	20/25mm	50/25mm
Marble RC	16.26 ± 1.30	15.3 ± 1.81	16.49 ± 1.01	16.34 ± 2.53	0.99	0.93	0.99
Marble EC	22.29 ± 0.66	23.17 ± 1.78	19.35 ± 1.14	19.88 ± 2.03	**1.15**	**1.20**	**1.03**

4.2.7. Principal Component Analysis in marble samples

The principal component analysis, or PCA, conducted for both marbles, uses the same parameters obtained from previously mentioned testing procedures, for the same reasons as in the case with granite samples: flexural strength (MPa), sample thickness (mm), p-wave propagation velocity in the direction of length, width and height (m/s), the Birch coefficient (%) and open porosity (%).

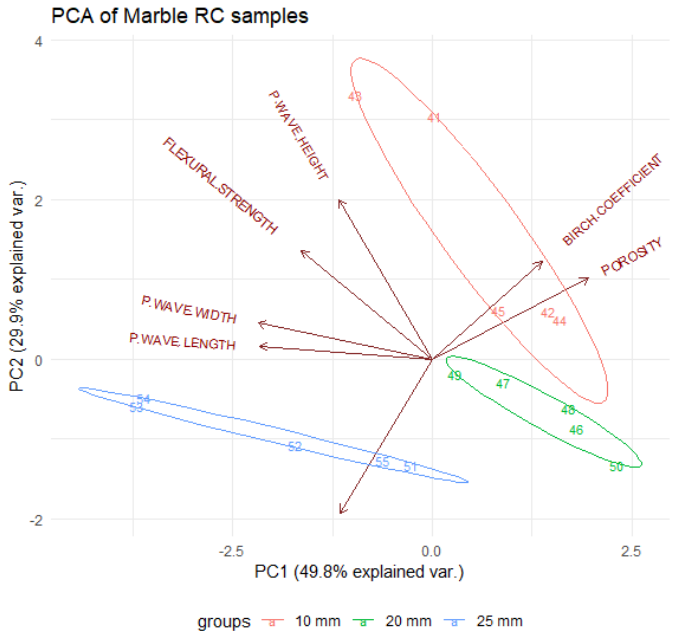

Figure 46 – PCA plot of the two main components PC1 and PC2, for the parameters of flexural strength (MPa), sample thickness (mm), p-wave propagation velocity in the direction of length, width and height (m/s), the Birch coefficient (%) and open porosity (%), obtained in Marble RC samples.

For the Marble RC, the resulting plot of PC1 and PC2 represents 79.7%, of the variation in the aforementioned parameters (Figure 46), in which it's possible to observe that flexural strength has practically no correlation with sample thickness, as vectors for both share a 90° angle, while having a slight positive correlation with P-wave propagation velocities. The lack of relation between flexural strength and sample thickness in the principal components is natural, given the high dispersion in the results obtained for Marble RC samples' flexural strength.

However, the same cannot be said for Marble EC samples (Figure 47), where the two first principal components, which describe 66.4% of the variation in the 7 parameters used, present an inverse correlation between flexural strength against sample thickness with a slight indication of a

positive correlation of flexural strength with open porosity and Birch coefficient variations, which could indicate that a variation in anisotropy in the different sample sizes could be slightly impacting the variation in flexural strength previously observed among these.

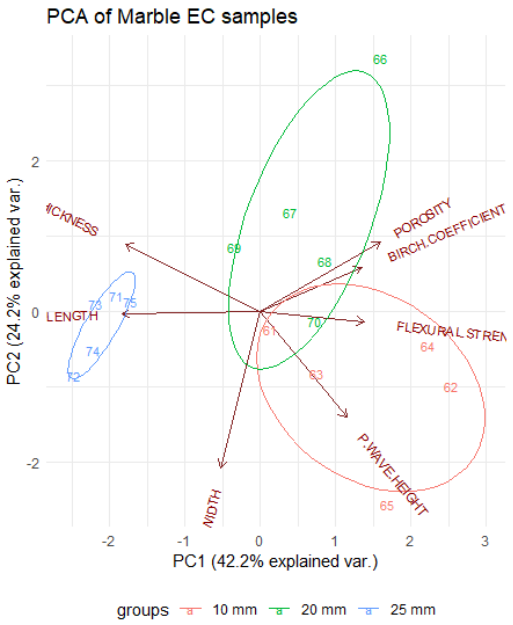

Figure 47 – PCA plot of the two main components PC1 and PC2, for the parameters of flexural strength (MPa), sample thickness (mm), p-wave propagation velocity in the direction of length, width and height (m/s), the Birch coefficient (%) and open porosity (%), obtained in Marble EC samples.

4.3. Results for Limestone samples

4.3.1. Stereomicroscopic Analysis

As observed through the stereomicroscopic analysis, depicted in Figure 48, the Limestone GM, a light grey oolitic and bioclastic limestone, is made up of almost only calcite components, with a base of relatively homogenous oolites and pellets, of 0.5 mm length and cemented in sparry calcite, which compose of around 85% of the limestone. There's also the presence of large bioclasts, with dimensions that vary between 2 mm and 7 mm in length, which in turn consist of around 15% the limestones composition, as well as a slight presence of microfracturing.

In the case of the Limestone MG samples, which present a light cream color, similar observations can be made regarding its oolitic and bioclastic composition. However, in this limestone's case, there's a wider range of grain size regarding the oolites and pellets in its composition, whose lengths vary between 0.5 mm and larger 1~3 mm grains, cemented in sparry calcite. The bioclastic components have the same dimensions as observed in the Limestone GM, and the Limestone MG samples also have a slight presence of microfractures.

As for the Limestone MMF, a light cream-colored oolitic limestone, it has a much less dense population of much smaller bioclastic components, which sizes of up to only 1 mm in length, a much

denser oolitic composition with sparry calcite cement, of grains with a length of around 0.5 mm, and a larger presence of cavities with signs of recrystallization.

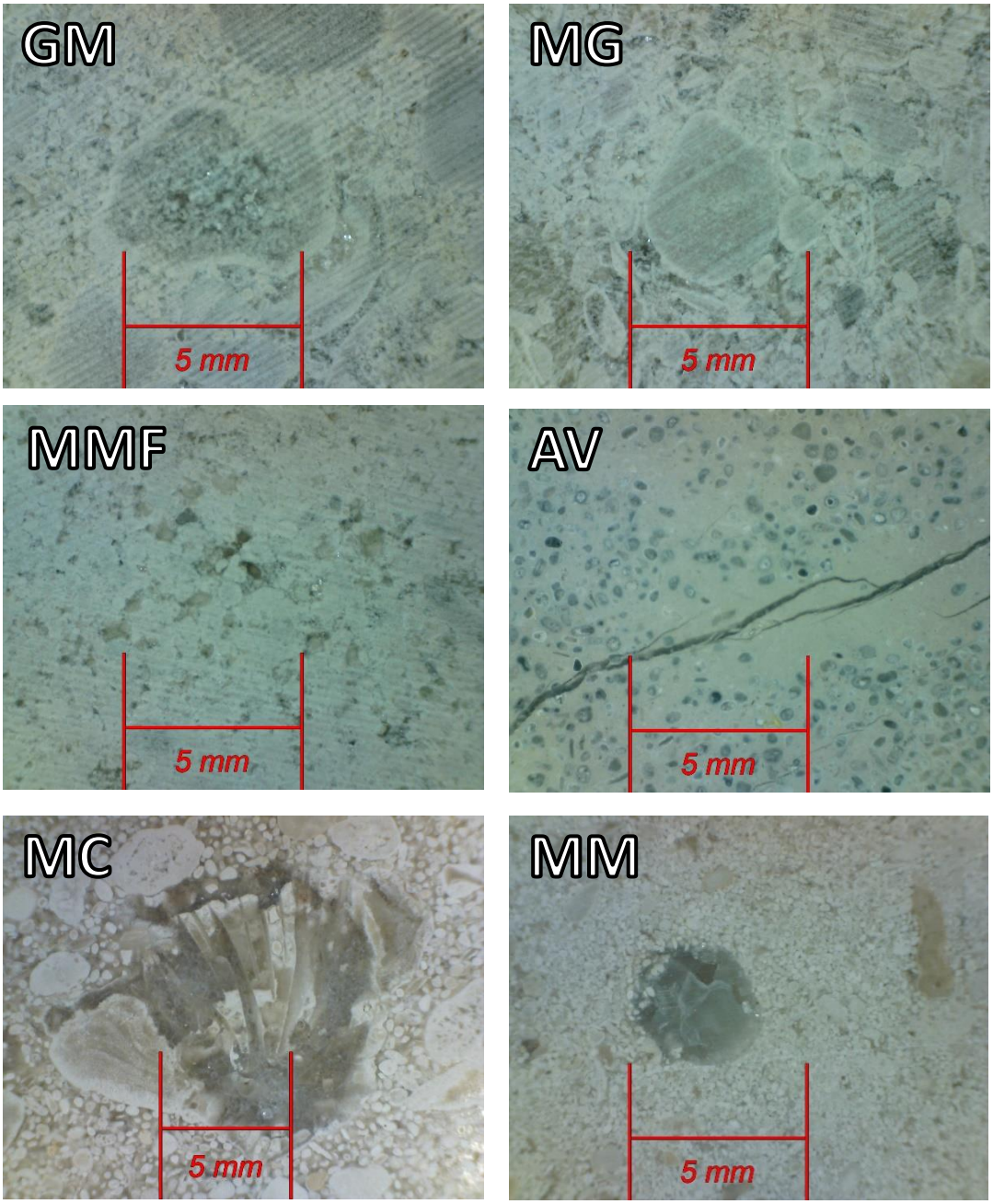

Figure 48 – Examples from the stereomicroscopic observation of the surfaces of Limestones GM (top left), MG (top right), MMF (middle left), AV (middle right), MC (bottom left) and MM (bottom right), taken from samples GM3, MG12, MMF4, AV8, MC9 and MM5, respectively.

The stereomicroscopic analysis of the Limestone AV, a blueish-grey limestone with a fine grain size and small light-colored patches, shows that this limestone is composed by mostly calcite, through the form of oolites, whose grains have dimensions of around 0.3 mm of length, and micrite, which not only cements the oolitic grains, but also forms the light colored patched which can are macroscopically observed on the Limestone AV samples. In this limestone's samples, there's a larger presence of

fracturing relative to other limestones, with both microfractures, fractures and larger sized fissures, in which it's possible to observe recrystallization, and in some cases even signs of weathering.

For the Limestone MC samples, a cream colored and heavily bioclastic limestone of compact nature, the stereoscopic observation presented a composition that, much like previous limestones observed, was based on calcite, in this case with based on oolites and pellets and pellets cemented in micrite, with a grain size of between 0.5 mm and 0.8 mm in diameter. The bioclasts observed in the Limestone MC samples were the largest observed across all limestones studied, particularly in the samples of 20 mm thickness relative to other sized samples, sometimes reaching more than 15 mm in length and having various forms, from linear to spheroidal, with some grouped and some isolated.

Finally, the Limestone MM, a compact limestone of whitish-cream color and oolitic nature, presented similar characteristics relative to the rest of the limestones tested, with a composition uniquely based on calcite, through the form of oolites in a micritic cement, whose grain size averaged around 0.2 mm in length, and a reduce presence of bioclast, compared to some of the other bioclastic limestones analyzed, with these having dimensions of 3 mm or sometimes more.

4.3.2. Gloss and Color

After following the testing procedures described in section 3.4.2, for assessing color and gloss in natural stone, the results obtained in the limestones studied for the a* and b* coordinates, of green/red and blue/yellow chromatic axes, respectively, are presented on Figure 49. From this, it's possible to observe that almost all types of limestone tested presented a similar tone of color, with the values averaging around 2.24 for the a* parameter, with low dispersion, with the exception of the Limestone AV samples, which averaged 0.54. For the b* measurements, the highest average belongs to the Limestone MM samples, with a value of 7.17, while the samples of Limestone MMF had the lowest, of 5.55, with an overall average of 6.29, where once again the Limestone AV samples were the exception, with an average of 3.86 for b* coordinates. This indicates that the limestones in study were generally of a yellowish tone, not as strong in the yellow as the Granite AM previously studied, while the Limestone AV stood closer to the greyscale in comparison to the rest.

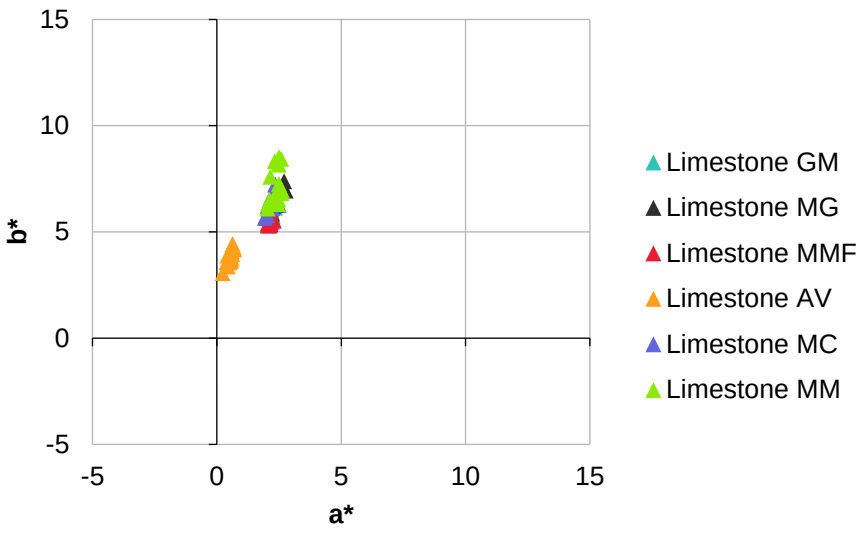

Figure 49 – Comparison between Limestones' GM, MG, MMF, AV, MC and MM sample results obtained for a (green/red color gradient) and b* (blue/yellow color gradient) parameters.*

In the analysis of the results obtained for the C^*_{ab} chroma coordinate (Figure 50), whose value is dependent on the a* and b* coordinates, and the L* lightness parameter, it becomes more evident in which of the limestones tested a superficial heterogeneity in appearance is more evident, due to the varying degrees of dispersion among the studied samples. For the Limestone MMF samples for example, the standard deviations for both of these parameters, C^*_{ab} and L* respectively, are of 0.19 and 0.31, the lowest in the group, while in the case of the Limestone MM these are 1.04 and 0.82, which are among the highest. Once again, the Limestone AV samples stand out from the rest, not only in C^*_{ab}, which was to be expected given the difference observed in a* and b* parameters, but also in terms of lightness, with these limestones being relatively darker than the rest. Besides this, it's worth noting that within the Limestone AV samples, there are 2 different groups of samples, one composed by the 10 mm and 25 mm thick samples, with a higher average L* value of 76.78, while the 20 mm thick samples averaged only 71.85.

Finally, in terms of the results obtained for the gloss tests, presented on Figure 51, the individual dispersion of values is relatively low for each limestone type, with samples from Limestone GM and MG having the lowest value for standard deviation at 0.07 while the Limestone AV samples had the highest, at 0.12. These samples from Limestone AV also had the lowest average gloss value, at 1.31, while the Limestone MG had the highest, averaging around 1.73.

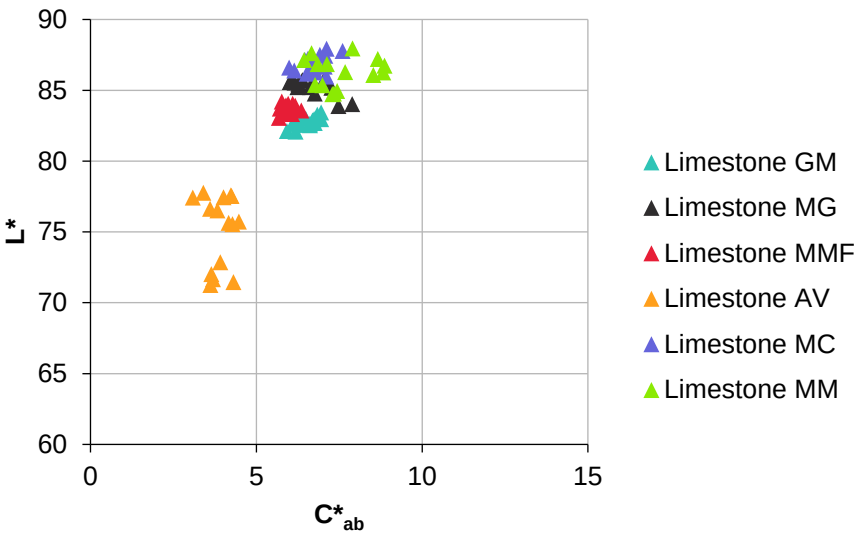

Figure 50 – Comparison between Limestones' GM, MG, MMF, AV, MC and MM sample results obtained for L (lightness parameter) and C^*_{ab} (chroma gradient) values.*

In terms of variations between sample sizes, the values obtained tend to be relatively uniform, as mentioned earlier, although a slightly increasing tendency can be observed in the Limestone GM and MMF samples and a slightly decrease can be seen in the Limestone MM samples, as sample size increases. Similarly, to what was noted in the L* parameter for the 20 mm thick samples in the Limestone AV, this same set of samples also presented the lowest average value for gloss, for this limestone type, although not as steeply as observed in the lightness parameter analysis.

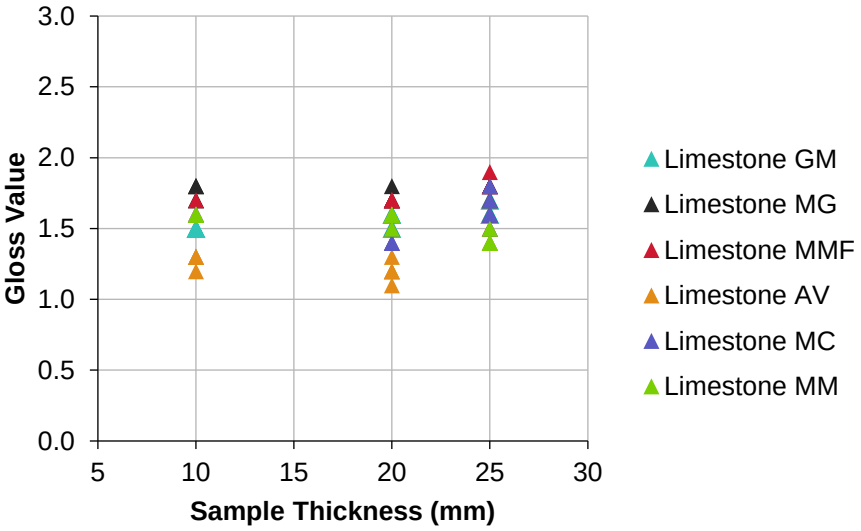

Figure 51 – Comparison between Limestones' GM, MG, MMF, AV, MC and MM sample results obtained for gloss values in relation to the different sets of sample sizes.

4.3.3. Apparent density and Open porosity

From the test procedure for determining open porosity, described in section 3.4.3, the results obtained (Figure 52, Table 7) for the 6 different limestones tested display a number of relatively different behaviors, when it comes to the percentage of open porosity in the different samples of each one. The Limestone GM and Limestone MMF types were the ones to display the most consistent values for open porosity in their samples, with overall standard deviations of just 0.23% and 0.26%, for average values for open porosity of 4.91% and 4.92%, respectively. On the other hand, samples from the Limestone MM had the highest overall standard deviation, of 1.93%, which is a result of different average values for each set of samples sizes, as 10 mm samples averaged 8.60% in open porosity, but 25 mm samples averaged a much higher 12.82%. Similarly, the 20 mm thick samples of Limestone MC also recorded a higher average open porosity, of 10.01%, in relation to the 10 mm and 25 mm sets, which averaged only 7.26%.

Table 7 – Average open porosity results for Limestones GM, MG, MMF, AV, MC and MM samples of sizes with 10 mm, 20 mm and 25 mm thickness.

	Average open porosity (%)		
	10mm	20mm	25mm
Limestone GM	4.95 ± 0.33	4.87 ± 0.23	4.92 ± 0.13
Limestone MG	7.02 ± 0.12	6.92 ± 0.57	6.14 ± 0.32
Limestone MMF	4.63 ± 0.13	4.20 ± 0.17	4.13 ± 0.05
Limestone AV	4.38 ± 0.14	3.01 ± 0.31	3.37 ± 0.33
Limestone MC	7.26 ± 0.69	10.01 ± 0.57	7.26 ± 0.85
Limestone MM	8.60 ± 0.18	9.26 ± 0.25	12.81 ± 0.38

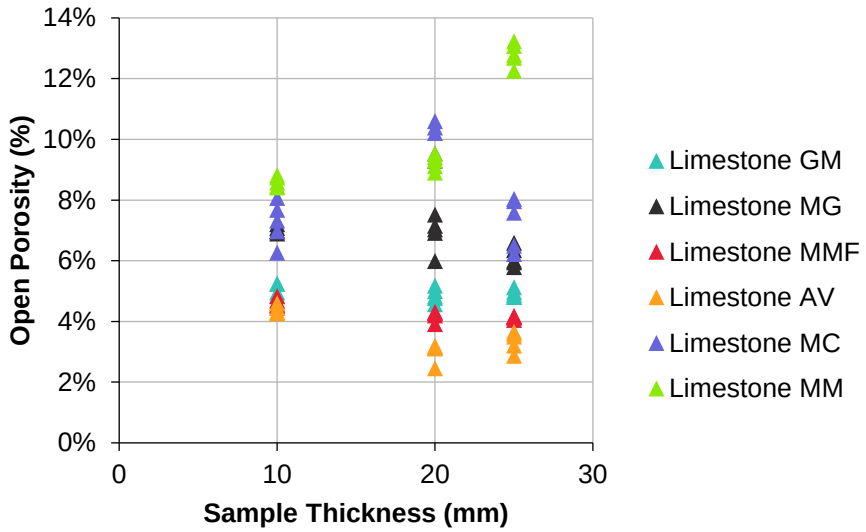

Figure 52 – Comparison between Limestones' GM, MG, MMF, AV, MC and MM sample results obtained for open porosity percentages and sample dimension (mm).

Although for both these limestones there's a high amount of overall dispersion, in each set of samples the open porosity percentages obtained are rather consistent, which indicates that these variations in behavior are a result of different intrinsic characteristics from the different sets of samples within these same limestones.

The results for apparent density in the limestones tested (Figure 53), calculated from Equation 2 through the data obtained from the weighing process, as expected, mirror the patterns observed in the results for open porosity (Figure 52), as previously observed in sections 4.1.3 and 0 for granite and marble samples. The Limestone MM samples now present a decreasing trend as sample size increases, with a reduction of 6.91% in apparent density from the 10 mm to the 25 mm thick samples, while the 20 mm thick samples of Limestone MC present a lower average, of 2371.11 kg/m^3, when compared to the 10 mm and 20 mm sets, of 2475.91 kg/m^3 and 2465.80 kg/m^3 respectively. Similar to the observed in open porosity, Limestones' GM and MMF samples present the lowest amount of variation from the limestones tested, with standard deviations of just 8.50 kg/m^3 and 5.28 kg/m^3, relative to averages of 2543.51 kg/m^3 and 2574.07 kg/m^3.

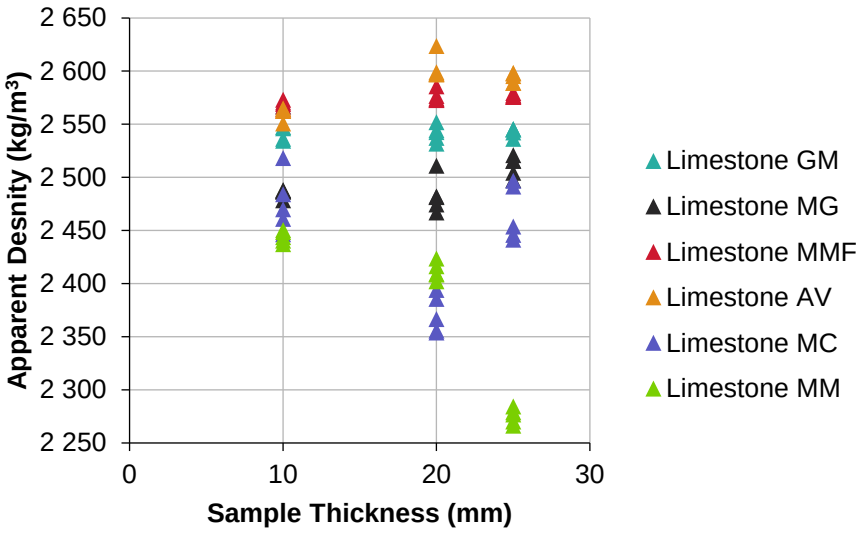

Figure 53 – Comparison between Limestones' GM, MG, MMF, AV, MC and MM sample results obtained for apparent density (kg/m^3) and sample dimension (mm).

4.3.4. Water absorption coefficient by capillarity

Through the process described in section 3.4.4, for the determination of the water absorption coefficient, the results obtained (Table 8) confirm the observations previously made through open porosity percentages, with the water absorption coefficient determination presenting a range of varied values for different limestones, as well as in between different sets of samples, of 20 mm and 25 mm thickness (Figure 54, Figure 55). For the Limestone GM samples (Figure 54), both sets of samples present similar results, with the first phase of water absorption curve ending at around 96 hours (587.88 $\sqrt{s}$), with an estimated water absorption coefficient of 7.20 g/m^2.s^{½} and 7.04 g/m^2.s^{½} for the 20 mm and

25 mm thick samples, respectively. For all Limestone GM samples, the coefficient of determination values for each individual estimation average around 99.31%, with the lowest being 98.59%.

In the case of Limestone MG (Figure 54), there's a visibly higher level of dispersion in the rate of water absorption between each sample, as the results for the coefficient range between 11.64 g/m^2.s^{½} and 23.20 g/m^2.s^{½}, with the 20 mm and the 25 mm sets having standard deviations of 3.84 g/m^2.s^{½} and 1.76 g/m^2.s^{½} respectively. In general, the water absorption coefficients obtained for 20 mm thick samples are higher than the obtained for 25 mm thick samples, with these sets averaging 18.21 g/m^2.s^{½} and 13.31 g/m^2.s^{½} in water absorption coefficient, while each sample's individual estimated rate maintained an accuracy equal or above 99.17%.

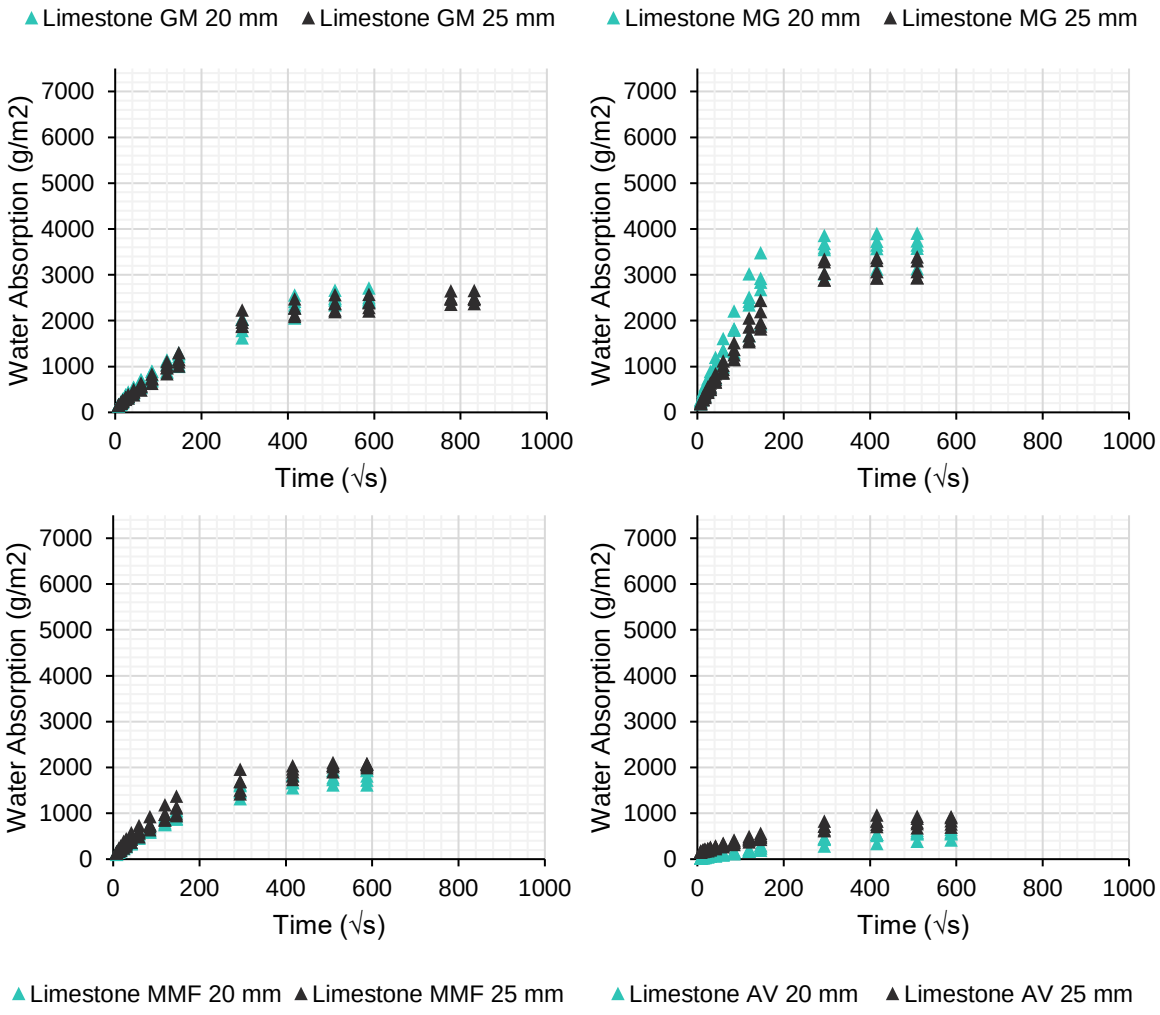

Figure 54 – Comparison between sample sizes' (of 20 mm and 25 mm thickness) and results obtained for water absorption (g/m^2), from Limestone GM (top left), Limestone MG (top right), Limestone MMF (bottom left) and Limestone AV (bottom right) samples.

The results obtained from the samples of Limestone MMF present a more consistent set of values for water absorption, with less dispersion and more similarity between the curves for 20 mm and 25 mm thick samples (Figure 54). The first phase tops off at about 48 hours, or 415.69 $\sqrt{s}$, for both of these sets, with an average estimation of the water absorption coefficient of 5.95 g/m^2.s^{½} and 6.98

g/m².s½, for the 20 mm and 25 mm sets respectively. The individual coefficients of determination, for each sample's estimation of water absorption, averaged around 99.00%, with the lowest minimum obtained being 97.54%.

For the Limestone AV samples (Figure 54), the values obtained present the lowest water porosity coefficients measured in across all limestones, which is not out of the ordinary given that these same samples also presented the lowest average open porosity percentages for all limestones. The 25 mm thick samples present an average of 2.37 g/m².s½ for the water absorption coefficient, while the 20 mm set averages a slightly lower 1.55 g/m².s½, a difference which relates well to the fact that the latter averaged a lower open porosity percentage. Both curves reach the ceiling for the first phase at around 72 hours (509.12 $\sqrt{s}$), and each individual estimation presented an accuracy of 98.08% in the case of 20 mm thick samples, and 99.37% for the rest.

The Limestone MC samples' results (Figure 55), show that the 20 mm thick samples have generally steeper curves than their 25 mm counterpart, while both show high dispersion, with standard deviations of 4.21 g/m².s½ for the 20 mm thick samples, which average a water absorption rate of 26.41 g/m².s½, and of 3.37 g/m².s½ for the 25 mm thick samples, which average a 17.56 g/m².s½ coefficient. Similarly, the total amount of water absorbed per surface unit is also higher for the smaller sized samples, which, along with the higher water absorption coefficient, appears logical, given the higher open porosity percentage observed in these samples. Finally, for the Limestone MC samples, the coefficient of determination of the estimated water absorption rates, of each sample tested, are all equal or above 99.19%, averaging 99.70%.

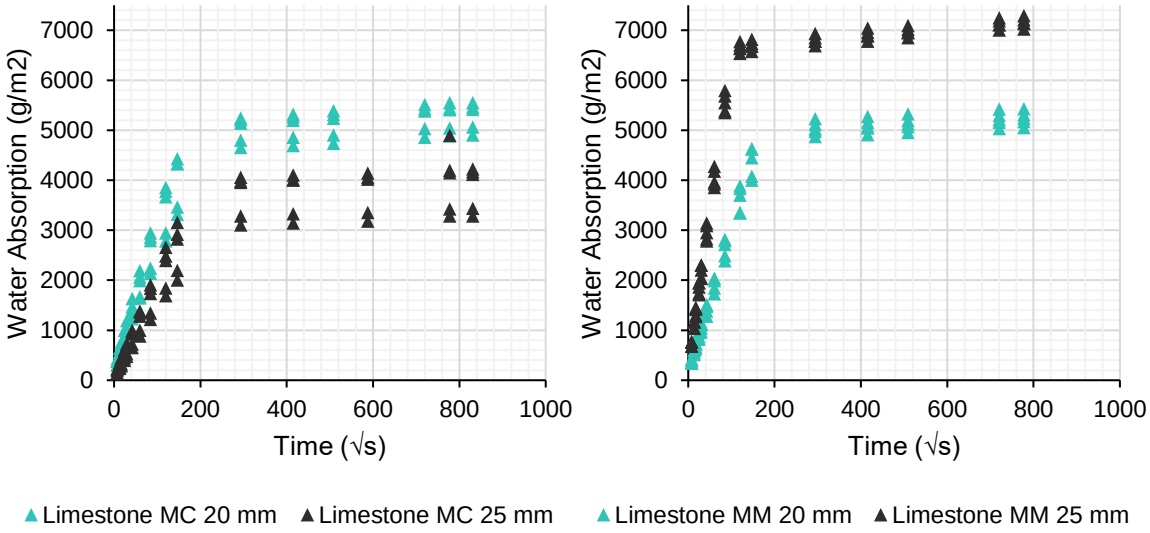

Figure 55 – Comparison between sample sizes' (of 20 mm and 25 mm thickness) and results obtained for water absorption (g/m²), from Limestone MC (left) and Limestone MM (right) samples.

Finally, the Limestone MM samples' results present a clear gap between water absorption rates and total water absorbed in the 20 mm and 25 mm thick samples (Figure 55), a phenomenon that's to be expected given the previously observed variation in open porosity percentages between these two

sets of sample sizes. However, unlike the in the results shown for the Limestone MC samples, in this case the values obtained maintain a relative low dispersion, with the 20 mm set averaging a water absorption coefficient of around 28.44 g/m².s½ and the 25 mm set averaging around 62.33 g/m².s½, which is the highest in all samples tested. Individually, each sample's estimated water absorption rate averaged an accuracy of around 99.95%, with the ceiling for the first phase ending at about 6 hours, or 146.97 $\sqrt{s}$.

Table 8 – Average water absorption coefficients for Limestone GM, MG, MMF, AV, MC and MM samples of sizes with 20 mm and 25 mm thickness.

Water Absorption Results in 20 mm thick samples			
	Average Coefficient	Standard Deviation	Average R² (%)
Limestone GM	7.20	0.92	98.97%
Limestone MG	18.21	3.84	99.54%
Limestone MMF	5.95	0.50	99.02%
Limestone AV	1.55	0.28	98.08%
Limestone MC	26.41	4.21	99.53%
Limestone MM	28.44	2.03	99.95%
Water Absorption Results in 20 mm thick samples			
	Average Coefficient	Standard Deviation	Average R² (%)
Limestone GM	7.04	0.74	99.65%
Limestone MG	13.31	1.76	99.82%
Limestone MMF	6.98	1.04	98.97%
Limestone AV	2.37	0.27	99.37%
Limestone MC	17.56	3.37	99.87%
Limestone MM	62.33	2.34	99.95%

4.3.5. P-wave propagation velocities

Through the process described in section 3.4.5, for the determination of P-wave propagation velocity, the results obtained for the samples of Limestone GM, MG, MMF and AV, in Figure 56, and also Limestone MC and MM, in Figure 57, all present similar patterns, with the velocities measured remaining more or less relatively consistent across all sample sizes, varying between each limestone, with the sole exception being the P-wave propagation velocities along the height of the 10 mm thick samples, which present much higher P-wave propagation velocity results in every single limestone tested.

For the Limestone GM samples, the velocities measured on the 20 mm, 25mm and 50 mm thick samples, across height, width and length, average around 4936.29 m/s, with relatively low dispersion, as this overall average of these 3 sample sizes presents a standard deviation of just 97.77 m/s. The P-wave propagation velocities from samples with 10 mm thickness, measured along sample length and width, also present similar values, with an average velocity of 4838.23 m/s, while along sample height

the velocities are much higher, as mentioned earlier, with an average velocity of 5863.81 m/s with an equally higher standard deviation of 229.44 m/s.

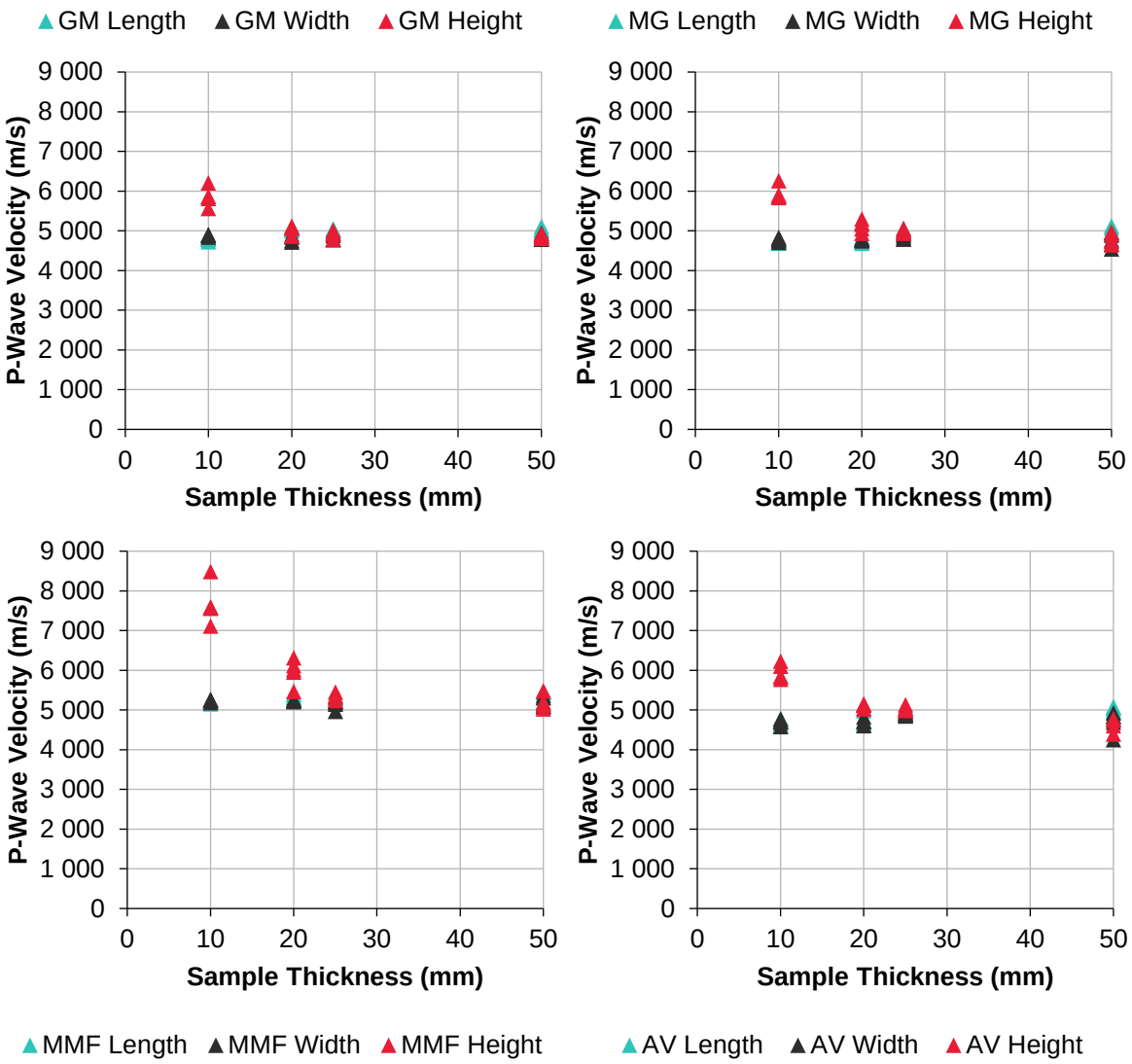

Figure 56 – Comparison between sample sizes' (from 10 mm to 50 mm thickness) and results obtained for P-wave propagation velocity (m/s), from Limestone GM (top left), Limestone MG (top right), Limestone MMF (bottom left) and Limestone AV (bottom right) samples.

From the results of the Limestone MG and Limestone AV samples (Figure 56), it's possible to observe very similar patterns, with a slight increase of P-wave propagation velocity measured along the length of the samples, as sample dimensions increase, from average velocities of respectively 4740.95 m/s and 4699.93 m/s in the 10 mm thick samples, to 5003.08 m/s and 5028.94 in the Limestone MG and AV samples of 50 mm thickness. However, the opposite occurs in the velocities measured in the height axis, as after the aforementioned spike observed in the 10 mm samples, with an increase of around 25% to an average velocity of 5956.08 m/s for both limestones, the values tend to continue a slight drop until the 50 mm thick samples, which average P-wave propagation velocities of 4792.5 m/s in the Limestone MG samples and 4655.56 m/s in the Limestone AV samples. Alongside sample width, the values tend to remain relatively constant around respective averages of 4797.84 m/s and 4776.30

m/s for both these limestones. Outside the measurements of P-wave propagation velocity across height in the 10 mm thick samples, the results obtained for all other combinations of direction of measurement and sample size present a low amount of dispersion, with standard deviations that tend to not pass the 100 m/s mark.

The results obtained from Limestone MMF samples (Figure 56) present some differences from the previous limestones analyzed, as the pattern of higher P-wave propagation velocity observed the 10 mm thick samples is a lot more prominent, with an average velocity parallel to height of 7667.22 m/s and a standard deviation of 498.84 m/s, which marks an increase of 46.89% relative to the velocities in other directions. These P-wave propagation velocities, measured along length and width, remain relatively constant, with respective averages of 5324.31 m/s and 5205.41 m/s across all sample sizes. However, in the P-wave propagation velocities along the height axis there's a variation, as from the 20 mm to 50 mm thick samples, the average velocity goes from 5970.30 m/s to 5196.14 m/s, outlining a gradual decrease in velocity of 32.23%, with a particularly high dispersion of results in the 20 mm thick samples.

From the results obtained for the Limestone MC samples (Figure 57), it's still possible to observe the same pattern mentioned for all previously analyzed limestones, where the values of P-wave propagation velocity for the 10 mm samples, in the direction parallel to the sample height, are around 31.07% higher than the rest of the velocities measured in the same sample size, averaging 6200.06 m/s. However, in the case of the other sample sizes, there's a slight increase in P-wave propagation velocity as sample size gets larger, a pattern that's different from the previously tested limestones, as average velocity in all directions goes from 4522.68 m/s, in the 20 mm thick samples, to 4791.10 m/s in the 50 mm ones, while presenting relatively low dispersion across these 3 sample sizes.

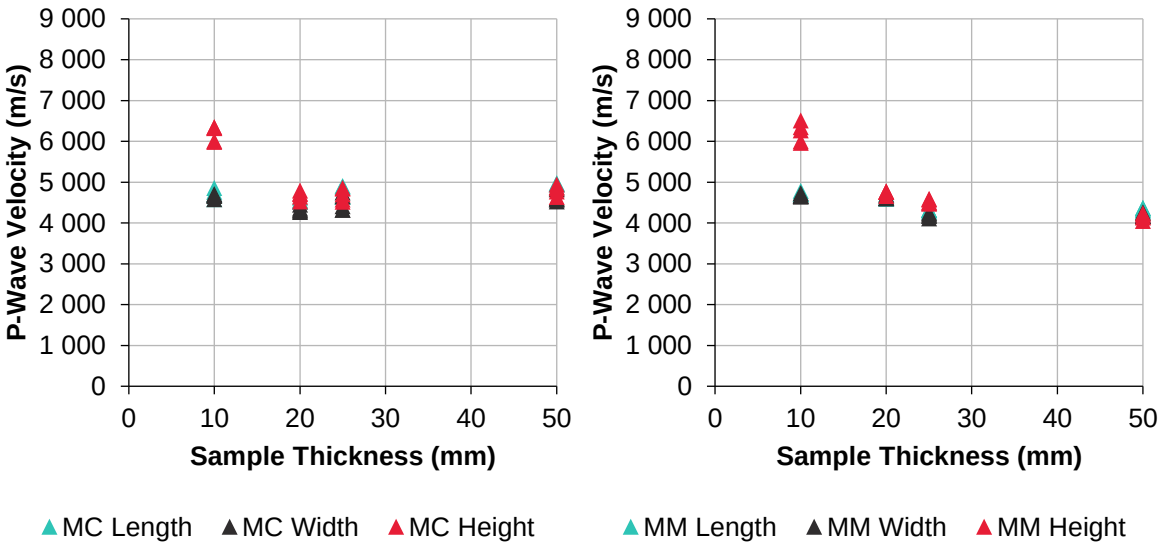

Figure 57 – Comparison between sample sizes' (from 10 mm to 50 mm thickness) and results obtained for P-wave propagation velocity (m/s), from Limestone MC (left) and Limestone MM (right) samples.

Finally, for the samples of Limestone MM, the main difference in behavior, relative to other limestones, is based around 2 separate averages for P-wave propagation velocity measured alongside sample length and width, with 10 mm and 20 mm thick samples averaging 4666.03 m/s and 25 mm and 50 mm thick samples averaging 4258.91 m/s. The results obtained in 20 mm and 50 mm thick samples, in particular, present low standard deviations, of just 63.76 m/s and 98.59 m/s, while the 10 mm samples have the highest, due to the previously mentioned increase in velocity parallel to height, which for the Limestone MM samples averages around 6215.60 m/s.

In terms of anisotropy in general for limestone samples, the Birch Coefficient tends to be relatively low for the samples of 20 mm, 25 mm and 50 mm thickness, not going above an average 8.46% per sample size in all limestones, with the exception of the Limestone MMF, where the 20 mm thick samples average a higher 13.14%. As for the samples of 10mm thickness, the Birch Coefficient values are much higher across all limestones, relative to other sample sizes, a product of the high P-wave propagation velocities obtained from the measurements parallel to sample height. This coefficient in limestones ranges between 20% and 30%, with the exception of, once again, the Limestone MMF samples, which have a coefficient of 40.75%. The fact that this limestone has higher values could be associated with the fact that its planes of anisotropy are perpendicular to the width axis, unlike all other limestones were these are perpendicular to the axis of height.

4.3.6. Flexural strength

The resulting flexural strength values obtained for the Limestone GM, Limestone MG, Limestone MMF and Limestone AV samples (Figure 58) all present very similar patterns between the size effect of increasing sample dimensions and the resulting flexural strength. The first characteristic present is the fact that 20 mm thick samples have the highest average flexural strength in each one of these limestones, to slightly different degrees of how large the difference between the rest of the sample sizes is. The second characteristic that stands out is the presence of a slight size effect on flexural strength, with the overall tendency in these 4 limestones being a decrease in such strength as sample size increases, although in a relatively negligible manner as overall data dispersion is relatively high compared to how little the flexural strength in the different sample sizes varies.

More specifically, in the Limestone GM samples, there's a decrease from an average of 12.26 MPa, in the 10 mm thick samples, to an average of 9.94 MPa in the 50 mm thick samples, as the highest flexural strength is obtained from the 20 mm thick samples, as previously mentioned, with an average of 12.54 MPa, marginally higher than the average of smallest samples. It's worth noting that the lowest measured value, of 7.87 MPa, in the last set of 50 mm thickness, in sample GM18, could be considered as an outlier when compared with the rest of the same sized samples, whose values for flexural strength all measured between 10.27 MPa and 11.40 MPa.

The Limestone MG samples present slightly lower values to the observed in Limestone MG, with the peak sample size of 20 mm thickness averaging 11.34 MPa of flexural strength, while from the 10 mm samples, to the 50 mm ones, the average decreases from 10.37 MPa down to 8.70 MPa. For both of these limestones, the dispersion in data is relatively small, with the standard deviations from

each sample size averaging around 0.97 MPa, and both also have similar linear regressions, with the slopes having values of -0.06 and -0.05 and coefficients of determination of 37.59% and 33.64%, for Limestone Gm and MG respectively.

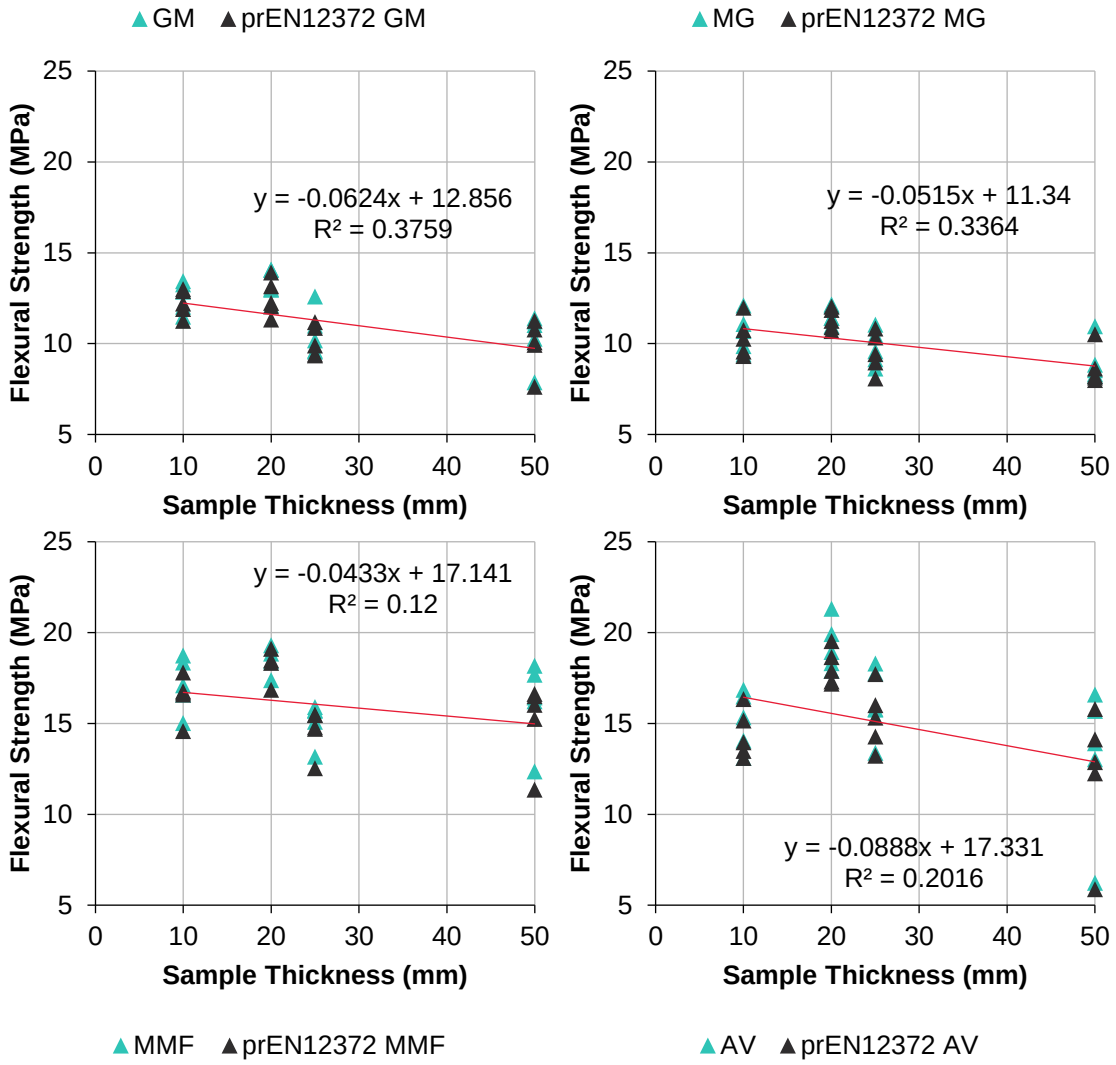

Figure 58 – Comparison between sample sizes' (from 10 mm to 30 mm thickness) and flexural strength results (MPa), obtained for Limestone GM (top left), Limestone MG (top right), Limestone MMF (bottom left) and Limestone AV (bottom right) samples.

For the Limestone MMF, the overall flexural strength is higher than the two previous cases, with the 20 mm thick samples averaging a value for flexural strength of 18.19 MPa. Unlike what occurs in Limestones GM and MG, the samples with thickness of 25 mm were the ones to have the lowest average flexural strength, of only 14.59 MPa, while 10 mm and 50 mm thick samples averaged 16.48 MPa and 15.15 MPa respectively. However, one of the 50 mm thick samples tested, MMF18, presents a measurement of flexural strength, of 12.36 MPa, which is much lower than the other 4 samples of this same size, who average around 16.10 MPa instead, which is closer to the average result obtained from the 10 mm thick samples.

As for the flexural strength results obtained from the Limestone AV samples, these present a more exacerbated version pattern observed in these 4 limestones, with the difference in average value between the 20 mm thick samples being higher, as this sample size averages a flexural strength of 18.11 MPa. Besides this, the tendency towards a decreasing flexural strength as sample size increases is also more accentuated at first glance. However, this is due to a particular sample of 50 mm thickness, AV19, which has a measured flexural strength of only 5.88 MPa, which below half the flexural strength obtained in all other samples of the same dimensions. This difference is likely the result of microfracturing in the central area of the sample (Figure 59), which facilitated the rupturing during the 3-point bending test, resulting in a lower load value at the point of rupture. Considering this measurement as an outlier, the 10 mm, 20 mm and 50 mm thick samples then have average flexural strength values of a respective 14.41 MPa, 15.30 MPa and 13.75 MPa, making this the only limestone so far where a smaller sample size averages a value below the minimum recommended of 25 mm thick samples.

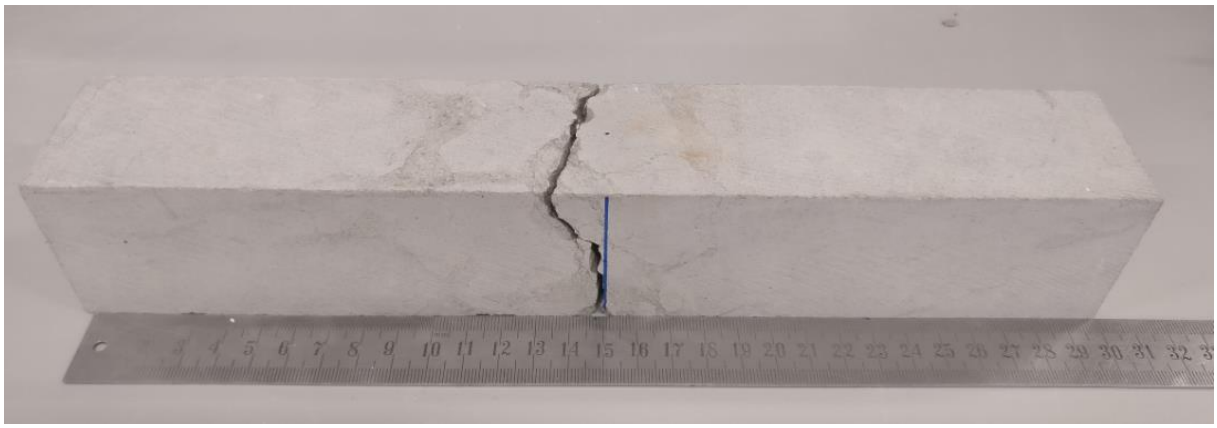

Figure 59 – Limestone AV sample AV19, after being put through the 3-point bending test to determine flexural strength, where it's possible to observe the resulting main fracture follow an already existing set of microfractures.

The dispersion of the obtained flexural strength values in the Limestone MMF and AV samples is higher than previously seen in the Limestone GM and MG results, particularly in the 50 mm thick samples, where standard deviation values for Limestone MMF and AV average 2.19 MPa and 3.77 MPa, respectively. However, taking out the measurements that were previously mentioned as likely outliers, these values drop to just 0.62 MPa and 1.56 MPa, which is more in line with the other sample sizes of these limestones. In terms of the linear regressions, although these are displayed while taking into account every sample tested, if not considering the outliers mentioned, the Limestone MMF linear regression would have a slope of -0.02 and the Limestone AV linear regression would have a slope of -0.04, both with low coefficients of determination of 3.08% and 8.06%, respectively, which are to be expected given the dispersion observed.

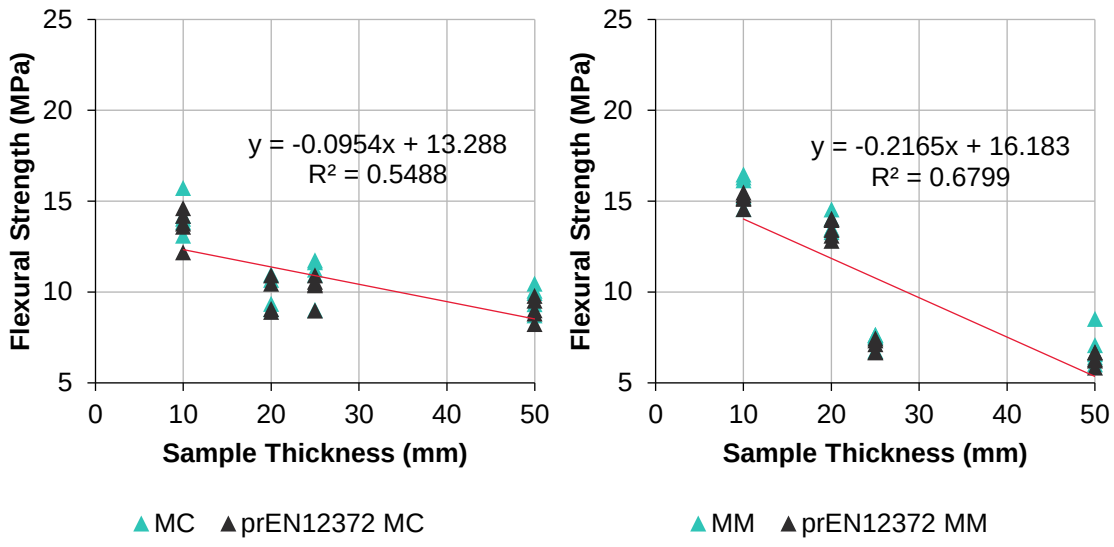

Figure 60 – Comparison between sample sizes' (from 10 mm to 30 mm thickness) and flexural strength results (MPa), obtained for Limestone MC (left) and Limestone MM (right) samples.

The Limestone MC and Limestone MM samples' results (Figure 60) present different patterns, in relation to the effect of size in flexural strength, when compared to the previous limestones, which all had strong similarities between them, regarding sample size versus flexural strength. In the case of Limestone MC samples, it's the 10 mm thick samples that present the highest average flexural strength values with an average of 13.67 MPa, while the rest of the sample sizes present more constant values that average around 9.72 MPa.

Meanwhile, in the Limestone MM samples' case, the 10 mm thick samples also average the highest flexural strength, of 15.13 MPa, followed by a small decrease in samples of 20 mm thickness, which averaged a flexural strength value of 13.47 MPa. However, the results obtained from the standard abiding sample sizes of Limestone MM present values that are much lower, with 25 mm and 50 mm thick samples averaging just 7.05 MPa and 6.35 MPa respectively. In these two cases, the differences observed in terms of behavior of flexural strength between the different sample sizes might be connected to factors outside size effect, as particular sample sizes in these two limestones have previously displayed varying results amongst each other in parameters such as open porosity/apparent density (section 4.3.3) and water absorption coefficient (section 4.3.4), unlike the previously analyzed granites, marbles and limestones.

In terms of the relation between sample size and flexural strength measured, linear regressions used to describe it present slopes of -0.10 and -0.22 for Limestone MC and MM samples, with coefficients of determination of 54.88% and 67.99%, whose higher approximation rate values are in part due to a relatively lower amount of dispersion in flexural strength values obtained for these two limestones, with standard deviation values that remain below 1.00 MPa in Limestone MC samples and below 0.53 MPa in Limestone MM samples.

Overall, the results obtained from the determination of flexural strength in limestone samples with thickness below the standard for testing, of 25 mm, show that the smaller sample dimensions are,

on average, almost always displaying values for flexural strength that are either higher or relatively equal to the ones obtained from sample sizes within regulation (Table 9). The only cases where this phenomenon doesn't occur is in the 10 mm thick samples of Limestone AV, a limestone which characterized by a large presence of fracturing and subsequent high statistical dispersion, and the 20 mm thick samples of Limestone MC, whose lower values in flexural strength might be tied to characteristics specific to this set of samples, as they displayed varying results in other parameters measured.

However, the actual variation of flexural strength that's observed is also, in most cases, either relatively small or negligible, only being considerable in the results obtained from the Limestone MM samples, which similarly to what occurs in the Limestone MC, could be a biproduct of differences in characteristics between sets of sample sizes of this limestone, rather than a direct product of sample size variations.

Table 9 – Comparison between average flexural strength results for Limestone GM, MG, MMF, AV, MC and MM samples of sizes with 10 mm, 20 mm and 50 mm thickness, with samples of 25 mm thickness, the minimum required.

	Average flexural strength (MPa)				*Ratio of average flexural strengths*		
	10mm	20mm	25mm	50mm	10/25mm	20/25mm	50/25mm
Limestone GM	12.26 ± 0.72	12.54 ± 1.01	10.14 ± 0.84	9.94 ± 1.40	**1.21**	**1.24**	**1.02**
Limestone MG	10.37 ± 1.06	11.34 ± 0.58	9.53 ± 1.09	8.7 ± 1.04	**1.09**	**1.19**	**1.10**
Limestone MMF	16.48 ± 1.17	18.19 ± 0.95	14.59 ± 1.20	15.15 ± 2.19	**1.13**	**1.25**	0.96
Limestone AV	14.41 ± 1.33	18.11 ± 0.98	15.30 ± 1.71	12.18 ± 3.77	0.94	**1.18**	**1.26**
Limestone MC	13.67 ± 0.92	9.84 ± 1.00	10.25 ± 0.74	9.07 ± 0.61	**1.33**	0.96	**1.13**
Limestone MM	15.13 ± 0.35	13.47 ± 0.53	7.05 ± 0.36	6.35 ± 0.35	**2.15**	**1.91**	**1.11**

4.3.7. Principal Component Analysis in limestone samples

The principal component analysis for the limestone samples tested was conducted using same parameters used previously for granite and marble samples, in sections 4.1.7 and 4.2.7, with results from flexural strength (MPa), sample thickness (mm), p-wave propagation velocity in the direction of length, width and height (m/s), the Birch coefficient (%) and open porosity (%), for sample sizes of 10 mm, 20 mm and 25 mm. In the case of Limestone GM samples, the resulting principal component plot (Figure 61) represents 75.2% of the variation present in the parameters mentioned, with sample thickness, P-wave propagation velocities and Birch coefficient weighing heavily on PC1, while PC2 is mainly defined by the variations in open porosity and flexural strength, with these last two having a strong positive correlation.

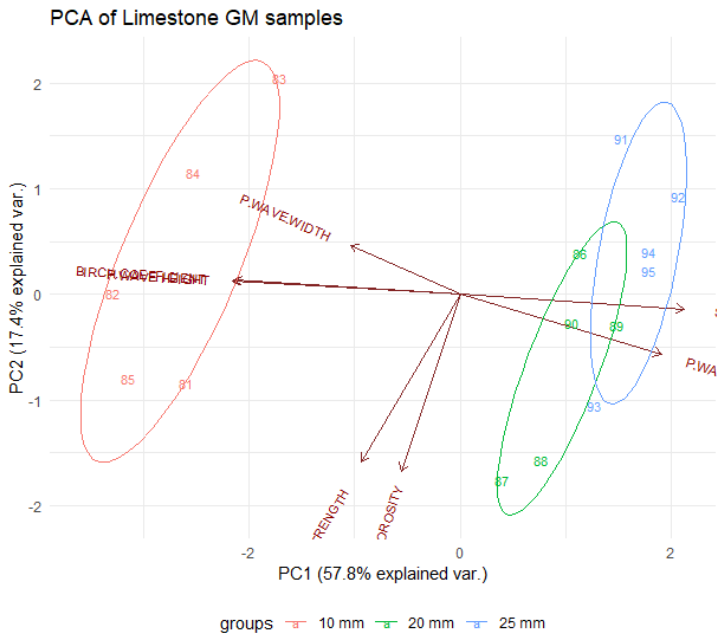

Figure 61 – PCA plot of the two main components PC1 and PC2, for the parameters of flexural strength (MPa), sample thickness (mm), p-wave propagation velocity in the direction of length, width and height (m/s), the Birch coefficient (%) and open porosity (%), obtained in Limestone GM samples.

This positive correlation with open porosity also occurs in the Limestone MG, although to a lesser extent, where the principal component analysis covered 83.7% of all variation, while in the Limestone MMF, flexural strength only bears a slight correlation with P-wave propagation velocity parallel to sample width. In these 3 limestones, flexural strength and sample thickness present a very low likelihood of being correlated, as vectors defining these parameters are always close to 90° apart. In the case of Limestone AV samples, whose principal component analysis covered for 85.6% of the parameters' variation within its two main components, there is a slight correlation between sample thickness and flexural strength variations, however, an inverse correlation with porosity is more apparent, which could indicate that the much higher presence of fissures and microfractures in this limestone's samples, relative to others, affects the resulting variation of flexural strength values.

The plot of the principal component analysis conducted with the results from the Limestone MC samples (Figure 62) describes 93.8% of the variation from its parameters, through the two principal components of PC1 and PC2, in which it's possible to observe that flexural strength variation is decently and inversely correlated with variations in not only sample thickness, but also open porosity, while having a slight positive correlation with P-wave propagation velocities and Birch coefficient.

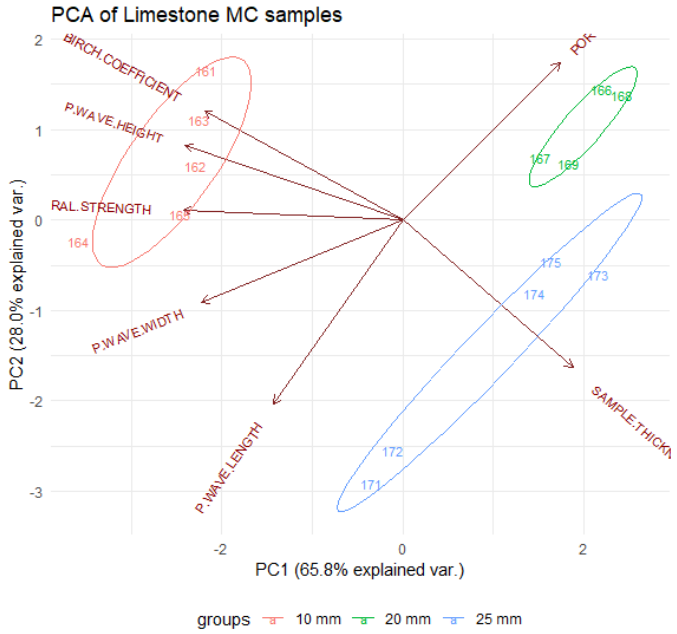

Figure 62 – PCA plot of the two main components PC1 and PC2, for the parameters of flexural strength (MPa), sample thickness (mm), p-wave propagation velocity in the direction of length, width and height (m/s), the Birch coefficient (%) and open porosity (%), obtained in Limestone MC samples.

These correlations imply that, for the results observed in the 10 mm, 20 mm and 25 mm thick samples, flexural strength variation between differing sample sizes could be, in part, a product of varying characteristics between these sample sets, as was pointed out in sections 4.3.3, 4.3.4 and 4.3.5, when analyzing results from open porosity (and apparent density), water absorption and P-wave propagation velocity tests.

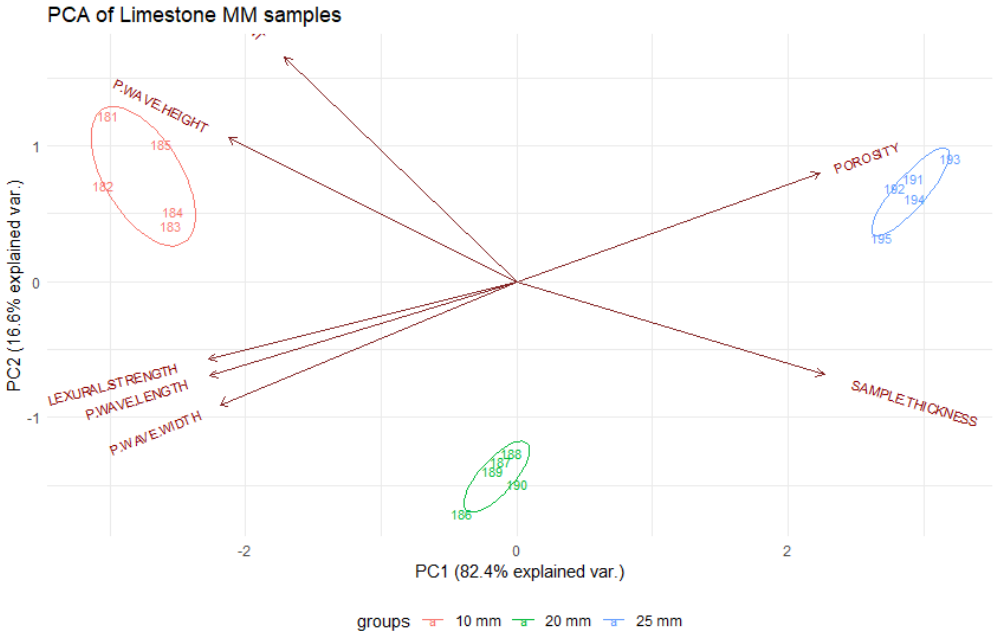

Figure 63 – PCA plot of the two main components PC1 and PC2, for the parameters of flexural strength (MPa), sample thickness (mm), p-wave propagation velocity in the direction of length, width and height (m/s), the Birch coefficient (%) and open porosity (%), obtained in Limestone MM samples.

.

A similar occurrence can be observed in the resulting plot for Limestone MM samples (Figure 63), where the two principal components, of PC1 and PC2, describe a staggering 99.00% of variation in results from the parameters in study. Through this, it's possible to observe a very strong inverse correlation of flexural strength and P-wave propagation velocities against open porosity, and a less salient inverse correlation with sample thickness, a factor which, as previously suggested in the flexural strength analysis, implies that the large variations in flexural strength observed between the 10 mm, 20 mm and 25 mm thick samples, are in fact skewed due to differing inherent characteristics between each of these sample sizes, on top of any effect of sample size variation, and not through it alone.

5. Final remarks

5.1.1. Conclusions

The purpose of the work carried out in this study is aimed towards a better understanding of the impact of sample size in the determination of a natural stone's flexural strength, particularly in regards to sizes below the minimum stipulated for testing this property, in which a limitation of 25 mm in thickness is described by the standard EN 12372 for flexural strength determination. This understanding is currently necessitated due to natural stone applications such as cladding, in which a stone panel's thickness is often inferior to 25 mm, even though their application and dimensioning takes into consideration the flexural strength value obtained in previously tested samples, whose thickness doesn't go below the minimum allowed of 25 mm.

Given the overall results of flexural strength obtained from the 200 samples of Portuguese granites, marbles and limestones, it's relatively straightforward to conclude that that a reduction in sample sizes, to below the standard minimum of 25 mm in thickness, does present, for the most part, an increase in flexural strength values. However, it's important to contextualize the increases observed, as not only do they, more often than not, occur as just marginal differences that often do not go beyond the statistical dispersion of the results, but they also do not present a direct inverse correlation with the reduction in sample size, presenting instead a set of increases and decreases in flexural strength averages that shape into a tenuous tendency (a fact highlighted by the generally low coefficients of determination obtained for any form of regression attempted).

The cases in which a decrease of flexural strength did appear to reflect a stronger relation to size effect occurred on the Granite AM, the Limestone MC and the Limestone MM, either through a more direct correlation between the two properties (Granite AM) or through a higher magnitude in the variations of flexural strength observed (Limestones MC and MM). In all these three natural stones, however, the determination of other physical properties, as well as stereomicroscopic analysis, was fundamental to understand that these variations of flexural strength were more than the sole product of a change in sample size, but also from other factors. For the limestones mentioned, and particularly for the Limestone MM, a variation in properties such as open porosity and P-wave propagation velocity between different sets of sample sizes proved to be more likely correlated to the variations in flexural strength observed, rather than the variation of sample thickness itself, implying that differences in characteristics, such as the connected pore structure, between the sets of 10 mm, 20 mm and 25 mm thick samples resulted in a skewing of the results obtained. In the case of the Granite AM, the different behavior observed is most likely connected to the fact that its degree of weathering is much higher than any other stone tested. As such, for cases like these, concluding remarks regarding size effect on flexural strength cannot be made without better understanding how these factors affect the variations in results observed.

Despite this, the fact is that, looking at the comparisons between the average flexural strength results obtained, the samples with thickness smaller than the minimum allowed by the EN 12372

standard do present values that are either slightly higher, or on equal terms to the values obtained for the 25 mm thick samples. In terms of natural stone application, however, this factor wouldn't be too relevant: an undervaluation of flexural strength through a laboratory testing, which follows the current minimum allow test sample dimensions, would only imply that in applications such as stone cladding with dowel anchorage, for example, these thinner natural stones would just present an actual higher resistance to bending stress, and consequently a higher partial safety factor (Camposinhos *et al.*, 2008; Camposinhos, 2012). In the samples tested, the only occurrences where a smaller set of samples has not presented a higher average flexural strength, are in the 20 mm thick samples in Limestone MC and Marble RC, and in the 10 mm thick samples of Limestone AV, but in either of these cases, the decrease observed relative to 25 mm thick samples is negligible, when compared to the statistical dispersion and the differences that also occur between samples of 25 mm and 50 mm thickness, or as mentioned earlier for the Limestone MC, due to variations in properties among the different samples sizes themselves.

5.1.2. Future Works

As per what's observed in the discussion of results and the presented conclusions, it is suggested that for future works in size effect in flexural strength of natural stone, certain deliberations should be taken into consideration, such as a more thorough study of petrographic properties in different natural stones, in particular with microscopic analysis; a more in-depth description and quantification of occurrences of fissures and microfracturing, a granulometric evaluation of a sample's composition, and a more complete determination of anisotropy, to further understand how heterogeneity in natural stone impacts the size effect observed. There's also a necessity for samples of each natural stone in study to be as homogenous as possible among themselves, as to avoid fluctuations in flexural strength that are a product of characteristics other than sample size, as was observed in the case of the Limestone MM samples.

Besides this, to better comprehend how the thickness affects flexural strength in a practical sense, a study on size effect on the natural stone's resistance in the various methods of application of stone cladding or roofing slates, where the thinner dimensions are currently being used, should be performed.

6. References

ASTM Committee D-18 on Soil and Rock. (2008). Standard test method for laboratory determination of pulse velocities and ultrasonic elastic constants of rock. ASTM International.

Aydin, A. (2013). Upgraded ISRM suggested method for determining sound velocity by ultrasonic pulse transmission technique. ISRM Suggested Methods for Rock Characterization, Testing and Monitoring: 2007-2014, pp. 95-99.

Bažant, Z. P. (1999). Size effect on structural strength: a review. Archive of applied Mechanics, Vol. 69, nº9, pp. 703-725.

Bellopede, R., Marini, P., & Collaro, L. (2015). Size effect in flexural strength test on dimension stones. Engineering Geology for Society and Territory, Vol. 5. pp. 303-307.

Bianconi, F., Bello, R., Fernández, A., & González, E. (2015) On comparing colour spaces from a performance perspective: application to automated classification of polished natural stones. New Trends in Image Analysis and Processing – ICIAP 2015 Workshops, pp. 71-78.

Birch, F. (1961). The velocity of compressional waves in rocks to 10 kilobars: Part 2. Journal of Geophysical Research, Vol. 66, nº7, pp. 2199-2224.

Birchall, J. D., Howard, A. J., & Kendall, K. (1981). Flexural strength and porosity of cements. Nature, Vol. 289, pp. 388-390.

Camposinhos, R. S. (2014). Stone cladding engineering, pp. 18-32.

Camposinhos, R. S. (2012). Dimension stone design–partial safety factors: a reliability based approach. Proceedings of the Institution of Civil Engineers-Construction Materials, Vol. 165, nº3, pp. 145-159.

Camposinhos, R. S., Amaral, P. M., Rosa, L. G., & Pires, V. (2008). Dimension stone cladding design – Dowel anchorage design. Second International Congress of Dimension Stones, pp. 203-207.

Çelik, M. Y., Akbulut, H., & Ergül, A. (2014). Water absorption process effect on strength of Ayazini tuff, such as the uniaxial compressive strength (UCS), flexural strength and freeze and thaw effect. Environmental Earth Sciences, Vol. 71, nº9, pp. 4247-4259.

Chadwick, A.C., Kentridge R.W. (2015). The perception of gloss: A review. Vision Research, Vol. 109, Part B, pp. 221-235.

European Committee for Standardization (1999). EN 1925 Natural stone test methods – Determination of water absorption coefficient by capillarity.

European Committee for Standardization (2006). EN 1936 Natural stone test methods – Determination of real density and apparent density, and of total and open porosity.

European Committee for Standardization (2006). EN 12372 Natural stone test methods – Determination of flexural strength under concentrated load.

European Committee for Standardization (2008). EN 13161 Natural stone test methods – Determination flexural strength under constant moment.

European Committee for Standardization (2021). prEN 12372 Natural stone test methods – Determination of flexural strength under concentrated load.

Fan, X., Lin, H., & Cao, R. (2019). Bending properties of granite beams with various section-sizes in three-point bending tests. Geotechnical and Geological Engineering, Vol. 37, pp. 1-11.

Fener, M. (2011). The effect of rock sample dimension on the P-wave velocity. Journal of Nondestructive Evaluation, Vol. 30, nº2, pp. 99-105.

Fernandes, J. C., Pires, V., Amaral, P. M., & Rosa, L. G. (2010). Analysis of strength scaling effect in Portuguese limestone: comparison between three-and four-point bending tests. Materials Science Forum, Vol. 636, pp. 1336-1341.

Gonçalves, T. C. D. (2007). Salt crystallization in plastered or rendered walls. Doctorate Thesis in Civil Engineering, pp.72-76.

Hammond III, H. K., & Nimeroff, I. (1950) Measurement of sixty-degree specular gloss. Journal of Research, p. 585.

Hunt, R. W. G., & Pointer, M. R. (2011). Measuring Colour, 4th Edition. John Wiley & Sons.

Hunter, R. S. (1937). Methods of determining gloss. Journal of Research of the National Bureau of Standards, Vol. 18, pp.19-39.

IMGranit, (n.d.). Granitos, Mármore, Calcário. Retrieved October 27, 2021, from https://www.imgranit.com/granit-jaune?lang=pt

Kahraman, S., Ulker, U. & Delibalta, M. (2007). A quality classification of building stones from P-wave velocity and its application to stone cutting with gang saws. Journal of the Southern African Institute of Mining and Metallurgy, Vol. 107, nº7, pp. 427-430.

Labuz, J. F., & Biolzi, L. (2007). Experiments with rock: remarks on strength and stability issues. International Journal of Rock Mechanics and Mining Sciences, Vol. 44, nº4. pp. 525-537.

Marini, P., Bellopede, R., & Luodes, N. M. (2017). Influence of thickness on flexural strength under concentrated load of natural stone in relation to EN 12372. Quarterly Journal of Engineering Geology and Hydrogeology, Vol. 50, nº4, pp. 417-421.

MARMOFOZ, (n.d.) MARMOFOZ – Stone Specialists. Retrieved October 27, 2021, from https://www.marmofoz.com/pt/produtos/detalhes/estremoz-ruivina-clara_87076

McGrath, J. R., Beck, M., & Hill Jr, M. E. (2017). Replicating red: analysis of ceramic slip color with CIELAB color data. Journal of Archaeological Science: Reports, Vol. 14, pp. 432-438.

Nourani, M. H., Moghadder, M. T., & Safari, M. (2017). Classification and assessment of rock mass parameters in Choghart iron mine using P-wave velocity. Journal of Rock Mechanics and Geotechnical Engineering, Vol. 9, nº2, pp. 318-328.

Primeira Pedra, (n.d.). First Stone – Primeira pedra. Retrieved October 27, 2021, from http://www.primeirapedra.com/stones/moca-creme-perlina/

Rajadell Rojas, O., & García Sevilla, P. (2008). Influence of color spaces over texture characterization. Research in Computing Science (1870-4069), Vol. 38, pp. 273-281.

ROP/LNEG, (n.d.) Rochas Ornamentais Portuguesas. Instituto Nacional de Engenharia, Tecnologia e Inovação I.P. Retrieved October 27, 2021, from https://rop.lneg.pt/rop/FormTipo.php

Sanmartín, P.; Silva-Sánchez, N.; Martínez-Cortizas, A.; Prieto, B. (2015). Usual and unusual CIELAB color parameters for the study of peat organic matter properties: Tremoal do Pedrido bog (NW Spain). Journal of Physics: Conference Series, Vol. 605, No. 1, p. 012014.

Sanmartín, P., Silva, B., Prieto, B. (2011). Effect of surface finish on roughness, color, and gloss of ornamental granites. Journal of materials in civil engineering, Vol. 23, nº8, pp. 1239-1248.

Schrenk, S. (2020) Natural stone cladding: anchored in the past, but ready for the future. Polycor. Retrieved October 27, 2021, from https://blog.polycor.com/natural-stone-cladding-anchored-in-the-past-but-ready-for-the-future

Tkalcic, M., & Tasic, J. F. (2003). Colour spaces: perceptual, historical and applicational background. The IEEE Region 8 EUROCON 2003. Computer as a Tool, Vol. 1, pp. 304-308.

Wang, L., Huang, T., Kamal, M. R., and Rey, A. D. (2000). The surface topography and gloss of polyolefin blown films. Polymer Engineering and Science, Vol. 40, nº3, pp. 747–760.

Weibull, W. (1949). A statistical representation of fatigue failures in solids. Transactions of the Royal Institute of Technology, Vol. 27, pp. 1–50.

Winkler, M. E. (1997). Stone in Architecture: Properties, Durability. Springer Science & Business Media, pp. 91-109.

Yagiz, S. (2011). P-wave velocity test for assessment of geotechnical properties of some rock materials. Bulletin of Materials Science, Vol. 34, nº4, pp. 947-953.

Yam, K. L., & Papadakis, S. E. (2004). A simple digital imaging method for measuring and analyzing color of food surfaces. Journal of food engineering, Vol. 61, pp. 137-142.

Appendices

Appendix A – Sample Measurements

Table 10 – Measurements for sample length (top) and sample width (bottom).

Length (mm)										
Sample	**AM**	**CV**	**EC**	**RC**	**GM**	**MG**	**MMF**	**AV**	**MC**	**MM**
1	59.76	59.81	58.91	60.33	59.73	60.05	60.06	60.55	59.57	60.59
2	60.16	59.84	59.47	60.35	59.94	60.14	60.09	61.56	60.95	59.84
3	60.11	60.10	59.79	60.31	59.88	60.16	59.94	61.38	61.04	60.84
4	60.05	60.05	60.45	60.37	59.76	59.71	57.31	61.64	60.72	60.26
5	60.17	60.61	60.15	60.36	60.08	60.03	59.76	59.82	59.51	60.30
6	120.44	120.39	120.42	120.43	119.31	120.13	119.52	120.80	120.82	120.77
7	119.86	119.98	120.49	120.54	119.67	120.15	119.91	121.11	121.07	121.23
8	120.07	120.13	120.26	120.52	120.13	119.77	120.04	120.80	120.76	121.22
9	120.35	119.23	120.38	120.56	119.68	119.62	120.01	120.71	121.20	120.70
10	120.45	119.35	120.59	120.52	120.26	119.71	119.61	121.04	121.11	120.75
11	150.06	150.30	150.19	150.46	150.12	150.87	150.90	149.35	150.46	149.40
12	149.72	149.42	150.47	150.47	150.70	150.75	150.78	151.44	150.40	150.91
13	150.09	149.62	150.41	150.51	150.56	150.42	151.02	152.07	151.40	150.24
14	150.31	150.39	150.39	150.52	150.66	151.01	150.68	150.82	150.84	150.21
15	149.87	149.61	150.48	150.55	151.08	150.96	150.76	150.04	150.85	151.40
16	300.00	299.50	300.00	300.50	301.00	300.50	300.00	300.00	300.50	300.50
17	300.50	299.50	300.00	300.50	300.50	300.00	300.50	300.50	300.50	300.50
18	300.00	300.00	300.50	301.00	301.00	300.50	300.00	300.00	301.00	300.50
19	300.00	300.50	300.00	300.50	300.00	300.00	300.00	300.00	301.00	300.50
20	300.00	300.00	300.00	300.50	300.00	300.00	300.00	300.50	300.50	301.50
Width (mm)										
Sample	**AM**	**CV**	**EC**	**RC**	**GM**	**MG**	**MMF**	**AV**	**MC**	**MM**
1	50.01	50.08	50.35	49.73	50.43	50.33	49.96	51.01	50.85	50.99
2	50.06	50.15	50.34	49.98	50.38	50.39	49.90	51.12	50.50	51.10
3	49.99	50.07	50.35	49.92	50.44	50.38	49.75	50.87	50.77	50.76
4	50.04	50.18	50.32	49.74	50.46	50.39	49.74	50.87	50.54	50.76
5	50.03	50.17	50.33	49.93	50.40	50.43	49.84	51.08	50.85	51.10
6	50.07	50.00	50.39	50.49	50.44	50.45	49.90	51.25	50.74	51.16
7	50.01	50.11	50.38	50.52	50.54	50.44	49.97	50.59	50.98	51.20
8	50.05	49.92	50.35	50.52	50.46	50.43	50.01	50.60	51.04	50.67
9	50.02	49.88	50.38	50.44	50.51	50.41	50.12	50.62	50.73	50.76
10	50.12	49.93	50.36	50.33	50.46	50.39	49.95	51.18	50.76	50.61
11	50.02	50.01	50.32	50.20	51.54	50.39	50.00	50.87	49.86	50.95
12	50.03	50.05	50.30	50.52	51.14	50.39	49.88	50.86	49.75	51.00
13	50.03	50.11	50.31	50.51	50.28	50.40	51.65	50.90	49.72	50.10
14	50.03	50.10	50.32	50.27	50.27	50.35	49.93	50.34	51.13	50.92
15	50.04	50.19	50.28	50.23	50.24	50.37	49.80	50.69	49.75	50.94
16	50.03	50.21	50.70	50.26	50.10	50.50	49.96	50.83	51.63	50.80
17	49.92	50.19	50.68	50.40	50.07	50.48	50.23	50.68	51.64	50.94
18	50.01	50.23	50.64	50.20	49.97	50.57	51.49	50.73	51.09	50.96
19	49.87	50.24	50.25	50.29	50.32	50.57	49.76	50.59	51.63	49.81
20	50.12	49.97	50.56	50.26	50.03	50.53	49.90	50.74	51.27	50.04

Table 11 – Measurements for sample height.

Height (mm)										
Sample	**AM**	**CV**	**EC**	**RC**	**GM**	**MG**	**MMF**	**AV**	**MC**	**MM**
1	10.10	9.88	10.06	9.74	10.55	10.57	10.18	10.59	11.38	9.76
2	10.02	9.73	10.05	9.79	10.56	10.51	9.96	10.52	11.42	10.15
3	10.18	9.82	10.08	9.81	10.58	10.62	9.83	10.39	11.41	10.13
4	10.08	9.72	10.03	9.80	10.55	10.61	9.86	10.37	11.42	10.20
5	10.13	9.71	10.37	9.82	10.47	10.65	9.87	10.52	11.37	10.03
6	20.49	20.04	20.48	20.04	20.31	20.31	20.17	20.58	19.05	20.97
7	20.17	19.80	20.41	19.92	20.49	20.23	20.21	20.63	18.70	20.96
8	20.04	19.82	19.56	19.47	20.31	20.25	20.24	20.45	18.88	20.94
9	19.89	19.83	19.85	19.82	20.44	20.16	20.44	20.61	18.37	20.97
10	20.14	19.89	19.95	19.53	20.29	20.13	20.20	20.58	19.01	20.97
11	26.02	25.51	25.16	24.83	25.05	25.23	25.04	24.96	25.18	25.24
12	26.01	24.96	25.26	24.65	25.23	25.25	25.17	25.11	25.26	25.14
13	25.99	25.24	25.26	24.88	25.11	25.22	25.13	25.06	25.29	25.06
14	25.89	24.87	25.33	24.82	24.96	25.09	25.19	25.24	25.17	25.13
15	25.98	24.93	25.26	24.69	24.92	25.28	25.08	24.95	25.37	25.24
16	28.88	30.46	50.27	50.26	50.30	50.76	50.45	51.11	50.03	50.44
17	28.43	30.14	50.26	50.28	50.29	50.23	50.29	52.03	49.95	50.59
18	28.97	30.47	50.31	50.20	49.59	50.52	50.40	51.82	49.93	50.50
19	28.54	30.50	50.55	50.28	50.35	50.32	50.33	52.22	50.07	50.40
20	28.60	30.73	50.24	50.40	49.66	50.55	50.34	52.30	49.76	50.40

Appendix B – Sample Color and Gloss

Table 12 – Measurements of gloss and color coordinates L, a*, b* and c* for Granite AM, Granite CV and Marble RC samples.*

Granite AM					
Sample	**Gloss**	**L***	**a***	**b***	C^*_{ab}
1	1.30	75.92	1.66	9.59	9.74
2	1.30	74.52	1.43	9.21	9.33
3	1.40	75.63	1.91	10.80	10.98
4	1.30	77.90	1.49	10.32	10.43
5	1.50	77.72	1.99	10.01	10.22
6	1.30	73.28	1.75	9.71	9.87
7	1.40	74.77	1.98	9.43	9.64
8	1.30	73.43	1.87	10.29	10.48
9	1.30	77.25	1.85	9.76	9.93
10	1.30	73.95	1.72	9.78	9.93
11	1.50	70.97	2.06	9.83	10.05
12	1.30	73.73	2.13	11.65	11.85
13	1.40	75.71	1.67	10.50	10.64
14	1.40	71.25	1.93	10.50	10.69
15	1.40	74.02	1.83	10.60	10.76
Granite CV					
Sample	**Gloss**	**L***	**a***	**b***	C^*_{ab}
1	1.90	76.42	0.18	1.78	1.80
2	2.00	77.31	0.05	2.57	2.60
3	1.80	71.75	-0.01	0.68	0.78
4	1.80	74.86	-0.02	1.73	1.76
5	2.10	76.18	0.09	1.73	1.75
6	1.90	75.76	-0.15	1.65	1.66
7	2.20	75.73	-0.24	1.84	1.88
8	1.90	75.46	-0.21	1.84	1.86
9	1.90	73.73	-0.23	1.51	1.55
10	2.10	74.60	-0.12	1.99	2.02
11	1.70	75.26	-0.13	1.48	1.55
12	1.90	76.32	-0.10	1.24	1.31
13	1.80	75.72	-0.07	1.88	1.90
14	1.90	74.44	0.05	1.75	1.77
15	2.10	73.63	-0.24	1.59	1.64
Marble RC					
Sample	**Gloss**	**L***	**a***	**b***	C^*_{ab}
1	1.90	76.74	-1.19	-1.91	2.25
2	1.60	77.54	-1.16	-1.77	2.11
3	1.90	78.13	-1.10	-1.81	2.12
4	1.80	76.84	-1.10	-1.90	2.20
5	1.60	76.35	-1.23	-2.24	2.56
6	1.80	76.12	-1.21	-1.78	2.15
7	1.50	76.17	-1.16	-1.91	2.24
8	1.70	77.09	-1.12	-1.57	1.94
9	1.70	77.65	-1.09	-1.47	1.84
10	1.60	76.44	-1.15	-1.40	1.81
11	1.60	74.47	-1.20	-1.93	2.28
12	1.50	74.17	-1.21	-1.89	2.26
13	1.60	75.08	-1.23	-2.07	2.41
14	1.60	75.43	-1.26	-2.09	2.44
15	1.70	75.59	-1.21	-2.01	2.34

Table 13 – Measurements of gloss and color coordinates L, a*, b* and c* for Marble EC, Limestone GM and Limestone MG samples.*

Marble EC					
Sample	**Gloss**	**L***	**a***	**b***	C^*_{ab}
1	2.60	88.30	-0.58	1.08	1.24
2	2.10	88.47	-0.42	1.34	1.51
3	2.20	88.04	-0.66	0.77	1.09
4	2.10	88.29	-0.55	1.00	1.15
5	2.40	88.27	-0.63	0.79	1.04
6	2.40	88.67	-0.63	1.34	1.48
7	2.20	88.15	-0.53	2.53	2.60
8	2.30	88.30	-0.59	1.64	1.77
9	2.10	87.17	-0.61	1.58	1.73
10	2.20	88.35	-0.44	1.74	1.83
11	2.10	87.09	0.46	2.99	3.05
12	2.20	87.59	0.37	2.62	2.69
13	2.20	88.08	-0.52	1.60	1.71
14	1.90	86.22	0.66	3.21	3.42
15	2.10	87.99	-0.23	1.69	1.78
Limestone GM					
Sample	**Gloss**	**L***	**a***	**b***	C^*_{ab}
1	1.50	82.65	2.28	6.21	6.62
2	1.50	82.56	2.18	5.93	6.32
3	1.50	82.13	2.16	5.51	5.92
4	1.50	82.72	2.19	5.81	6.21
5	1.50	82.61	2.16	5.70	6.10
6	1.50	82.53	2.26	6.22	6.62
7	1.50	82.69	2.32	6.35	6.76
8	1.60	82.95	2.25	6.35	6.74
9	1.60	82.88	2.22	6.31	6.69
10	1.60	83.02	2.08	5.91	6.26
11	1.70	82.08	2.12	5.81	6.18
12	1.70	82.99	2.14	6.13	6.49
13	1.60	83.44	2.18	6.59	6.95
14	1.60	82.96	2.21	6.59	6.95
15	1.60	83.27	2.21	6.48	6.84
Limestone MG					
Sample	**Gloss**	**L***	**a***	**b***	C^*_{ab}
1	1.80	85.70	2.16	6.01	6.38
2	1.70	85.23	2.25	6.23	6.62
3	1.80	85.69	2.16	6.01	6.39
4	1.80	85.23	2.20	5.84	6.24
5	1.70	85.54	2.24	6.33	6.72
6	1.70	85.73	2.36	6.63	7.04
7	1.80	83.88	2.77	6.95	7.48
8	1.70	84.02	2.70	7.39	7.89
9	1.60	85.18	2.48	6.82	7.26
10	1.70	84.76	2.48	6.29	6.76
11	1.70	85.54	2.06	5.79	6.15
12	1.80	85.58	2.01	5.67	6.01
13	1.60	85.26	2.19	5.92	6.31
14	1.80	85.71	2.08	5.71	6.07
15	1.80	85.44	2.15	5.88	6.27

Table 14 – Measurements of gloss and color coordinates L, a*, b* and c* for Limestone MMF, Limestone AV and Limestone MC samples.*

Limestone MMF					
Sample	**Gloss**	**L***	**a***	**b***	C^*_{ab}
1	1.60	83.60	2.29	5.53	5.98
2	1.60	83.77	2.24	5.66	6.09
3	1.70	84.21	2.04	5.40	5.77
4	1.60	83.65	2.12	5.48	5.87
5	1.60	84.04	2.12	5.57	5.96
6	1.70	83.78	2.13	5.41	5.82
7	1.70	83.70	2.12	5.30	5.71
8	1.70	83.82	2.14	5.43	5.84
9	1.60	83.39	2.16	5.37	5.79
10	1.70	83.93	2.11	5.49	5.89
11	1.80	84.05	2.08	5.73	6.10
12	1.90	83.32	1.97	5.74	6.08
13	1.70	83.05	2.05	5.30	5.68
14	1.80	83.92	2.14	5.79	6.17
15	1.60	83.58	2.17	5.98	6.36
Limestone AV					
Sample	**Gloss**	**L***	**a***	**b***	C^*_{ab}
1	1.30	75.55	0.65	4.23	4.28
2	1.30	75.72	0.63	4.43	4.47
3	1.30	75.63	0.60	4.11	4.16
4	1.20	76.63	0.40	3.58	3.60
5	1.30	77.42	0.23	3.06	3.08
6	1.20	71.67	0.58	3.64	3.69
7	1.20	71.26	0.52	3.57	3.61
8	1.10	72.86	0.43	3.89	3.91
9	1.20	71.45	0.68	4.26	4.31
10	1.30	72.02	0.43	3.62	3.64
11	1.40	76.52	0.59	3.78	3.83
12	1.40	77.44	0.62	3.96	4.01
13	1.50	77.59	0.67	4.17	4.23
14	1.50	77.77	0.44	3.37	3.40
15	1.50	77.53	0.68	4.19	4.25
Limestone MC					
Sample	**Gloss**	**L***	**a***	**b***	C^*_{ab}
1	1.60	86.25	2.23	6.41	6.79
2	1.60	86.18	2.23	6.13	6.52
3	1.60	87.14	2.10	6.11	6.46
4	1.60	86.39	2.03	5.79	6.14
5	1.60	86.59	1.93	5.67	5.99
6	1.50	87.77	2.34	7.23	7.60
7	1.40	87.94	2.29	6.74	7.12
8	1.40	87.43	2.30	6.70	7.08
9	1.40	86.69	2.25	6.29	6.68
10	1.50	87.51	2.20	6.56	6.92
11	1.50	85.97	2.35	6.70	7.11
12	1.80	86.61	2.15	6.37	6.73
13	1.60	87.24	2.05	6.23	6.56
14	1.70	86.94	2.14	6.38	6.73
15	1.60	86.67	2.20	6.71	7.06

Table 15 – Measurements of gloss and color coordinates L, a*, b* and c* for Limestone MM samples.*

Limestone MM					
Sample	**Gloss**	**L***	**a***	**b***	C^*_{ab}
1	1.60	85.37	2.46	6.31	6.77
2	1.60	84.72	2.58	6.82	7.29
3	1.60	84.77	2.59	6.87	7.34
4	1.60	84.96	2.61	6.96	7.44
5	1.60	85.36	2.47	6.53	6.99
6	1.60	87.14	2.03	6.11	6.44
7	1.60	87.61	2.06	6.33	6.66
8	1.60	86.28	2.49	7.26	7.68
9	1.60	86.84	2.12	6.51	6.85
10	1.50	86.84	2.34	6.73	7.13
11	1.50	87.96	2.15	7.60	7.90
12	1.40	86.74	2.49	8.51	8.87
13	1.40	87.22	2.33	8.34	8.66
14	1.40	86.07	2.48	8.16	8.53
15	1.40	86.26	2.59	8.44	8.83

Appendix C – Sample Open Porosity and Apparent Density

Table 16 – Results obtained for open porosity and apparent density, in 10 mm, 20 mm and 25 mm thick samples.

Open Porosity (%)										
Sample	**AM**	**CV**	**RC**	**EC**	**GM**	**MG**	**MMF**	**AV**	**MC**	**MM**
1	2.66%	1.56%	0.54%	0.59%	5.24%	7.08%	4.60%	4.45%	7.68%	8.82%
2	2.39%	1.04%	0.57%	0.62%	4.96%	6.97%	4.51%	4.31%	7.32%	8.41%
3	2.39%	1.47%	0.54%	0.65%	4.45%	7.21%	4.68%	4.60%	8.07%	8.46%
4	2.44%	1.11%	0.50%	0.99%	4.85%	6.89%	4.54%	4.27%	6.26%	8.75%
5	2.53%	1.13%	0.49%	0.55%	5.24%	6.97%	4.83%	4.29%	6.97%	8.58%
6	2.35%	0.97%	0.58%	1.01%	4.57%	7.03%	4.28%	3.16%	10.60%	8.90%
7	2.35%	0.93%	0.57%	0.59%	5.18%	7.52%	4.20%	3.12%	9.53%	9.54%
8	2.32%	0.92%	0.53%	0.60%	5.00%	6.92%	4.27%	3.20%	10.39%	9.42%
9	2.30%	0.97%	0.49%	0.51%	4.83%	7.15%	3.91%	3.11%	9.29%	9.11%
10	2.27%	0.99%	0.52%	0.52%	4.77%	5.99%	4.31%	2.46%	10.21%	9.31%
11	2.26%	0.86%	0.40%	0.49%	4.81%	6.35%	4.17%	3.66%	6.23%	13.08%
12	2.30%	0.91%	0.35%	0.44%	4.81%	5.95%	4.13%	3.20%	6.49%	12.69%
13	2.39%	0.88%	0.36%	0.41%	5.12%	6.00%	4.05%	3.59%	8.03%	13.23%
14	2.39%	0.86%	0.34%	0.41%	4.97%	5.80%	4.17%	2.87%	7.58%	12.78%
15	2.44%	0.93%	0.38%	0.46%	4.89%	6.59%	4.14%	3.50%	7.97%	12.25%
Apparent Density (kg/m^3)										
Sample	**AM**	**CV**	**RC**	**EC**	**GM**	**MG**	**MMF**	**AV**	**MC**	**MM**
1	2574.64	2604.83	2696.69	2693.08	2536.15	2486.92	2569.02	2562.51	2460.91	2437.24
2	2581.38	2617.97	2702.80	2694.84	2546.07	2488.04	2573.06	2563.85	2469.98	2450.43
3	2583.25	2607.46	2697.31	2694.77	2566.78	2478.36	2566.83	2550.62	2446.48	2448.61
4	2578.64	2616.89	2699.44	2683.09	2547.38	2486.44	2570.55	2564.81	2518.14	2440.53
5	2576.92	2614.49	2698.45	2695.39	2534.46	2487.01	2563.94	2562.57	2484.03	2443.75
6	2577.64	2618.96	2695.52	2683.20	2551.91	2481.98	2572.70	2597.77	2353.87	2423.41
7	2580.78	2606.18	2695.85	2697.32	2531.78	2466.90	2576.69	2596.68	2385.50	2402.11
8	2582.29	2636.56	2697.66	2691.73	2537.06	2481.49	2574.26	2597.54	2355.59	2408.99
9	2582.93	2617.81	2697.87	2694.81	2544.32	2474.49	2585.66	2598.96	2393.98	2416.40
10	2584.85	2619.03	2696.94	2694.64	2542.64	2510.97	2573.24	2623.76	2366.62	2408.53
11	2582.87	2619.69	2701.59	2698.56	2545.22	2504.25	2575.72	2588.87	2496.87	2270.30
12	2580.74	2618.55	2703.26	2699.64	2545.35	2515.33	2577.27	2597.58	2491.36	2278.85
13	2578.28	2618.16	2702.72	2699.48	2536.39	2515.75	2579.32	2589.07	2441.28	2266.27
14	2578.05	2621.16	2704.15	2700.61	2542.21	2520.94	2575.82	2598.28	2453.54	2276.82
15	2578.89	2618.06	2700.71	2698.71	2544.90	2497.39	2577.01	2595.36	2445.92	2284.24

Appendix D – Sample Water Absorption Coefficient

Table 17 – Water absorption coefficient and respective coefficients of determination, obtained for 20 mm and 25 mm thick samples.

Water Absorption Coefficient ($g/m^2.s^{½}$)										
Sample	**AM**	**CV**	**RC**	**EC**	**GM**	**MG**	**MMF**	**AV**	**MC**	**MM**
1	11.60	0.99	0.75	0.59	6.04	19.41	5.54	1.57	28.92	26.06
2	12.92	1.06	0.80	0.55	8.13	23.20	6.38	1.45	20.74	28.87
3	12.21	0.98	0.79	0.50	7.90	17.47	6.50	1.78	28.79	30.18
4	12.55	1.03	0.73	0.51	7.51	18.43	5.38	1.82	23.18	30.49
5	12.08	1.04	0.68	0.43	6.43	12.54	5.95	1.13	30.45	26.61
6	12.45	1.16	0.75	0.36	7.03	14.37	5.89	2.46	13.42	62.74
7	12.55	1.22	0.67	0.30	7.03	12.02	6.91	2.22	14.65	65.31
8	13.75	1.17	0.46	0.43	8.11	11.64	8.58	2.73	21.34	63.60
9	13.36	1.14	0.57	0.41	7.01	12.66	7.24	2.00	18.90	59.50
10	12.03	1.07	0.64	0.34	6.01	15.84	6.26	2.45	19.48	60.52
Coefficient of Determination (%)										
Sample	**AM**	**CV**	**RC**	**EC**	**GM**	**MG**	**MMF**	**AV**	**MC**	**MM**
1	99.81%	94.78%	92.56%	96.95%	99.10%	99.82%	99.17%	98.07%	99.76%	99.87%
2	99.45%	97.20%	89.33%	93.62%	98.87%	99.75%	98.37%	98.19%	99.61%	99.97%
3	99.86%	94.55%	87.13%	93.81%	98.59%	99.27%	99.17%	98.57%	99.19%	99.98%
4	99.91%	98.33%	73.78%	90.91%	99.09%	99.70%	98.53%	96.79%	99.54%	99.96%
5	99.79%	97.86%	86.79%	86.84%	99.22%	99.17%	99.85%	98.78%	99.56%	99.98%
6	99.97%	98.56%	87.51%	80.37%	99.09%	99.81%	97.54%	99.14%	99.90%	99.98%
7	99.86%	99.77%	93.77%	91.43%	99.65%	99.93%	98.90%	99.29%	99.87%	99.93%
8	99.88%	99.57%	88.07%	93.75%	99.76%	99.75%	98.97%	99.50%	99.93%	99.92%
9	99.94%	99.45%	86.15%	90.80%	99.82%	99.74%	99.59%	99.72%	99.88%	99.93%
10	99.84%	99.21%	86.65%	96.67%	99.94%	99.89%	99.83%	99.22%	99.77%	100.00%

Appendix E – Sample P-wave Propagation Velocity

Table 18 – P-wave propagation velocities obtained in the axes parallel to length (top) and width (bottom).

P-wave propagation velocity in length (m/s)										
Sample	**AM**	**CV**	**RC**	**EC**	**GM**	**MG**	**MMF**	**AV**	**MC**	**MM**
1	2900.97	4241.84	4462.88	5156.41	4816.94	4765.87	5222.61	4767.72	4582.31	4696.90
2	2864.76	4016.11	4188.03	5158.12	4833.87	4773.02	5225.22	4772.09	4688.46	4787.20
3	2917.96	4144.83	4599.23	5154.70	4790.40	4700.00	5212.17	4615.04	4695.38	4716.28
4	2929.27	4057.43	4444.85	5204.31	4780.80	4701.57	5210.00	4634.59	4857.60	4707.81
5	2906.76	4067.79	4235.92	5203.45	4730.71	4764.29	5151.72	4710.24	4760.80	4710.94
6	2794.43	3973.27	4378.91	5102.97	5077.02	4843.95	5312.00	4664.09	4525.09	4699.22
7	2867.46	3920.92	4349.82	5310.13	5070.76	4711.76	5329.33	4622.52	4620.99	4609.51
8	2886.30	3964.69	4310.39	5380.36	5026.36	4848.99	5382.96	4682.17	4522.85	4591.67
9	2838.44	3934.98	4330.22	5505.02	5007.53	4690.98	5405.86	4642.69	4556.39	4660.23
10	2867.86	3925.99	4033.11	5478.18	5095.76	4788.40	5316.00	4981.07	4519.03	4644.23
11	2815.38	3873.71	4378.72	5593.31	5020.74	4930.39	5351.06	4880.72	4900.98	4317.92
12	2742.12	3952.91	4746.69	5531.99	5040.13	4958.88	5309.15	5064.88	4883.12	4324.07
13	2738.87	3927.03	4715.05	5533.46	5052.35	5064.65	5336.40	4921.36	4658.46	4268.18
14	2600.52	3947.24	4947.04	5513.55	4939.67	4951.15	5305.63	4944.92	4641.23	4304.01
15	2765.13	3968.44	4491.94	5514.65	4969.74	4917.26	5308.45	4919.34	4641.54	4325.71
16	2901.40	4102.70	4784.70	5463.60	5025.00	4902.10	5444.60	5076.10	4950.60	4355.10
17	2816.30	4047.30	5050.50	5463.60	5000.00	4966.90	5309.20	4983.40	4942.40	4367.70
18	3000.00	4059.50	5375.70	5844.70	5110.40	5128.00	5434.80	5050.50	4975.20	4323.70
19	2935.40	4044.40	5474.50	5493.60	5016.70	5076.10	5464.50	4958.70	4862.70	4361.40
20	2938.30	4054.10	4846.50	5812.40	5050.50	4942.30	5454.50	5076.00	4958.70	4301.00
P-wave propagation velocity in width (m/s)										
Sample	**AM**	**CV**	**RC**	**EC**	**GM**	**MG**	**MMF**	**AV**	**MC**	**MM**
1	2890.75	4317.24	3964.57	4736.19	4849.04	4839.42	5258.95	4723.15	4581.08	4677.98
2	2910.47	4438.05	3647.83	4715.09	4891.26	4799.05	5252.63	4777.57	4675.93	4731.48
3	2957.99	4353.91	4303.42	4846.60	4897.09	4708.41	5236.84	4582.88	4657.80	4656.88
4	2926.32	4252.54	3494.44	4829.13	4899.03	4753.77	5181.25	4710.19	4679.63	4656.88
5	2942.94	4215.97	3841.98	5094.90	4893.20	4802.86	5246.32	4686.24	4708.33	4645.45
6	2594.30	4201.68	3846.56	4104.88	4850.00	4804.76	5252.63	4701.83	4300.00	4693.58
7	2717.93	4175.83	3966.93	4377.82	4906.80	4758.49	5260.00	4599.09	4357.26	4612.61
8	2734.97	4230.51	3729.63	4470.80	4760.38	4757.55	5209.38	4819.05	4325.42	4606.36
9	2718.48	4156.67	3845.80	4544.14	4720.56	4755.66	5220.83	4730.84	4450.00	4614.55
10	2753.85	4267.52	3473.10	4617.43	4851.92	4799.05	5257.89	5118.00	4265.55	4600.91
11	2733.33	4033.06	3755.22	4735.85	4955.77	4845.19	5208.33	4844.76	4748.57	4210.74
12	2719.02	4069.11	4056.45	5001.98	4779.44	4892.23	5142.27	4890.38	4649.53	4180.33
13	2592.23	3976.98	4573.64	4720.56	4881.55	4990.10	4966.35	4990.20	4323.48	4106.56
14	2452.45	4040.32	4574.55	4833.65	4787.62	4795.24	5201.04	4935.29	4407.76	4173.77
15	2633.68	4147.93	3809.09	4738.68	4784.76	4797.14	5187.50	4874.04	4326.09	4245.00
16	2960.40	4082.10	3755.60	4741.50	4817.30	4549.50	5098.00	4841.00	4825.20	4233.30
17	2655.30	3983.30	3868.70	4666.70	4861.20	4901.00	5178.40	4692.60	4569.90	4175.40
18	2841.50	3986.50	4403.50	4921.60	4947.50	4770.80	5363.50	4925.20	4602.70	4177.00
19	2833.50	3955.90	5234.40	5079.80	4792.40	4957.80	5077.60	4251.30	4528.90	4257.30
20	2800.00	4199.20	3560.60	5181.40	4904.90	4678.70	5308.50	4832.40	4577.70	4170.00

Table 19 – P-wave propagation velocities obtained in the axis parallel to height.

P-wave propagation velocity in height (m/s)										
Sample	**AM**	**CV**	**RC**	**EC**	**GM**	**MG**	**MMF**	**AV**	**MC**	**MM**
1	2885.71	6175.00	5294.74	5126.32	5861.11	5872.22	8483.33	6229.41	6322.22	6506.67
2	2783.33	6081.25	4020.00	6118.75	6211.76	5838.89	7114.29	5844.44	6010.53	6343.75
3	2827.78	6137.50	5600.00	5450.00	5568.42	5900.00	7561.54	5772.22	6338.89	5958.82
4	2880.00	5400.00	4012.00	5764.71	5861.11	5894.44	7584.62	6100.00	6344.44	6000.00
5	2813.89	5711.76	4508.70	6137.50	5816.67	6264.71	7592.31	5844.44	5984.21	6268.75
6	2410.59	4175.00	3471.19	5138.46	5077.50	5207.69	6112.12	5145.00	4646.34	4765.91
7	2553.16	4304.35	3518.97	5383.78	5122.50	5057.50	5462.16	5031.71	4794.87	4763.64
8	2505.00	4217.02	3315.25	5726.47	5077.50	4939.02	5952.94	5112.50	4720.00	4759.09
9	2652.00	4310.87	3544.64	5215.79	4866.67	5169.23	6011.76	5026.83	4710.26	4765.91
10	2456.10	4231.91	3381.36	5744.12	5072.50	5297.37	6312.50	5145.00	4526.19	4660.00
11	2344.14	4114.52	3755.22	5397.83	5010.00	5046.00	5327.66	4992.00	4842.31	4589.09
12	2322.32	4160.00	4009.52	5358.70	4947.06	4950.98	5243.75	5124.49	4857.69	4570.91
13	2147.93	4206.67	4592.73	5408.70	4923.53	4945.10	5235.42	5012.00	4516.07	4475.00
14	2332.43	4077.05	4367.24	5515.56	4800.00	5018.00	5359.57	5048.00	4576.36	4487.50
15	2061.90	4225.42	3946.88	5367.39	4792.31	5056.00	5452.17	4990.00	4698.15	4507.14
16	2256.30	3955.80	4260.20	4879.60	4836.50	4743.90	5201.00	4776.60	4632.40	4203.30
17	2221.10	3588.10	4447.80	4929.40	4882.50	4650.90	5029.00	4604.40	4849.50	4047.20
18	2541.20	3671.10	4658.30	5070.70	4814.60	4904.90	5478.30	4754.10	4943.60	4139.30
19	2378.30	3812.50	5055.00	5078.80	4936.30	4982.20	5135.70	4388.20	4768.60	4235.30
20	2648.10	4043.40	4331.00	5090.90	4868.60	4680.60	5136.70	4754.50	4878.40	4131.10

Appendix E – Sample Flexural Strength

Table 20 – Flexural strength results obtained in all sample, along with average and standard deviation values for 10 mm, 20 mm, 25 mm and 30/50 mm thick samples.

Sample	AM	CV	EC	RC	GM	MG	MMF	AV	MC	MM
1	6.14	17.89	18.12	21.86	12.22	10.75	16.58	13.96	13.76	15.48
2	6.22	13.67	15.59	22.43	13.00	10.27	16.76	15.16	14.20	15.12
3	7.55	17.78	17.12	21.38	11.91	9.56	16.70	13.09	12.18	15.17
4	7.12	17.47	15.21	22.71	11.26	11.98	17.79	16.34	14.62	15.33
5	5.90	16.92	15.25	23.04	12.90	9.31	14.57	13.48	13.59	14.56
6	5.69	17.27	13.39	21.02	12.05	10.90	-	17.19	10.91	13.42
7	5.88	14.95	16.25	23.03	13.91	11.25	16.85	17.30	10.46	13.97
8	6.67	15.87	14.37	22.09	13.17	12.02	19.11	18.65	8.91	14.03
9	6.08	17.51	17.96	24.12	11.32	11.85	18.47	19.52	9.06	13.10
10	6.55	16.58	14.52	25.60	12.24	10.70	18.33	17.89	-	12.81
11	5.63	14.49	15.51	20.40	9.41	10.34	15.48	13.21	10.37	6.68
12	4.88	15.54	15.87	20.00	9.35	8.08	15.46	17.72	10.91	7.44
13	4.57	16.26	17.17	17.76	11.19	10.83	14.69	16.00	8.99	7.12
14	5.07	16.56	17.92	18.55	9.89	9.43	14.79	14.27	10.42	7.33
15	5.34	15.71	15.99	20.03	10.87	8.96	12.54	15.31	10.56	6.68
16	4.57	12.37	13.98	18.72	9.94	8.64	16.50	15.78	9.53	6.68
17	4.81	14.70	15.83	17.22	11.26	7.99	16.62	12.24	9.00	5.84
18	5.74	14.90	16.51	21.71	7.62	10.52	11.34	14.12	8.81	6.30
19	4.92	13.31	20.52	19.69	10.08	8.23	15.24	5.88	8.23	6.67
20	4.64	14.77	14.84	22.04	10.79	8.14	16.03	12.87	9.79	6.24
$\bar{x}$(10mm)	6.58	16.75	16.26	22.29	12.26	10.37	16.48	14.41	13.67	15.13
σ(10mm)	± 0.71	± 1.76	± 1.30	± 0.66	± 0.72	± 1.06	± 1.17	± 1.33	± 0.92	± 0.35
$\bar{x}$(20mm)	6.17	16.44	15.30	23.17	12.54	11.34	18.19	18.11	9.84	13.47
σ(20mm)	± 0.42	± 1.05	± 1.81	± 1.78	± 1.01	± 0.58	± 0.95	± 0.98	± 1.00	± 0.53
$\bar{x}$(25mm)	5.10	15.71	16.49	19.35	10.14	9.53	14.59	15.30	10.25	7.05
σ(25mm)	± 0.41	± 0.80	± 1.01	± 1.14	± 0.84	± 1.09	± 1.20	± 1.71	± 0.74	± 0.36
$\bar{x}$(50mm)	4.93	14.01	16.34	19.88	9.94	8.70	15.15	12.18	9.07	6.35
σ(50mm)	± 0.47	± 1.12	± 2.53	± 2.03	± 1.40	± 1.04	± 2.19	± 3.77	± 0.61	± 0.35

Appendix F – Principal Component Analysis Results

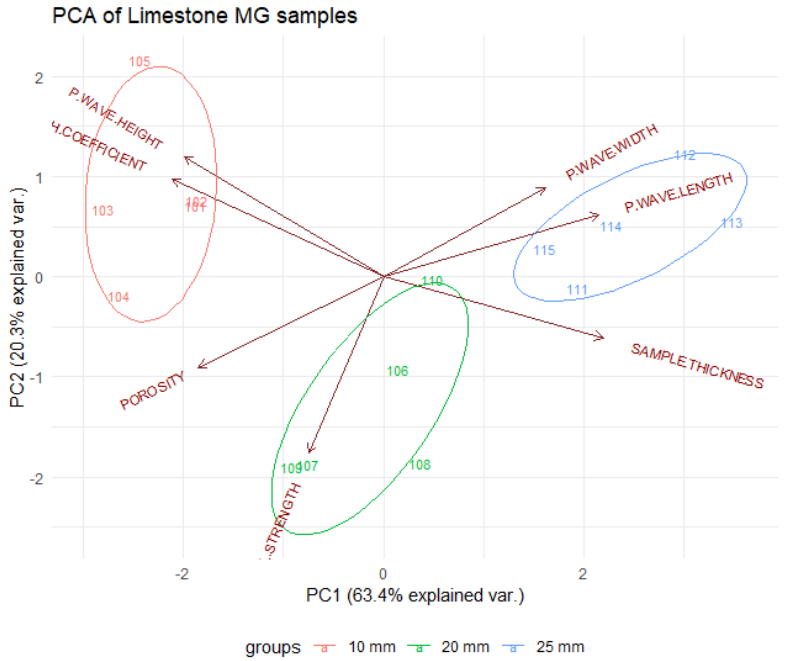

Figure 64 – PCA plot of the two main components PC1 and PC2, for the parameters of flexural strength (MPa), sample thickness (mm), p-wave propagation velocity in the direction of length, width and height (m/s), the Birch coefficient (%) and open porosity (%), obtained in Limestone MG samples.

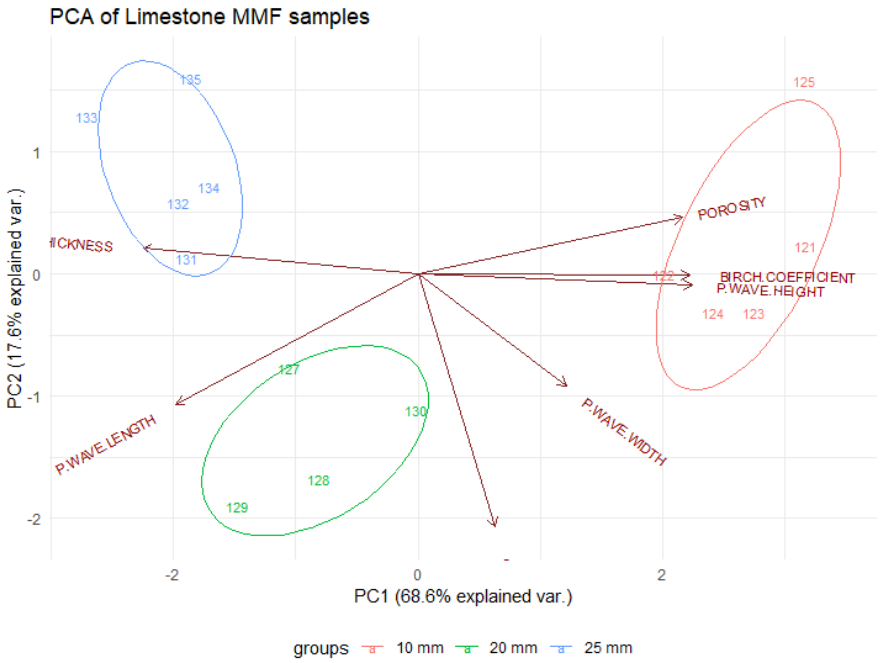

Figure 65 – PCA plot of the two main components PC1 and PC2, for the parameters of flexural strength (MPa), sample thickness (mm), p-wave propagation velocity in the direction of length, width and height (m/s), the Birch coefficient (%) and open porosity (%), obtained in Limestone MMF samples.

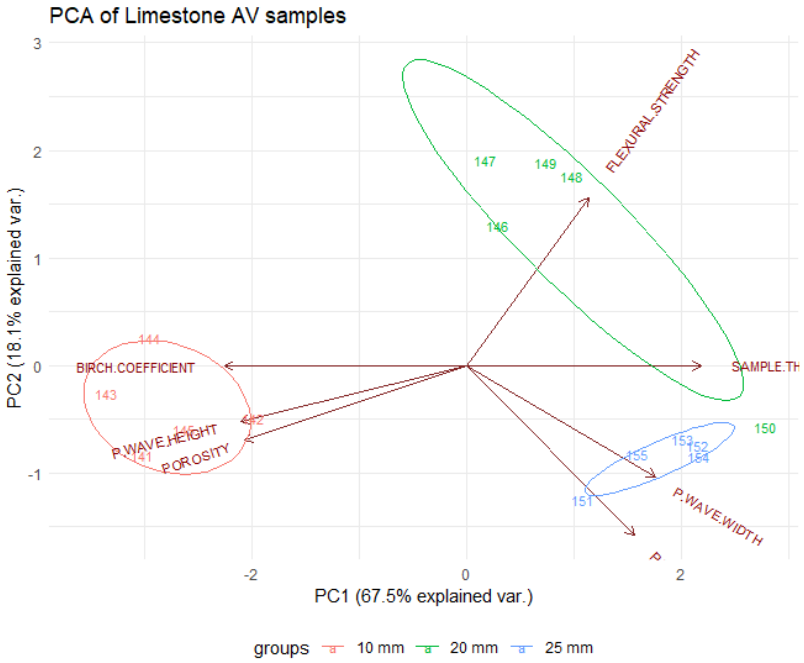

Figure 66 – PCA plot of the two main components PC1 and PC2, for the parameters of flexural strength (MPa), sample thickness (mm), p-wave propagation velocity in the direction of length, width and height (m/s), the Birch coefficient (%) and open porosity (%), obtained in Limestone AV samples.